

REGULATION OF MITOCHONDRIAL SIRTUINS SIRT3 AND SIRT5 BY SMALL MOLECULES

A dissertation submitted to

The Faculty of Biology, Chemistry and Geosciences
University of Bayreuth, Germany

To attain the degree
Doctor of Natural Sciences (Dr. rer. nat.)

Presented by
Giang Thi Tuyet Nguyen

Bayreuth, 2013

This doctoral thesis was prepared at the Department of Biochemistry, University of Bayreuth, Germany from October 2010 until September 2013, under the supervision of Prof. Dr. Clemens Steegborn. This work was funded by Elite Network of Bavaria, BioMedTech International graduate School of Science (BIGSS) Ph.D. program, University of Bayreuth, Germany.

This is a full reprint of the dissertation submitted to attain the academic degree of Doctor of Natural Sciences (Dr. rer. nat.) and approved by the Faculty of Biology, Chemistry and Geosciences, University of Bayreuth, Germany.

Acting dean: Prof. Dr. Rhett Kempe

Date of submission: 30th September, 2013

Date of defense: 27th January, 2014

Doctoral Committee:

Prof. Dr. Clemens Steegborn 1st reviewer

Prof. Dr. Paul Rösch 2nd reviewer

Prof. Dr. Stephan Förster Chairman

Prof. Dr. Matthias Breuning

Acknowledgements

This work is dedicated to my parents, Dau Dinh Nguyen and Tuyet Thi Than for their love, encouragement and support throughout my life, and to my beloved husband, Trieu Nguyen and my little daughter, My Kim Nguyen who have always stood by me.

I would like to express my deepest appreciation to my supervisor, Prof. Dr. Clemens Steegborn for his guidance and continuous support throughout this work. His extensive knowledge and broad vision led me to the right way in research.

I would also like to extend my appreciation to my doctoral committee members: Prof. Dr. Paul Rösch (Department of Biopolymers, University of Bayreuth, Germany), Prof. Dr. Stephan Förster (Department of Physical Chemistry, University of Bayreuth, Germany) and Prof. Dr. Matthias Breuning (Department of Organic Chemistry, University of Bayreuth, Germany) for their feedback and assistance.

I am indebted to all members of the Department of Biochemistry, University of Bayreuth, Germany for their support during my work here. I am very grateful to Dr. Melanie Gertz for detailed and in-depth discussions. I would like to thank Dr. Micheal Weyand and Dr. Sebastien Moniot for their help in crystallography study. Also thanks to Dr. Frank Fischer for his help in mass spectrometry experiments. Special thanks to Ms. Gabriele Kassler and Ms. Renate Crowe for all their help. Thanks to Benjamin Sünkel, Martin Pannek, Ningna Xu, Norbert Grillenbeck, Susanne Schäfer and the other members for their help and encouragement.

I would also like to thank to my Master supervisor, Prof. Dr. Kyeong Kyu Kim (Sungkyunkwan University, South Korea) for providing me the plasmid vector pVFT3S.

I thank Prof. Dr. Paul Rösch, PD. Dr. Stephan Schwarzinger and Ms. Violaine Zigan for helping me in Elite Network of Bavaria, BioMedTech International graduate School of Science (BIGSS) Ph.D. program.

I am thankful to Elite Network of Bavaria, BioMedTech International graduate School of Science (BIGSS) Ph.D. program, University of Bayreuth, Germany for funding this research.

I would like to thank my aunt, Nguyet Thi Nguyen for her help and other family members and friends for their encouragement.

Publications and presentations relate to this work:

Publications:

Nguyen, G.T.T.*, Gertz, M.*, and Steegborn, C. (2013). Crystal structures of Sirt3 complexes with the resveratrol derivative 5-(2-(4-bromophenyl)vinyl)-1,3-benzenediol reveal binding sites and inhibition mechanism. *Chem Biol* 20, 1375-138.

Nguyen, G.T.T., Schaefer, S., Gertz, M., Weyand, M., and Steegborn, C. (2013). Structures of human sirtuin 3 complexes with ADP-ribose and with carba-NAD⁺ and SRT1720: binding details and inhibition mechanism. *Acta Crystallogr D* 69, 1423-1432.

Gertz, M.*, Fischer, F.*, Nguyen, G.T.T., Lakshminarasimhan, M., Schutkowski, M., Weyand, M., and Steegborn, C. (2013). Ex-527 inhibits Sirtuins by exploiting their unique NAD⁺-dependent deacetylation mechanism. *P Natl Acad Sci* 110, E2772-E2781.

Gertz, M., Nguyen, G.T., Fischer, F., Suenkel, B., Schlicker, C., Franzel, B., Tomaschewski, J., Aladini, F., Becker, C., Wolters, D., and Steegborn, C. (2012). A molecular mechanism for direct sirtuin activation by resveratrol. *PLoS One* 7, e49761.

* = Equal contribution

Conferences, courses and symposiums:

Poster presentation entitled “Regulation of mitochondrial sirtuins by small molecules” at the Elite Network of Bavaria Structure Days, Thurnau, Germany, July 2012.

Protein crystallography practical course entitled “From data to structures”, Oulu, Finland, January 2012.

Oral and poster presentation entitled “Regulation of mitochondrial sirtuins by small molecules” at the Elite Network of Bavaria Structure Days symposium, Thurnau, Germany, July 2011.

Another publication not included in this thesis:

Ta, H.M., Nguyen, G.T.T., Jin, H.M., Choi, J., Park, H., Kim, N., Hwang, H.-Y., and Kim, K.K. (2010). Structure-based development of a receptor activator of nuclear factor- κ B ligand (RANKL) inhibitor peptide and molecular basis for osteopetrosis. *P Natl Acad Sci* 107, 20281-20286.

TABLE OF CONTENTS

Abbreviations:	1
Abstract	5
Zusammenfassung	7
1. Introduction	9
1.1. Caloric restriction (CR) and aging	9
1.2. Sirtuins and their roles in CR, aging and human age-related diseases.....	9
1.3. The mammalian sirtuin enzyme family.....	10
1.3.1. Overview of the mammalian sirtuin family: classification, localization and function	10
1.3.2. Mitochondrial sirtuins	12
1.3.3. Structure of sirtuins	13
1.3.4. Enzymatic activity of sirtuins	15
1.4. Sirtuin modulators	17
1.4.1. Activators	17
1.4.1.1. Resveratrol	17
1.4.1.2. Other activators.....	19
1.4.2. Inhibitors	20
1.5. Objectives.....	21
2. Materials and Methods	23
2.1. Materials.....	23
2.1.1. Chemicals, peptides and compounds.....	23
2.1.2. Plasmid vectors	23
2.1.3. Oligonucleotide primers	24

2.1.4. Bacterial strains.....	24
2.2. Methods.....	25
2.2.1. Agarose gel electrophoresis	25
2.2.2. Cloning	25
2.2.3. Site-directed mutagenesis.....	26
2.2.4. Expression	26
2.2.5. Cell disruption.....	27
2.2.6. SDS-Polyacrylamide gel electrophoresis (SDS-PAGE)	27
2.2.7. Purification.....	27
2.2.7.1. Affinity chromatography (AC)	28
2.2.7.2. Tag cleavage	28
2.2.7.3. Ion exchange chromatography (IEC)	29
2.2.7.4. Size exclusion chromatography (SEC).....	29
2.2.8. Fluorescence-based Flour-de-Lys assay.....	29
2.2.9. Enzyme-coupled continuous assay	30
2.2.10. Mass spectrometry (MS)	30
2.2.11. Thermal denaturation shift assay	31
2.2.12. Binding analysis by microscale thermophoresis (MST)	31
2.2.13. Crystallization and structure determination	31
3. Results.....	33
3.1. Sirt3 studies.....	33
3.1.1. Sirt3 purification	33
3.1.2. Resveratrol and its related compounds.....	35
3.1.2.1. Resveratrol and its related compounds are hSirt3 inhibitors	35

3.1.2.2. Crystallization trials of hSirt3 in complex with resveratrol related compounds ...	36
3.1.2.3. Crystal structures and inhibition mechanisms of hSirt3 in complex with resveratrol related compounds.....	38
3.1.2.3.1. hSirt3 in complex with FdL-1 peptide and piceatannol/polydatin	38
3.1.2.3.2. hSirt3 in complex with FdL-1 peptide and 4'-bromo-resveratrol.....	39
3.1.2.3.3. hSirt3 in complex with ACS2 peptide and 4'-bromo-resveratrol.....	44
3.1.3. Resveratrol unrelated compounds.....	49
3.1.3.1. SRT1720.....	49
3.1.3.2. Ex-527	54
3.2. Sirt5 studies.....	57
3.2.1. Sirt5 purification	57
3.2.2. Resveratrol and its related compounds are zSirt5 activators on FdL-1 peptide	59
3.2.3. Crystallization trials and crystal structures of zSirt5 in complex with peptide substrates in the presence of resveratrol	61
4. Discussion	66
4.1. Sirt3 studies.....	66
4.1.1. Resveratrol and its related compounds.....	66
4.1.2. Resveratrol unrelated compounds.....	68
4.2. Sirt5 studies.....	71
References.....	72
Appendix.....	83
(Eidesstattliche) Versicherungen und Erklärungen	92

Abbreviations:

ACS	acetyl-CoA synthetase
ADP	adenosine diphosphate
ADPR	ADP-ribose
AC	affinity chromatography
AIF	apoptosis-inducing factor
AMP	adenosine monophosphate
AMPK	AMP-activated protein kinase
ATP	adenosine-5'-triphosphate
brRESV	4'-bromo-resveratrol (5-(2-(4-hydroxyphenyl)vinyl)-1,3-benzenediol)
CPS1	caobamoyl phosphate synthetase 1
CR	caloric restriction
DMSO	dimethyl sulfoxide
DTT	dithiothreitol
<i>E. coli</i>	<i>Escherichia coli</i>
EDTA	ethylenediaminetetraacetic acid
FA	formic acid
FdL	Fluor de Lys
FOXO	forkhead box protein O1
GDH	glutamate dehydrogenase

H3	histone 3
HEPES	hydroxyethyl piperazineethanesulfonic acid
HIF-1 α	hypoxia-inducible factor 1- α
His-tag	hexahistidine tag
HPLC	high performance liquid chromatography
HPSF	high purity salt free
hSirt1	human Sirt1
hSirt2	human Sirt2
hSirt3	human Sirt3
hSirt5	human Sirt5
IC ₅₀	median inhibition concentration (concentration that reduces the effect by 50%)
IEC	ion exchange chromatography
IGF-1	insulin-like growth factor-1
IPTG	isopropyl β -D-thiogalactopyranoside
K _d	dissociation constant
K _m	Michaelis constant
ME	mutant electron-transferring flavoprotein dehydrogenase
MS	mass spectrometry
MST	microscale thermophoresis
NAD ⁺	nicotinamide adenine dinucleotide oxidized
NADPH	nicotinamide adenine dinucleotide phosphate hydrogen

NAM	nicotinamide
NF- κ B	nuclear factor- κ B
2'-OAADPr	2'-O-acetyl-ADP-ribose
OD ₆₀₀	optical density at 600 nm
Par-3	protease activated receptor 3
PCR	polymerase chain reaction
PCT	piceatannol (3,5,3',4'-tetrahydroxy- <i>trans</i> -stilbene)
PD	polydatin (reservatrol-3- β -D-glucoside)
PDB	protein data bank
RESV	resveratrol (3,4',5-trihydroxystilbene)
ROS	reactive oxygen species
SDS-PAGE	sodium dodecyl sulfate-Polyacrylamide gel electrophoresis
Sir2Tm	<i>Thermotoga maritima</i> Sirtuin
SEC	size exclusion chromatography
Sir	silent information regulator
SRT	Sirtris
STACs	Sirtuin activating compounds
TAE	Tris-acetate-EDTA
TEV	tobacco etch virus
TFA	trifluoroacetic acid
T _m	temperature of melting

TNF	tumor necrosis factors
Trx-tag	thioredoxin tag
TSA	thermal shift assay
V_{\max}	maximum reaction velocity
XDS	X-ray detector software
yHst2	yeast Hst2
ySirt2	yeast Sirt2
zSirt5	zebrafish Sirt5

Abstract

Sirtuins are a highly conserved family of protein deacylases that are important regulators of metabolism, longevity and aged-related diseases. There are seven sirtuin isoforms in mammals with different subcellular localization, substrates and biological functions. Three sirtuin isoforms, Sirt3-5, are located in the mitochondria and play significant roles in all mitochondrial processes. This study investigates the modulations of small molecule compounds on mitochondrial sirtuins Sirt3 and Sirt5 using structural characterization as well as biochemical and biophysical analysis.

Resveratrol, a polyphenol found in red wine, was reported to activate Sirt1. Testing resveratrol and its related compounds including piceatannol, polydatin, 4'-bromo-resveratrol against Sirt3 showed an inhibitory effect. Among these compounds, brRESV is the most potent Sirt3 inhibitor. Crystal structures of Sirt3 in complex with FdL-1 peptide and piceatannol/polydatin showed a direct interaction between the compounds and the peptide coumarin ring to induce non-productive substrate binding, thus inhibit the enzyme activity. Crystal structures of the complex Sirt3/FdL-1/4'-bromo-resveratrol and Sirt3/ACS2/4'-bromo-resveratrol revealed two different compound binding sites. Biochemical and binding data indicated that the binding site of 4'-bromo-resveratrol in the FdL-1 complex involved in inhibition mechanism whereas the compound binding site in the ACS2 complex might imply the site for the activation mechanism of resveratrol on Sirt1.

Resveratrol unrelated compounds including SRT1720, a potent synthetic Sirt1 activator, and Ex-527, a potent Sirt1 inhibitor, also inhibited Sirt3. In the crystal structure of the complex Sirt3/carba-NAD⁺/SRT1720, the compound showed competition with substrate peptide by occupying the binding region of acetyl lysine. SRT1720 interacts with NAD⁺ and the binding analysis indicated that the NAM moiety of NAD⁺ is essential for SRT1720 binding. The crystal structure of Sirt3 in the presence of NAD⁺ and SRT1720 only showed the ADP-ribose part implying the hydrolysis of NAD⁺ and the importance of NAM moiety in SRT1720 binding. In contrast to the SRT1720 inhibition mechanism, Ex-527 stabilized a closed sirtuin conformation

and prevented the product 2'-O-acetyl-ADP-ribose release. Crystal structure of the complex of Sirt3/native O-alkylamidate intermediate provided more information about the deacetylation reaction.

Zusammenfassung

Sirtuine sind eine Familie hochkonservierter Proteindeacylasen, die wichtige Regulatoren des Metabolismus, der Lebensdauer und alters-assoziiertes Krankheiten sind. Säugetiere besitzen sieben Sirtuinisoformen, die sich in ihrer subzellulären Lokalisation, ihren Substraten und biologischen Funktionen unterscheiden. Drei Sirtuinisoformen, Sirt3-5, sind mitochondrial lokalisiert und spielen eine entscheidende Rolle in allen mitochondrialen Prozessen. Diese Arbeit untersucht die Modulation von niedermolekularen Wirkstoffen auf die mitochondrialen Sirtuine Sirt3 und Sirt5 mittels struktureller Charakterisierung als auch anhand biochemischer und biophysikalischer Analyse.

Über Resveratrol, ein in Rotwein vorkommendes Polyphenol, ist bekannt, dass es Sirt1 aktiviert. Die Untersuchung von Resveratrol und dessen verwandten Wirkstoffen wie Piceatannol, Polydatin, 4'-Bromoresveratrol gegen Sirt3 zeigte eine inhibitorische Wirkung. Von diesen Wirkstoffen ist 4'-Bromoresveratrol der stärkste Sirt3-Inhibitor. Kristallstrukturen von Sirt3 komplexiert mit dem FdL-1-Peptid und Piceatannol/Polydatin zeigten eine direkte Interaktion dieser Wirkstoffe mit dem Coumarinring des Peptids. Dies induziert eine unproduktive Substratbindung, die dadurch die Enzymaktivität inhibiert. Kristallstrukturen der Sirt3/FdL-1/4'-bromo-resveratrol- und Sirt3/ACS2/4'-bromo-resveratrol-Komplexe offenbarten zwei unterschiedliche Wirkstoffbindestellen. Biochemische Daten und Bindungsdaten deuteten an, dass die 4'-bromo-resveratrol-Bindestelle im FdL-1-Komplex im Inhibitionsmechanismus involviert ist. Die Wirkstoffbindestelle im ACS2-Komplex hingegen könnte die Bindestelle für den Aktivierungsmechanismus von Resveratrol gegenüber Sirt1 implizieren.

Wirkstoffe wie SRT1720, ein potenter synthetischer Sirt1-Aktivator, und Ex-527, ein potenter Sirt1-Inhibitor, die beide Resveratrol nicht ähneln, inhibierten auch Sirt3. In der Komplexstruktur von Sirt3/carba-NAD⁺/SRT1720 kompetierte der Wirkstoff mit dem Substratpeptid, indem er die Bindestelle des Acetyllysins besetzt. SRT1720 interagiert mit NAD⁺ und Bindestudien deuten an, dass die Nikotinamidgruppe des NAD⁺ für die SRT1720-Bindung

essenziell ist. Im Gegensatz zum Inhibitionsmechanismus von SRT1720 stabilisiert Ex-527 die geschlossene Sirtuinkonformation und verhinderte dadurch die Freisetzung des Produkts 2'-O-acetyl-ADP-Ribose. Die Kristallstruktur des Komplexes aus Sirt3/nativem O-alkylamidat-Intermediats lieferte mehr Information über die Deacetylierungsreaktion.

1. Introduction

1.1. Caloric restriction (CR) and aging

Caloric restriction (CR) is a dietary regimen based on low calorie intake up to 40 percent. Over 75 years ago, Clive McCay and colleagues first found that rats fed a caloric restricted diet live longer than *ad libitum* (freely fed) (McCay, et al., 1989). Since then, similar observations were reported in a variety of species including yeast, fruit flies, worms, etc. (Lin, et al., 2002; Masoro, 2005). In addition, many studies found that CR without malnutrition can prevent or delay a wide number of chronic diseases, such as cancer, diabetes, autoimmune, respiratory disease, Alzheimer disease and Parkinson disease (Cohen, et al., 2009; Longo and Fontana, 2010; Masoro, 1990) indicating that CR retards aging processes.

1.2. Sirtuins and their roles in CR, aging and human age-related diseases

Sirtuins are a family of NAD⁺-dependent protein deacetylases conserved throughout evolution from archaeobacteria to eukaryotes. They are homologs to the yeast Sir2 (silent information regulator 2) (Lin, et al., 2000).

Sir2 was proven to be required for lifespan extension in yeast by CR (Kaeberlein, et al., 1999; Lin, et al., 2000). The ability of glucose restriction to extend lifespan was blocked in yeast deleting *Sir2* gene (Lin, et al., 2000). Since then, many studies focus on Sir2 homologs and their relation to aging. Sir2 homolog induces lifespan extension in worms (Wang and Tissenbaum, 2006) and flies (Rogina and Helfand, 2004). Sirt1 was described as a key role in regulating the metabolic response to CR (Cantó and Auwerx, 2009). Sirt3 mediates CR to age-related hearing loss, the hallmark of mammalian aging and required for the reduction of oxidative damage (Someya, et al., 2010). Sirt6 prolongs lifespan in male mice (Kanfi, et al., 2012) and can be act as a tumor suppressor (Lombard and Miller, 2012).

Many reports suggested the relation of sirtuins to various age-related diseases such as metabolic abnormalities, cancer, neurodegenerative diseases, cardiovascular, etc. (Sebastian, et

al., 2012). Sirtuins can control tumorigenesis due to their ability in regulation of genomic stability such as Sirt1 modulates cellular stress responses and DNA repair, deacetylates the proto-oncogene Myc to prevent transformation (Martinez-Pastor and Mostoslavsky, 2012; Yuan, et al., 2009). Some reports suggested that Sirt3 and Sirt6 seem to be tumor suppressors due to their ability to destabilize HIF-1 α (hypoxia-inducible factor 1- α) through down regulation of ROS (reactive oxygen species) and induce apoptosis in cancer cell lines (Sebastian, et al., 2012). Sirt1 was described as a protector against neurodegenerative diseases such as Alzheimer disease, Parkinson disease and Huntington disease (Arima, et al., 1998; Haass and Selkoe, 2007; Jiang, et al., 2012). Sirt2 supports differentiation and migration of some brain cells through deacetylating α -tubulin and Par-3 (protease activated receptor 3) (Beirowski, et al., 2011; Li, et al., 2007). Moreover, Sirt1 and Sirt7 possess cardiovascular protective properties by deacetylating p53 or regulating fatty acid oxidation (Sebastian, et al., 2012). Sirt3 is a regulator of cardiac function by reducing cellular ROS or suppressing Akt phosphorylation via AMPK (AMP-activated kinase) (Pillai, et al., 2010; Sack, 2011). Sirt6 protect against cardiac hypertrophy by inhibiting NF- κ B (nuclear factor- κ B) or IGF (insulin-like growth factor)-Akt signaling (Sundaresan, et al., 2012; Yu, et al., 2012).

1.3. The mammalian sirtuin enzyme family

1.3.1. Overview of the mammalian sirtuin family: classification, localization and function

In mammals, there are seven members of the sirtuin family, Sirt1–7 that differ in their cellular localization and function (Haigis and Sinclair, 2010; Michan and Sinclair, 2007). The seven mammalian sirtuins share a highly conserved catalytic core domain but have differences in their N- and C-terminal ends (Frye, 2000) (Figure 1.1).

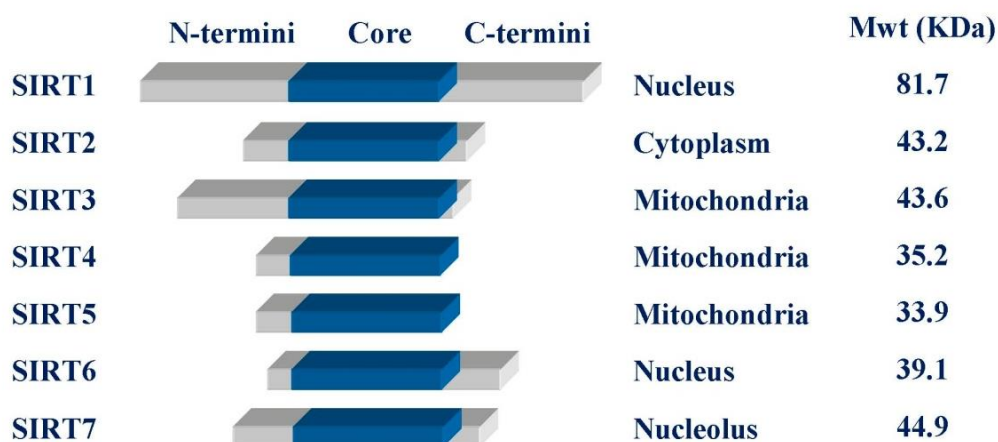


Figure 1.1. Schematic illustration of seven mammalian sirtuins.

Based on phylogenetic analysis, mammalian sirtuins can be divided into four classes. Sirt1-3 belong to class I, Sirt4 to class II, Sirt5 to class III and Sirt6, Sirt7 to class IV (Frye, 2000). Sirt1 is mainly found in the nucleus but also present in the cytosol (Michan and Sinclair, 2007), Sirt2 in the cytoplasm (North, et al., 2003), Sirt3-5 in mitochondria (Gertz and Steegborn, 2010), and Sirt6 and Sirt7 in the nucleus (Michishita, et al., 2005).

Sirt1-3 have robust deacetylation activity, whereas Sirt4 and Sirt6 were reported to be ADP-ribosyltransferases (Haigis, et al., 2006; Mao, et al., 2011). Sirt6 can also act as a deacetylase (Michishita, et al., 2008). Sirt7 was recently confirmed as a deacetylase due to its important role in deacetylation of H3K18Ac (acetylated lysine 18 of histone H3) (Barber, et al., 2012). Sirt5 was initially reported to deacetylate CPS1 (carbamoyl phosphate synthase 1) (Nakagawa, et al., 2009) but recently described as a protein desuccinylase and demalonylase (Du, et al., 2011) indicating that sirtuins are a family of deacylases.

Sirt1 is the most studied mammalian sirtuin isoform which was first described as a histone deacetylase (Haigis and Sinclair, 2010) but also has other protein targets such as p53 which is deacetylated upon DNA damage or oxidative stress (Vaziri, et al., 2001) and forkhead transcription factors (FOXO) in lipid and glucose metabolism (Motta, et al., 2004). Sirt2 is a tubulin deacetylase (North, et al., 2003). Sirt3-5 play important roles in metabolism, apoptosis and intracellular signaling (Verdin, et al., 2010). More details of Sirt3-5 are in the Mitochondrial

sirtuins section (see below). Sirt6 is involved in DNA repair (Lombard, 2009), regulates immune response that relates to NF- κ B targets (Kawahara, et al., 2009; Michishita, et al., 2008) and controls TNF (tumor necrosis factors) production (Van Gool, et al., 2009). Sirt7 is H3K18Ac deacetylase that functions in chromatin regulation, cellular transformation programs and tumour formation (Barber, et al., 2012).

1.3.2. Mitochondrial sirtuins

NAD⁺-dependent protein deacylase is a major enzymatic activity of sirtuins. Proteomic studies implied that a large number of mitochondrial proteins are acetylated (Verdin, et al., 2010). NAD⁺ is an essential electron carrier in various metabolic processes such as energy production, fatty acid metabolism, urea cycle, etc., which are integrated by mitochondria. Since sirtuins use NAD⁺ as a cosubstrate, Sirt3-5 which have been identified in the mitochondrial matrix are directly linked to mitochondrial processes and influence mitochondrial functions (Figure 1.2).

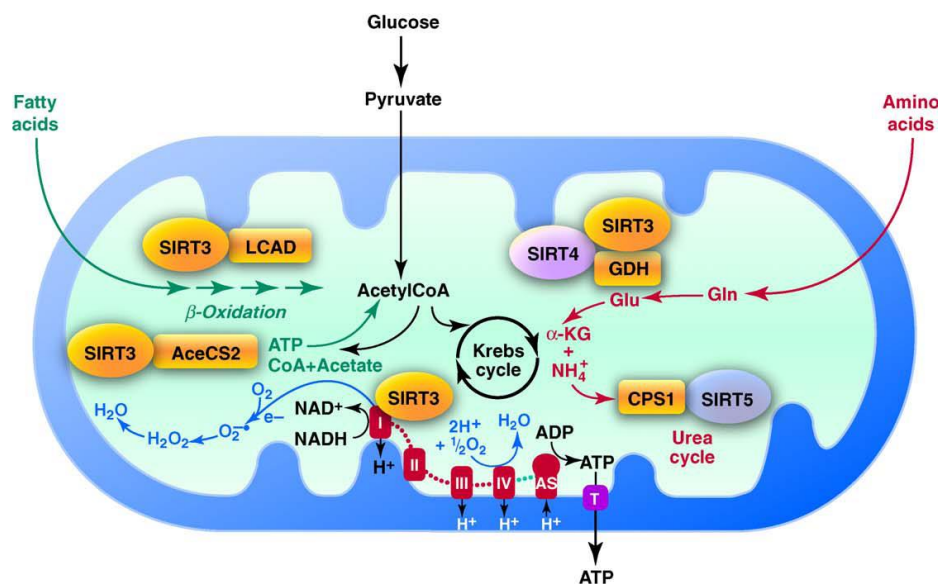


Figure 1.2. Mitochondrial sirtuins and their links to mitochondrial processes. Figure is reused with permission from Elsevier Limited (Verdin, et al., 2010).

Sirt3 seems to be the major mitochondrial deacetylase since mice lacking Sirt3 showed a hyperacetylation of mitochondrial proteins (Lombard, et al., 2007). The mitochondrial protein acetylcoenzyme A synthase 2 (ACS2) which converts acetate to acetyl-CoA in the presence of ATP is the first identified Sirt3 substrate (Hallows, et al., 2006). Glutamate dehydrogenase (GDH) is also Sirt3 substrate since Sirt3 deacetylates and activates GDH activity by 10% (Schlicker, et al., 2008). Sirt3 interacts with Complex I of the electron transport chain and deacetylates various proteins in this complex (Ahn, et al., 2008). The mitochondrial matrix enzyme CPS1 which plays an important role in the rate-limiting step of the urea cycle was identified as a Sirt5 substrate (Nakagawa, et al., 2009). Recently, Sirt5 has been determined as a major demalonylase and desuccinylase since mice lacking Sirt5 showed hypermalonylation and hypersuccinylation (Peng, et al., 2011). Two Sirt5 residues in the catalytic pocket, Tyr102 and Arg105, are mandatory for the demalonylase and desuccinylase activities (Du, et al., 2011). These two residues are conserved in sirtuin class III of different species (Du, et al., 2011). The enzymatic function of Sirt4 remains unclear. So far, Sirt4 has no detectable deacetylase activity and weak ADP-ribosyltransferase activity (Ahuja, et al., 2007; Haigis, et al., 2006).

1.3.3. Structure of sirtuins

Crystal structures of different sirtuin homologs including apo protein or in complex with substrates or small molecules have been published. The structure of yeast Hst2 (PDB ID 1Q14) (Zhao, et al., 2003) contains the full-length protein whereas the remaining structures show only the core domain. The full length yHst2 structure implies the role of N- and C-terminal region of sirtuins in the regulation of substrate binding (Zhao, et al., 2003).

The conserved catalytic core consists of two domains, a large Rossmann-fold domain for NAD⁺ binding and a variant small zinc-binding domain that may be involved in substrate binding (Sanders, et al., 2010; Sauve, et al., 2006) (Figure 1.3). The Rossmann-fold domain consists of six parallel β strands forming a β sheet which is sandwiched between several α helices on each side (Min, et al., 2001). The two modules of the zinc-binding domain include three β strands forming an antiparallel β sheet and a helical region with three or four helices

dependent on the sirtuin member. Four cysteine residues coordinate the zinc ion in a tetrahedral conformation to stabilize the structure (Min, et al., 2001). A cleft where catalysis takes place is formed between two domains by four linking loops. This region is the most conserved with high sequence homology among sirtuin family.

The largest of these four linking loops, called cosubstrate binding loop, is very dynamic. The cosubstrate binding loop is highly flexible when NAD^+ is not bound and becomes well-ordered through NAD^+ binding (Zhao, et al., 2004) indicating that its conformation is dependent on the presence of NAD^+ . The NAD^+ binding site can be divided in three pockets: an adenine binding pocket (pocket A), a nicotinamide (NAM) ribose binding pocket (pocket B) and a NAM binding pocket (pocket C). Different ligands in NAD^+ site induce slightly conformational changes of the cosubstrate binding loop (Avalos, et al., 2005; Sanders, et al., 2007).

The acetyl lysine of peptide substrate inserts into a hydrophobic tunnel of the cleft between two domains. When comparing the protein conformation with and without peptide substrate, peptide binding induces a shift in the linking loop between two domains and brings two domains closer together (Cosgrove, et al., 2006). The substrate peptide orientation and interaction with protein residues described in different crystal structures strengthen one mechanism that different sirtuins discriminate among substrates.

The NAD^+ cosubstrate inserts from opposite site with the acetylated substrate into the cleft between two domains (Sanders, et al., 2010). The conformation of NAM ribose is variable dependent on NAD^+ analogs, substrate peptides and sirtuin homologs. The density of the ADPR part including the adenine ribose and NAM ribose is well defined whereas the NAM moiety is almost invisible in different sirtuin structures in the presence of NAD^+ (Chang, et al., 2002; Nguyen, et al., 2013; Pan, et al., 2011) indicating the flexibility of this part or the hydrolysis of NAD^+ during crystallization.

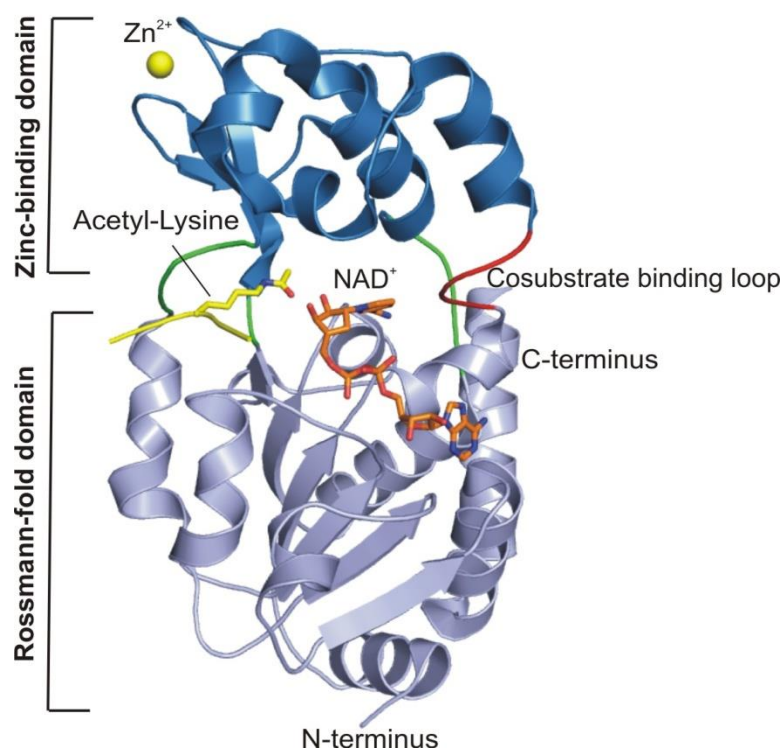


Figure 1.3. Overall structure of sirtuins. The catalytic core of human Sirt3 (ribbon) in complex with carba-NAD⁺ (stick, orange) and ACS2 peptide (acetyl lysine in stick, yellow) (PDB ID 4FVT) (Szczepankiewicz, et al., 2012) is shown as a representative. The large Rossmann-fold domain is in purple. The small zinc-binding domain that contains Zn²⁺ ion (sphere, yellow) is in blue. The loops connecting two domains are in green. The cosubstrate binding loop is highlighted in red.

1.3.4. Enzymatic activity of sirtuins

Although the initial activity of sirtuins was reported as NAD⁺-dependent ADP-ribosylation (Tanny, et al., 1999), protein deacetylation is the most prevalent reaction that sirtuin enzymes catalyze. The deacetylation reaction occurs in two continuous stages to generate deacetylated protein, NAM and 2'-O-acetyl-ADP-ribose (2'-OAADPr) (Sauve, et al., 2006; Tanner, et al., 2000) (Figure 1.4). In the first stage, sirtuins cleave NAD⁺ to produce NAM and the nucleophilic addition of the acetyl oxygen to C1' of the ADP-ribose moiety to form C1'-O-alkylamidate intermediate (Sauve, 2010). The nucleophilic attack mechanism has been subject to debate between S_N1 and S_N2 type for the cleavage of the glycosidic bond between NAM and the

rest of NAD^+ (Smith and Denu, 2007). NAM can inhibit sirtuins by rebinding to reverse the reaction through the base-exchange mechanism (Sauve, et al., 2006). In the second stage, the $\text{C1}'\text{-O-alkylamidate}$ intermediate converts to the bicyclic intermediate by using the conserved Histidine as a general base to induce nucleophilic attack of the $2'$ -OH group of the ribose onto the iminium carbon of the O-alkylamidate intermediate. The crystal structure of the bicyclic intermediate between thiosuccinyl H3 peptide and NAD^+ on Sirt5 was recently solved to provide an evidence for the mechanism (Zhou, et al., 2012). The bicyclic intermediate is disrupted by a base activated water molecule to form deacetylated protein and $2'$ -O-acetyl-ADP-ribose (Sauve and Youn, 2012). Both $2'$ -O-acetyl-ADP-ribose and $3'$ -O-acetyl-ADP-ribose exist in equilibrium as solution products of sirtuins (Jackson and Denu, 2002).

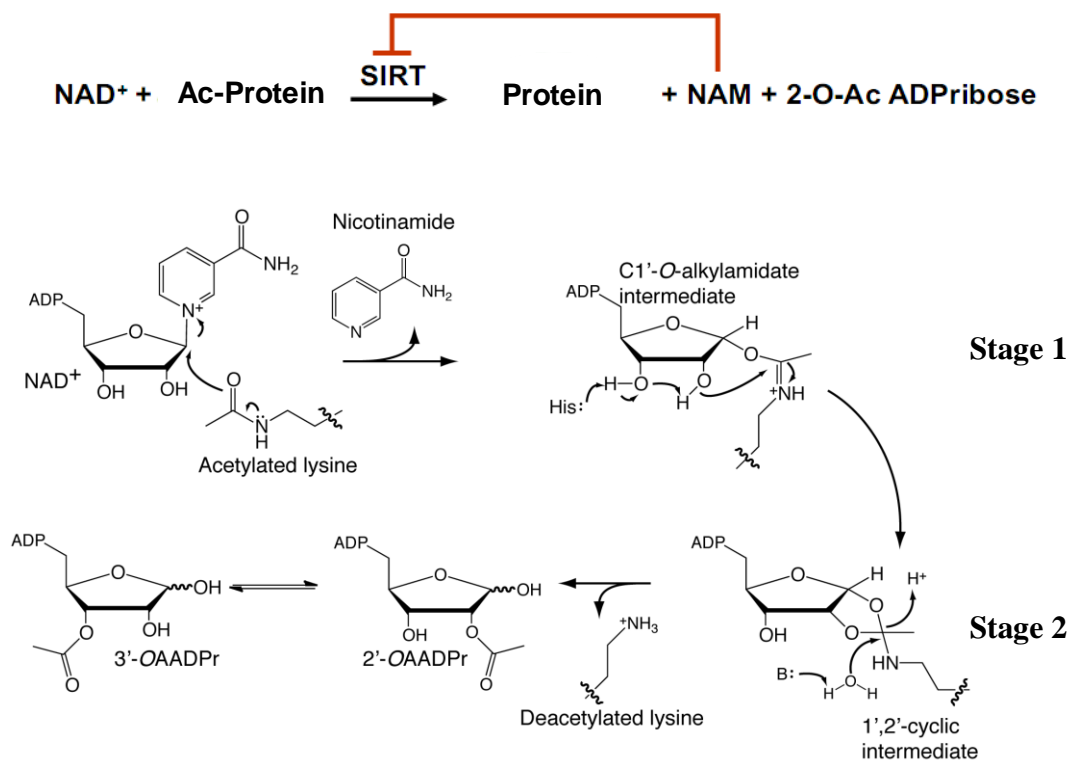


Figure 1.4. Mechanism of sirtuin-catalyzed deacetylation. Protein deacetylation reaction with two continuous stages catalyzed by sirtuins. Figure is reused with permission from American Society for Biochemistry and Molecular Biology (Feldman, et al., 2012).

1.4. Sirtuin modulators

1.4.1. Activators

1.4.1.1. Resveratrol

CR extends lifespan of a variety of species and delays or prevents many age-related diseases. The role of sirtuins in CR-mediated longevity has been proven in several studies (Cantó and Auwerx, 2009; Kanfi, et al., 2012; Someya, et al., 2010). Due to the fact that not many people would be willing to keep a CR lifestyle, recent studies focus on mimicking CR's effects, especially enhancing the activity of sirtuins by small molecules providing a foundation for drug development.

Howitz and colleagues screened small molecule compounds to identify several activators and inhibitors of Sirt1. They reported that two polyphenols, quercetin and piceatannol (Figure 1.5), can activate Sirt1 activity 5- and 8-fold, respectively. The sirtuin activating compounds were called STACs. Subsequently, they screened the polyphenol family and found resveratrol (3,4',5-trihydroxystilbene) (Figure 1.5) as the most potent activator candidate with ~13-fold increase in substrate deacetylation of Sirt1 and lower K_m of the enzyme for the substrate and NAD^+ (Howitz, et al., 2003). Resveratrol, a natural polyphenol found in red wine and other plant-based foods, is able to mimic CR in anti-aging and possess many other benefits such as antiviral, anti-inflammation, anti-diabetic and cardioprotective effects (S. Mohar, 2012). Resveratrol was reported to extend lifespan of different organisms including yeast, worm and fly dependent on sirtuin activity (Howitz, et al., 2003; Wood, et al., 2004). This compound can also induce lifespan extension in fish but the relation of its effect to sirtuins is unclear (Valenzano, et al., 2006).

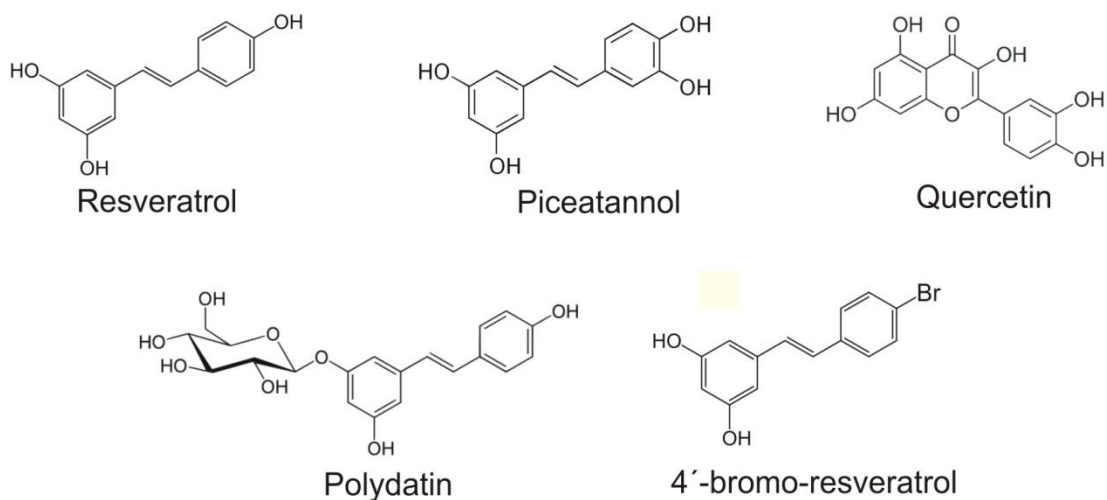


Figure 1.5. Resveratrol and its related compounds. Figures are adapted with permission from Blum et al. (Blum, et al., 2011). Copyright (2011) American Chemical Society.

However, the role of resveratrol as a Sirt1 activator has been questioned in some reports. Resveratrol effect was initially found with a fluorophore labeled substrate (Howitz, et al., 2003). It was later shown that for this substrate, the enhancement of Sirt1 activity by resveratrol depends on the fluorophore labeling (Borra, et al., 2005; Kaeberlein, et al., 2005). Resveratrol did not activate Sirt1 when using fluorophore-free peptide substrates (Beher, et al., 2009; Pacholec, et al., 2010). In addition, the crystal structure of Sirt5 in complex with resveratrol and of Sirt3 in complex with piceatannol revealed the direct interaction of the compounds to the coumarin tag of the Fluor-de-lys peptide (Gertz, et al., 2012), indicating the fluorophore influence in compound binding. In another study, resveratrol induced metabolic changes mediated via AMPK rather than Sirt1 (Um, et al., 2010).

Subsequently, a study found that Sirt1 fluorophore-free substrates containing a hydrophobic amino acid residue (Trp, Tyr or Phe) at position +1 or +6 were selectively activated by STACs (Hubbard, et al., 2013). In the same report, Glu230 of Sirt1, a conserved residue from flies to humans, was identified as the critical residue for Sirt1 activation by STACs. The compounds stimulate Sirt1 via allosteric activation mechanism mediated by Glu230 containing N-terminal domain of the enzyme. In addition, another study testing many physiological deacetylation sites in parallel using peptide arrays showed that substrate sequence determines

resveratrol effects (Lakshminarasimhan, et al., 2013). Moreover, there is no evidence of Sirt1 independent AMPK phosphorylation in STAC-treated cells that goes against a report about resveratrol mediated AMPK pathway (Park, et al., 2012). Therefore, sirtuins could be directly activated by STACs.

1.4.1.2. Other activators

Resveratrol is a natural compound which might have benefits in prevention or treatment of age related diseases via sirtuin activation. However, the compound has low bioavailability and might not specific for sirtuin target (Alcaín and Villalba, 2009; Pirola and Frojdo, 2008). New synthetic sirtuin activators that are much more effective than resveratrol have been developed. Milne and colleagues identified resveratrol unrelated activators including SRT1460, SRT1720, and SRT2183 (Figure 1.6) that work up to 1000 fold more potently than resveratrol (Milne, et al., 2007). Among these compounds, SRT1720 is the most effective with $EC_{1.5} = 0.16 \mu\text{M}$ and maximum activation = 781%. This small molecule compound was demonstrated as therapeutics for treatment of many diseases such as type 2 diabetes, metabolic disorders, inflammation, etc. (Villalba and Alcaín, 2012).

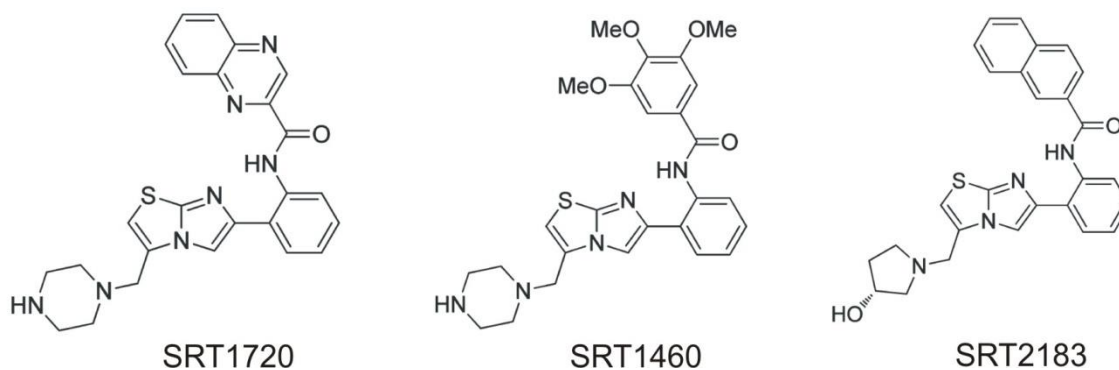


Figure 1.6. Resveratrol unrelated activators. Figures are adapted with permission from Blum et al. (Blum, et al., 2011). Copyright (2011) American Chemical Society.

1.4.2. Inhibitors

While sirtuin activators have mainly been developed for Sirt1, sirtuin inhibitors have been studied on different sirtuin members including ySir2 (yeast Sir2), Sir2Tm (*Thermotoga maritima* sirtuin), and mammalian Sirt1, Sirt2, Sirt3 and Sirt5.

The first sirtuin inhibitors are mostly based on substrates and products of the deacetylation reaction. NAM inhibits Sir2 activity by rebinding to attack the O-alkylamidate intermediate (Sauve and Schramm, 2003). Carba-NAD⁺ is a weak inhibitor of sirtuins (Landry, et al., 2000). Thioacetyllysine derived peptides have been described as sirtuin inhibitors by hindering the reaction via formation of a stable S-alkylamidate intermediate instead of the native, transient O-alkylamidate intermediate (Smith and Denu, 2007). Moreover, the replacement of N-acetyl group with other groups and chemical modifications of peptide substrate have also reported as an approach to develop sirtuin inhibitors (Chen, 2011).

Besides substrate and product based inhibitors, a variety of small molecule compounds have been studied (Blum, et al., 2011; Cen, 2010). Some of these compounds such as splitomicin, sirtinol, cambinol (Figure 1.7) have weak effects on sirtuins with micromolar range of IC₅₀ value. Their derivatives showed improved potency but still moderate isoform selectivity. Splitomicin showed a moderate inhibition on Sir2 with an IC₅₀ value of 60 μM (Bedalov, et al., 2001) but a weak inhibition on Sirt1. HR73, a splitomicin derivative, inhibited Sirt1 with an IC₅₀ value of less than 5 μM (Pagans, et al., 2005). Sirtinol inhibited both Sir2 and Sirt2 (Grozingler, et al., 2001) but its analogs, *meta*- and *para*-sirtinol, are more potent (Mai, et al., 2005). Cambinol inhibited Sirt1 and Sirt2 with IC₅₀ values of 56 and 59 μM, respectively but showed weak inhibition against Sirt5 and no inhibition against Sirt3 (Heltweg, et al., 2006). Phenyl ring modifications of cambinol improved potency and selectivity of this compound on Sirt1 and Sirt2 (Medda, et al., 2009). Other compounds such as Ex-527 and suramin (Figure 1.7) have higher effects on sirtuins with nanomolar range of IC₅₀ value. Ex-527, an indole derivative, has high selectivity for Sirt1 with an IC₅₀ value of 0.098 μM and lower potency against Sirt2 (IC₅₀ 19.6 μM) and Sirt3 (IC₅₀ 48.7 μM) (Solomon, et al., 2006). Suramin, a symmetric polyanionic naphthylurea, is a potent inhibitor of many sirtuin isoform including Sirt5 (IC₅₀ 22 μM) (Schuetz, et al., 2007), Sirt1 (IC₅₀ 0.297 μM) and Sirt2 (IC₅₀ 1.15 μM) (Trapp, et al., 2007).

Among these compounds, the inhibition mechanisms of suramin and Ex-527 on sirtuins were revealed based on crystal structures (Gertz, et al., 2013; Schuetz, et al., 2007; Zhao, et al., 2013). In Sirt5-suramin complex structure, one suramin molecule links two monomers of Sirt5 together. Suramin inhibits Sirt5 by binding into the B- and C-pockets of the NAD⁺ binding site and the substrate binding site (Schuetz, et al., 2007). Ex-527 stabilizes the closed sirtuin conformation to prevent product release (Gertz, et al., 2013).

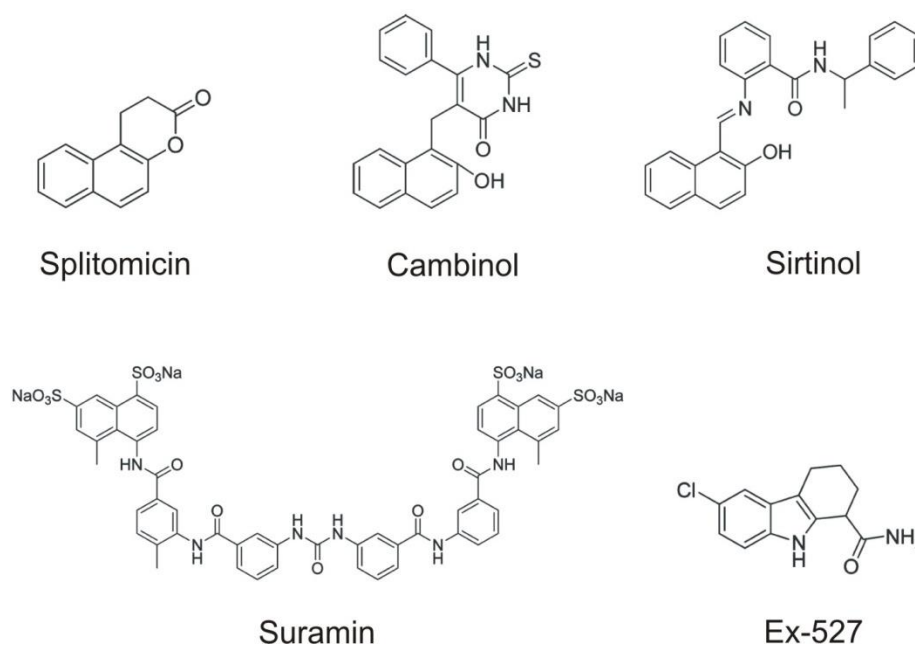


Figure 1.7. Representative sirtuin inhibitors. Figures are adapted with permission from Blum et al. (Blum, et al., 2011). Copyright (2011) American Chemical Society.

1.5. Objectives

Sirtuins modulation by small molecule compounds could have benefits to treat many human age-related diseases such as cancer and neurodegenerative diseases. Resveratrol is a natural polyphenol that can mimic CR to activate Sirt1 and has important role in delaying and preventing some diseases. SRT1720, a resveratrol unrelated compound, is the most potent activator of Sirt1. The molecular mechanisms of these activators on Sirt1 are unclear, especially their structural information. So far, all activators have been described only for Sirt1 whereas inhibitors have been identified for different sirtuin isoforms. In this study, the mitochondrial

sirtuins Sirt3 and Sirt5 are used as models to investigate the regulation of small molecule compounds on the sirtuin family. The small molecule compounds used in this study include resveratrol and its related compounds with improved solubility due to an additional hydroxyl group (piceatannol (3,5,3',4'-tetrahydroxy-*trans*-stilbene)) or glucose group (polydatin (resveratrol-3- β -D-glucoside)) or bromide group (4'-bromo-resveratrol (5-(2-(4-hydroxyphenyl)vinyl)-1,3-benzenediol)) (Figure 1.5) and resveratrol unrelated compounds including SRT1720 (N-(2-(3-(piperazin-1-ylmethyl)imidazo[2,1-b]thiazol-6-yl)phenyl)quinoxaline-2-carboxamide) and Ex-527 (6-chloro-2,3,4,9-tetrahydro-1H-carbazole-1-carboxamide). To obtain the purpose of this study, crystal structures of Sirt3 and Sirt5 in complex with different substrate peptides in the presence of different small molecule compounds were solved. In addition, biochemical and biophysical studies were conducted to support the regulation mechanisms of small molecule compounds on sirtuins implied by crystal structures.

2. Materials and Methods

2.1. Materials

2.1.1. Chemicals, peptides and compounds

All chemicals were from Sigma, Roth and Applichem if not stated differently. Fluor-de-lys 1 (FdL-1) peptide was from Enzo Life Science (New York, USA). The fluorophore-free peptides listed in Table 2.1 were synthesized and HPLC (high performance liquid chromatography) purified by GL Biochem (Shanghai, China). 4'-bromo-resveratrol was from Matrix Scientific (Columbia, USA). SRT1720 was from Cayman Chemical (Ann Arbor, USA).

Table 2.1. List of peptides used in this study.

Peptide	Protein	Sequence	Acetylated position
ACS2	Acetyl-coenzyme A synthetase 2	TRSG(acK)VMRRL	Lys642
p53-short	p53	RHK(acK)LMFK	Lys382
p53-long	p53	STSRHK(acK)LMFKTE	Lys382
CPS1	Carbamoyl-phosphate synthetase 1	FKRGVL(acK)EYGVKV	Lys527
ME	Mutant electron-transferring flavoprotein dehydrogenase	ILTE(acK)YRI	Lys153
ME-long	Mutant electron-transferring flavoprotein dehydrogenase	FGILTE(acK)YRIPVP	Lys153
H3	Histone 3	IHA(acK)RVT	Lys116
Lamin-B2	Lamin-B2	YKFTP(acK)YILRA	Lys500
AIF	Apoptosis-inducing factor 1	DFRSLE(acK)ISREVK	Lys295

2.1.2. Plasmid vectors

The catalytic core domain gene of zebrafish Sirt5 (zSirt5) (residues 30-298) was cloned into the vector pET151/D-TOPO (Life Technologies, USA) coding for His-tag (hexahistidine tag) and carrying the resistance marker to ampicillin. The catalytic core domain gene of human Sirt3 (hSirt3) (residues 118-399) was cloned into the vector pVFT3S (Sungkyunkwan university,

South Korea) coding for His-Trx-tag (hexahistidine-thioredoxin tag) and carrying the resistance marker to kanamycin.

2.1.3. Oligonucleotide primers

All primers using for cloning or site-directed mutagenesis listed in Table 2.2 were HPLC purified or HPSF (high purity salt free) from Sigma, USA or Eurofins MWG Operon, Germany.

Table 2.2. List of primers used in this study. Restriction sites or stop codon are underlined. Positions of mutation labeled as bold and italic.

Name	Sequence
zSirt5-5'TOPO	5'- <u>CACCACCAGACCAAGCTCGGATT</u> TA-3'
zSirt5-3'stop	5'-CTATTCCAGCGCGGGGGGCAA-3'
hSirt3-5'BamHI	5'-CTAGCTGGATCCAGTGACAAGGGGAAGCT-3'
hSirt3-3'XhoI	5'-GACCCGCTCGAGTCATTTGTCTGGTCCATC-3'
R139A_F	5'-GCCAGAGCCTGCCAGG CG GGTGGTGGTCATGGTG-3'
R139A_R	5'-CACCATGACCACCAC CG CCTGGCAGGCTCTGGC-3'
M311A_F	5'-GTGGTTGATTTCCCC CG GCAGATCTGCTGCTC-3'
M311A_R	5'-GAGCAGCAGATCTGCC CG GGGAAATCAACCAC-3'
R335A_F	5'-TTGACCGAGGCCGTGG CG AGCTCAGTTCCCCGA-3'
R335A_R	5'-TCGGGGA ACT GAGCT CG CCACGGCCTCGGTCAA-3'
R384A_F	5'-TGGACAGAAGAGATGG CG GACCTTGTGCAGCGG-3'
R384A_R	5'-CCGCTGCACAAGGTCC CG CCATCTCTTCTGTCCA-3'

2.1.4. Bacterial strains

The *E. coli* strain TOP10 (Life Technologies, USA) was used for cloning, plasmid propagation and site-directed mutagenesis. The *E. coli* strain Rosetta (DE3) (Merck, Germany) was used for overexpression of recombinant proteins.

The strains have the following genotypes:

TOP10: F⁻ mcrA Δ (mrr-hsdRMS-mcrBC) Φ 80lacZ Δ M15 Δ lacX74 recA1 araD139 Δ (ara leu) 7697 galU galK rpsL (StrR) endA1 nupG

Rosetta (DE3): F⁻ ompT hsdSB(rB – mB⁻) gal dcm lacY1(DE3) pRARE (CamR)

2.2. Methods

2.2.1. Agarose gel electrophoresis

Bio-Rad Sub-cell horizontal gel electrophoresis system (Bio-Rad, USA) was used to perform nucleic acid electrophoreses with 1x TAE (Tris-acetate-EDTA (ethylenediaminetetraacetic acid)) as the running buffer. Samples and DNA maker (New England Biolabs, USA) were mixed with loading buffer (6 mM EDTA, 6 % glycerol and 0.015 % bromophenol blue) before loading on a 1 % (w/v) agarose matrix (in 1x TAE buffer) containing 1 μ g/ml ethidium bromide. After electrophoresis, the gel was placed under UV light for DNA visualization.

2.2.2. Cloning

The catalytic core domain genes of zSirt5 and hSirt3 were amplified using PCR (polymerase chain reaction). 50 μ l of a PCR reaction contains the following: 10-50 ng of template DNA, 0.5 μ M of each primer, 2 Units of DNA polymerase (Thermo Scientific, USA) and 1x HF buffer, 0.2 μ M of each deoxynucleotide. The PCR program included 1) initial denaturation at 95 °C for 2 minutes; 2) denaturation at 95 °C for 1 minute, annealing at 60 °C for 1 minute, extension at 72 °C for 1 minute and 3) final elongation at 72 °C for 10 minutes. Step 2 was repeated 30 times. The PCR products were visualized and purified using agarose gel electrophoresis and gel extraction kit (Qiagen, USA).

zSirt5 gene was directly mixed with the vector pET151/D-TOPO without using restriction enzymes. hSirt3 gene and the vector pVFT3S were treated with restriction enzymes

BamHI and XhoI (Thermo Scientific, USA). After visualized and purified using agarose gel electrophoresis, hSirt3 gene was ligated into the vector using a molar ratio of 3:1 (gene : vector) in the presence of T4 DNA ligase (New England Biolabs, USA) and incubation at 20 °C overnight. 3 µl of the ligated products was used for the transformation of the recombinant plasmids into 50 µl of TOP10 competent cells to amplify the plasmids. The mixture was placed on ice for 30 minutes, heat shock at 42 °C for 30 seconds, and then put on ice for 5 minutes. 450 µl of LB media was added to recover the cells at 37 °C for 1 hour followed by plating on LB agar plates containing appropriate antibiotics and incubated at 37 °C overnight. Subsequently, the plasmids were extracted using plasmid extraction kit (Qiagen, USA).

2.2.3. Site-directed mutagenesis

50 µl of the PCR reaction for site-directed mutagenesis contains the following: 5-50 ng of template DNA, 125 ng of each forward and reverse primers, 0.2 mM deoxynucleotide mix, 1.25 Units of *Pfu Turbo* DNA polymerase (Agilent Technologies, USA), 1x cloned *Pfu* DNA polymerase reaction buffer. The PCR program for site-directed mutagenesis was: 1) initial denaturation at 95 °C for 5 minutes; 2) denaturation at 95 °C for 1 minute, annealing at 55 °C for 1 minute, extension at 68 °C for 10 minutes; 3) final elongation at 68 °C for 10 minutes. Step 2 was repeated 18 times. Subsequently, the PCR product was treated with 5 Units of DpnI restriction enzyme at 37 °C for 1 hour to digest the template plasmid vector and 1 µl of the reaction mixture was transformed into 50 µl of TOP10 competent cells using the transformation protocol as in the Cloning section.

2.2.4. Expression

The recombinant plasmids were transformed into 50 µl of *E. coli* Rosetta (DE3) competent cells for expression. The cells were placed on a 1 millimeter electroporation cuvette (Serva, Germany) and pulsed with a voltage of 2.5 kV using the Bio-Rad Gene Pulser electroporation system (Bio-Rad, USA). 450 µl of LB media was added to recover the cells at 37 °C for 1 hour followed by transferring to LB media containing appropriate antibiotics and

incubation at 37 °C by shaking. When the OD₆₀₀ reached 0.6 – 0.8, the temperature was reduced to 15 °C. IPTG (isopropyl β-D-thiogalactopyranoside) was added into media to induce protein expression. The cells were grown at 15 °C overnight and harvested by centrifugation at 5,000 RPM for 20 minutes at 4 °C and stored at -80 °C.

2.2.5. Cell disruption

Frozen cells were resuspended in an appropriate lysis buffer and disrupted using Microfluidizer (Microfluidics, USA) at 4 °C. The lysed cells were then centrifuged at 18,000 RPM for 45 minutes in a refrigerated Beckman Coulter Avanti J-26XP centrifuge fitted with a JA-30.50 Ti rotor (Beckman Coulter, USA) to remove cell debris.

2.2.6. SDS-Polyacrylamide gel electrophoresis (SDS-PAGE)

SDS-PAGE was performed to analyze the purity and size of proteins. The stacking gel, running gel (15% acrylamide), buffers were prepared by following a published protocol (Sambrook and Russell, 2001). Protein samples were denatured for 5 minutes at 95 °C before loading on the gel. The Mini-PROTEAN Tetra Cell vertical electrophoresis system (Bio-Rad, USA) was used for electrophoresis. After electrophoresis, the gel was rinsed in water, followed by a quick soaking in hot Coomassie blue solution (0.025 % (w/v) Coomassie-Briliant Blue R-250 (Appllichem, Germany), 50 % (v/v) methanol, 10 % (v/v) acetic acid). Subsequently, the gel was transferred to a destaining solution containing 20 % (v/v) methanol and 12 % (v/v) acetic acid.

2.2.7. Purification

The catalytic core domain of zSirt5 and hSirt3 were purified using similar protocols. The fusion proteins were purified by affinity chromatography with TALON resin followed by removing the His-tag of zSirt5 or His-Trx-tag of hSirt3 using tobacco etch virus (TEV) protease.

To separate tag and protease, the tag-cleaved hSirt3 was resubjected to a TALON column while the digested zSirt5 was loaded into a HiTrap SP column. Finally, zSirt5 and hSirt3 were subjected to Superose-12 gel filtration column (GE Healthcare, Waukesha, USA), and the purified proteins were shock frozen and stored at -80 °C.

2.2.7.1. Affinity chromatography (AC)

The first step to purify His-tagged hSirt3 and zSirt5 was affinity chromatography. 1 ml bed volume of TALON resin was used for every liter of *E. coli* culture. The resin was washed with water followed by equilibration in lysis buffer. The supernatant containing the recombinant protein in lysis buffer was incubated with the equilibrated resin at 4 °C for 1 hour. After the incubation, the flow through was collected by gravity flow using a glass column (Bio-Rad, USA). The column was washed twice with 20 bed volumes of two wash buffers and the protein was then eluted with elution buffer. The purity and size of the proteins were analyzed using SDS-PAGE.

Lysis buffer: 50 mM Tris, pH 7.8 for hSirt3 and 8.5 for zSirt5, 200 mM NaCl

The first wash buffer: 50 mM Tris, pH 7.8 for hSirt3 and 8.5 for zSirt5, 500 mM NaCl

The second wash buffer: 50 mM Tris, pH 7.8 for hSirt3 and 8.5 for zSirt5, 200 mM NaCl, 5 mM Imidazole

Elution buffer: 50 mM Tris, pH 7.8 for hSirt3 and 8.5 for zSirt5, 200 mM NaCl, 250 mM Imidazole

In the second AC of hSirt3 purification, the protein was eluted using gel filtration buffer.

2.2.7.2. Tag cleavage

The His-tag of zSirt5 and the His-Trx-tag of hSirt3 were cleaved using TEV protease. The purified proteins after AC step were dialyzed in the buffer containing 30 mM HEPES, pH

6.5, 50 mM NaCl for zSirt5 and gel filtration buffer for hSirt3 at 4 °C. The ratio of protease : protein is 1:20 mg and incubated at 4 °C overnight.

2.2.7.3. Ion exchange chromatography (IEC)

IEC was performed using a 1 ml HiTrap SP cation exchange column (GE Healthcare, USA) that was equilibrated with buffer A (30 mM HEPES, pH 6.5). After tag cleavage, zSirt5 was applied on the column. The column was washed with 3 column volumes of buffer A followed by elution of the protein using a linear gradient against buffer B (30 mM HEPES, pH 6.5, 1 M NaCl). Protein fractions were analyzed using SDS-PAGE and then pooled.

2.2.7.4. Size exclusion chromatography (SEC)

Elution samples from the second AC of hSirt3 or from the IEC of zSirt5 purification were pooled and concentrated to 1 ml using an Amicon centrifugal concentrator (Millipore, USA) and injected to an equilibrated Superose-12 size exclusion column (GE Healthcare, USA) and eluted with gel filtration buffer containing 20 mM Tris, pH 7.8 for hSirt3 and 8.5 for zSirt5, 150 mM NaCl. Subsequently, the purity of the eluted fractions was assessed using SDS-PAGE before appropriate fractions were pooled and concentrated.

2.2.8. Fluorescence-based Flour-de-Lys assay

Deacetylase activity of sirtuins was tested using a commercial FdL assay kit (Enzo Life Sciences, USA) containing the p53-derived FdL-1 substrate peptide RHK(acK) with a C-terminally attached fluorophore. 50 µl of a reaction mixture consisting of 1.5 µg of sirtuin, 100 µM FdL-1, 2.5 mM NAD⁺ in the appropriate protein buffer was incubated at 37 °C for 30 minutes. Subsequently, a developer mixture containing 2 mM NAM and 10 mg/ml trypsin was added to the reaction mixture and incubated at room temperature for 45 minutes. Trypsin cleaves the coumarin tag from deacetylated FdL-1. Fluorescence was determined at an excitation wavelength of 360 nm and an emission wavelength of 460 nm using a FluoDiat70 microplate

reader (Photol Otsuka Electronics, Japan). A blank containing all the components of the assay except the enzyme was subtracted.

2.2.9. Enzyme-coupled continuous assay

The continuous assay was performed using a published protocol (Smith, et al., 2009). NAM, one of the products of the deacetylation reaction, is first converted to nicotinic acid and ammonia by nicotinamidase. The ammonia is then transferred to α -ketoglutarate via glutamate dehydrogenase yielding glutamate, under consumption of NADPH which is measured spectrophotometrically at 340 nm and thus proportional to sirtuin activity. 100 μ l of a reaction mixture contains 2 μ M of hSirt3 or 10 μ M of zSirt5, 500 μ M substrate peptide, 640 μ M NAD⁺, 1 mM DTT, 3.3 mM α -ketoglutarate, 2 μ M nicotinamidase, 2 units of bovine GDH and 0.2 mM NADPH in a buffer containing 20 mM Na-PO₄, pH 7.5. The reaction was performed at room temperature for 1 hour and continuously measured using a spectrophotometer (Cary 50, Agilent technologies, USA).

2.2.10. Mass spectrometry (MS)

50 μ l of a reaction mixture consisting of 10 μ M hSirt3 (in 20 mM Tris pH 7.8, 150 mM NaCl) or zSirt5 (in 20 mM Tris pH 8.5, 150 mM NaCl), 0.5 mM ACS2 peptide and 2.5 mM NAD⁺ in the presence of different compound concentrations in 2% (v/v) DMSO, or with 2% (v/v) DMSO as a control was incubated at 37 °C. The reaction was stopped after different time points by adding 0.25% (v/v) trifluoroacetic acid (TFA) followed by dilution to 1 μ M peptide in 0.1% (v/v) formic acid (FA). Subsequently, the solution was filtered to separate the substrate peptide from the reaction mixture using 10 kDa cutoff concentrators (Pall Life Sciences, USA). Finally, 5 μ l of each sample containing the filtered substrate peptide was subjected to nano-LC-MS/MS analysis as described before (Fischer, et al., 2012). Specific deacetylation activity was determined by linear fitting of the time-series experiments. The results were analyzed using Xcalibur (Thermo Scientific, USA).

2.2.11. Thermal denaturation shift assay

Protein thermal denaturation assay measures the thermal stability of a target protein and a subsequent increase in protein melting temperature due to the binding of a ligand to the protein based on the fluorescence change of the dye SYPRO Orange (Life Technologies, USA). 50 μ l of a sample mixture contains 0.1 mg/ml of protein, 1 μ l of 1:10 diluted SYPRO dye, 500 μ M NAD⁺, compounds or 2% (v/v) DMSO as a control followed by adding 15 μ l of mineral oil. The temperature was gradually increased from 25 °C to 73 °C using 2 °C intervals. The change in fluorescence was measured at an excitation wavelength of 465 nm and an emission wavelength of 580 nm using a FluoDiaT70 microplate reader (Photal Otsuka Electronics, Japan).

2.2.12. Binding analysis by microscale thermophoresis (MST)

Binding affinities were measured by microscale thermophoresis (Wienken, et al., 2010) with 1 μ M hSirt3 in 20 mM Tris pH 7.8, 150 mM NaCl in the presence or absence of different concentrations of compounds or ACS2 peptide. Protein and ligands were mixed at room temperature and transferred to capillaries for scanning before thermophoresis analysis at 25 °C using the NanoTemper Monolith NT.label-free instrument (NanoTemper Technologies, Germany) with the intrinsic protein fluorescence signal (excitation at 280 nm, emission at 360 nm). The excitation UV-LED power was set to 25% and IR-laser power to 20; 40 and 80%. The K_d values were determined through non-linear fitting (1-site equation) of the measured thermophoresis values using Prism (Graphpad Software, CA, USA). Each experiment was repeated at least twice.

2.2.13. Crystallization and structure determination

Crystallization trials were performed using a Phoenix robot (Art Robbins, USA) for initial screening with a mixture of 0.15 μ l of protein and 0.15 μ l of reservoir solution on a 96 well sitting drop plate (Corning, Intelli, Greiner etc. plates) and incubated at 20 °C in a Formulatrix imager (Formulatrix Inc., USA). The selected conditions were further optimized

manually by mixing 1 μ l of protein and 1 μ l of reservoir solutions on a 24 well sitting drop corning plates and incubation at 20 °C.

The X-ray diffraction data were collected at 100 K with an MX-225 CCD detector (Rayonix, Evanston, IL, USA) at beam line MX14.1 of the BESSY II electron storage ring (Berlin, Germany) (Mueller, et al., 2012). The wavelength was 0.92 Å allowing to observe the anomalous diffraction of the Br atom. Diffraction data were processed using XDS (Kabsch, 2010). Crystal structures were solved by Patterson searches with the program MolRep (Vagin and Isupov, 2001) using chain A of the complex hSirt3/FdL-1/PCT (PDB ID 4HD8) (Gertz, et al., 2012) as a search model for hSirt3 structures and the complex hSirt5/suramin (PDB ID 2NYR) (Schuetz, et al., 2007) as a search model for zSirt5 structures. Structure refinement was performed using Refmac (Murshudov, et al., 1997), and manual rebuilding was done in Coot (Emsley and Cowtan, 2004). Parameter files for 4'-bromo-resveratrol, polydatin and SRT1720 were generated using ProDrg (Schuttelkopf and van Aalten, 2004). The quality of the refined structures was evaluated using Coot and MolProbity (Chen, et al., 2010). The structure figures were prepared using Pymol (The PyMOL Molecular Graphics System, Schrödinger, LLC).

3. Results

3.1. Sirt3 studies

3.1.1. Sirt3 purification

hSirt3 purification was first performed using the published protocol with the vector pET21b coding for a His-tag (Jin, et al., 2009) but the solubility and purity of the expressed protein were very low. pVFT3S, a vector coding for a His-Trx-tag, was then used to improve protein solubility. The hSirt3 purification protocol in this study was illustrated by a diagram in figure 3.1A. After the first AC step, the highly expressed proteins with the size of ~60 and ~45 kDa were collected. The hSirt3 construct (118-399) is ~31 kDa and the His-Trx-tag is ~14 kDa indicating that the second band (~45 kDa) is the target protein. MS analysis was used to identify the protein shown in the first band (~60 kDa) and found that it was an *E. coli* chaperon. After TEV protease incubation and the second AC, the His-Trx-tag was removed but the *E. coli* chaperon had not yet separated. After SEC, the last step of purification, the purified hSirt3 was obtained in the fractions B3 – B10 shown in the second peak of SEC profile with the purity \geq 95%, the *E. coli* chaperon was eluted in the fractions A4 – A8 shown in the first peak (Figure 3.1B). The yield of purification was 8-10 mg of the purified protein per 12 liters of the expressed media.

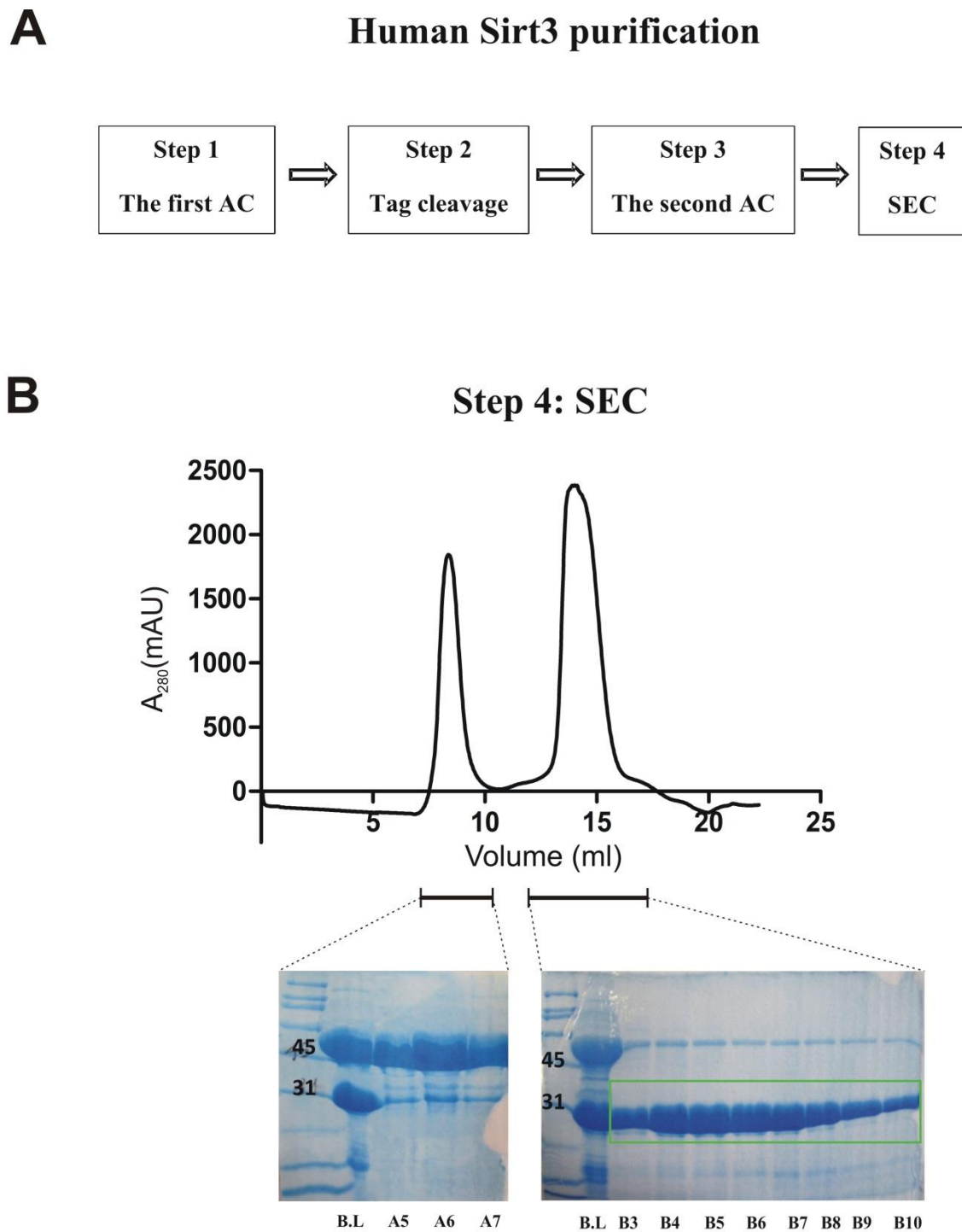


Figure 3.1. Human Sirt3 purification. (A) Four steps of hSirt3 purification. (B) Step 4: SEC, hSirt3 and *E. Coli* chaperon were separated. Fractions B3-B10 (green box) were pooled for further studies. B.L, before loading.

3.1.2. Resveratrol and its related compounds

3.1.2.1. Resveratrol and its related compounds are hSirt3 inhibitors

The FdL assay was performed to investigate the effects of resveratrol (RESV) and its related compounds including piceatannol (PCT), polydatin (PD) and 4'-bromo-resveratrol (brRESV) on hSirt3. The protein is weakly inhibited by RESV, PCT and PD (Figure 3.2A). brRESV showed a much more potent effect and inhibited hSirt3 activity almost completely at 0.2 mM compound concentration (Figure 3.2A). In comparison to human Sirt1 (hSirt1), the same inhibition effect of 0.2 mM brRESV but ~17-fold activation by 0.2 mM RESV was observed (Figure 3.2B).

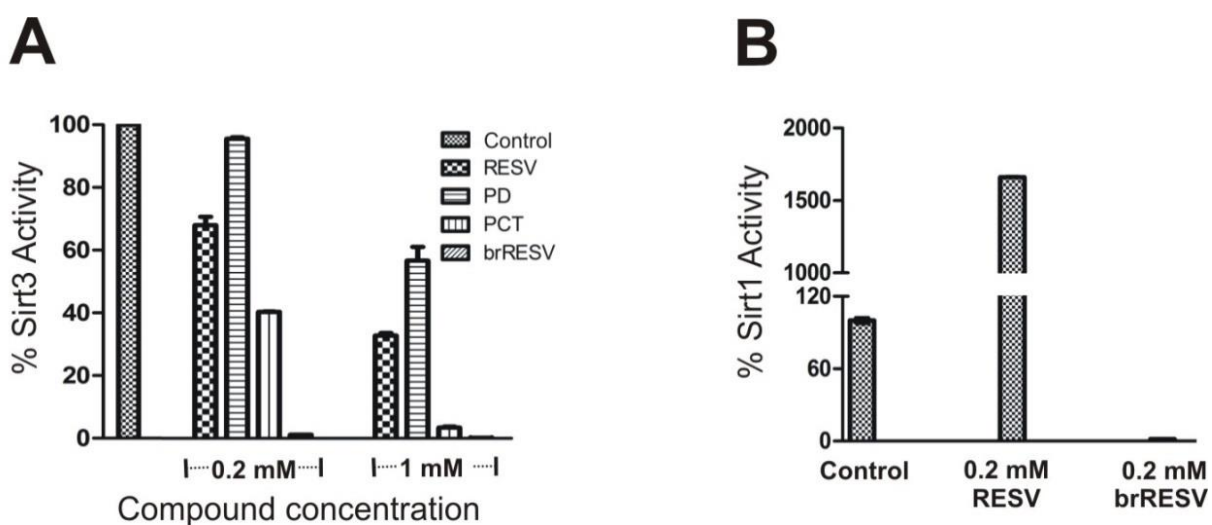


Figure 3.2. FdL assay. (A) Inhibition of hSirt3 activity by resveratrol-related compounds at 0.2 mM and 1 mM compound concentration. (B) 0.2 mM RESV activates whereas brRESV inhibits hSirt1. Activities were normalized to the control in the absence of compound. Error bars represent standard errors of two independent measurements.

The FdL substrate peptide is attached with a fluorophore that can interact with small molecules, potentially leading to artificial effects on sirtuin activity (Borra, et al., 2004; Gertz, et al., 2012; Pacholec, et al., 2010). Therefore, a MS-based assay and ACS2 peptide, the acetylated

peptide derived from a physiological Sirt3 substrate, were used to confirm and quantify hSirt3 inhibition by brRESV. A dose-response experiment at 500 μM ACS2 peptide yielded an IC_{50} value of $143.0 \pm 3.6 \mu\text{M}$ (Figure 3.3). This result confirms that inhibition by brRESV applies to non-modified peptides.

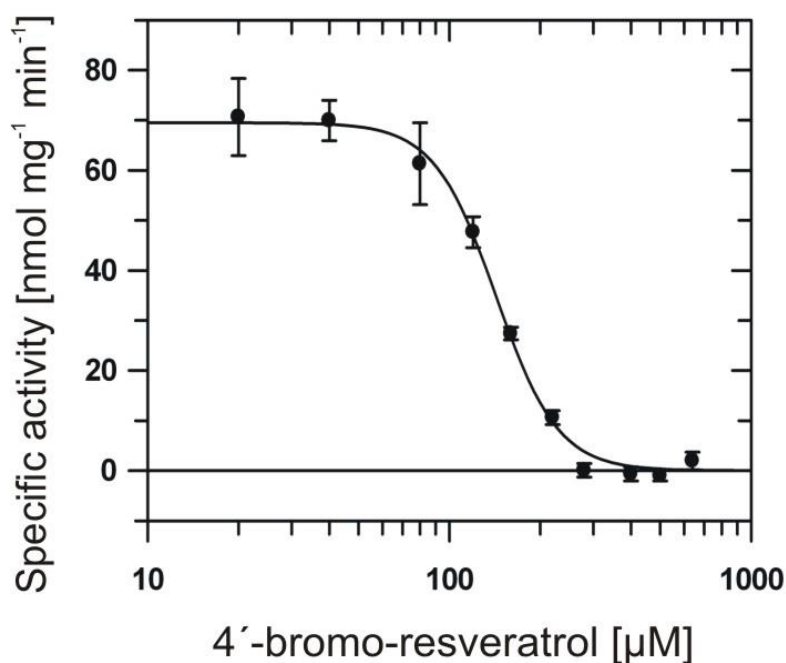


Figure 3.3. IC_{50} determination of brRESV on hSirt3 against 500 μM ACS2 peptide using MS. Error bars represent standard errors of linear fits to time series experiments.

3.1.2.2. Crystallization trials of hSirt3 in complex with resveratrol related compounds

To determine the inhibition mechanisms of resveratrol related compounds on hSirt3, different complexes of the protein with FdL-1 or ACS2 peptide and compounds in the presence or absence of NAD^+ were crystallized (Table 3.1) and crystals were obtained in different morphologies. The complex hSirt3/FdL-1/PCT, hSirt3/FdL-1/PD and hSirt3/FdL-1/brRESV form rod-shaped crystals, the crystals of the complex hSirt3/ACS2 and hSirt3/ACS2/ NAD^+ / brRESV have plate shapes and crystals of the complex hSirt3/ACS2/brRESV are in diamond shapes (Figure 3.4). Especially, Sirt3 crystals in the presence of ACS2 peptide and brRESV were

obtained in 30 different conditions of the screening core suite JCSG I – IV with the same morphology (Figure 3.5).

Table 3.1. Crystallization trials of hSirt3 complexes

Crystallization trials	Number of crystal conditions
hS3 + FdL-1 + PCT/PD/brRESV	1
hS3 + NAD ⁺ + brRESV	0
hS3 + ACS2 + brRESV	30
hS3 + ACS2 + NAD ⁺ + brRESV	1

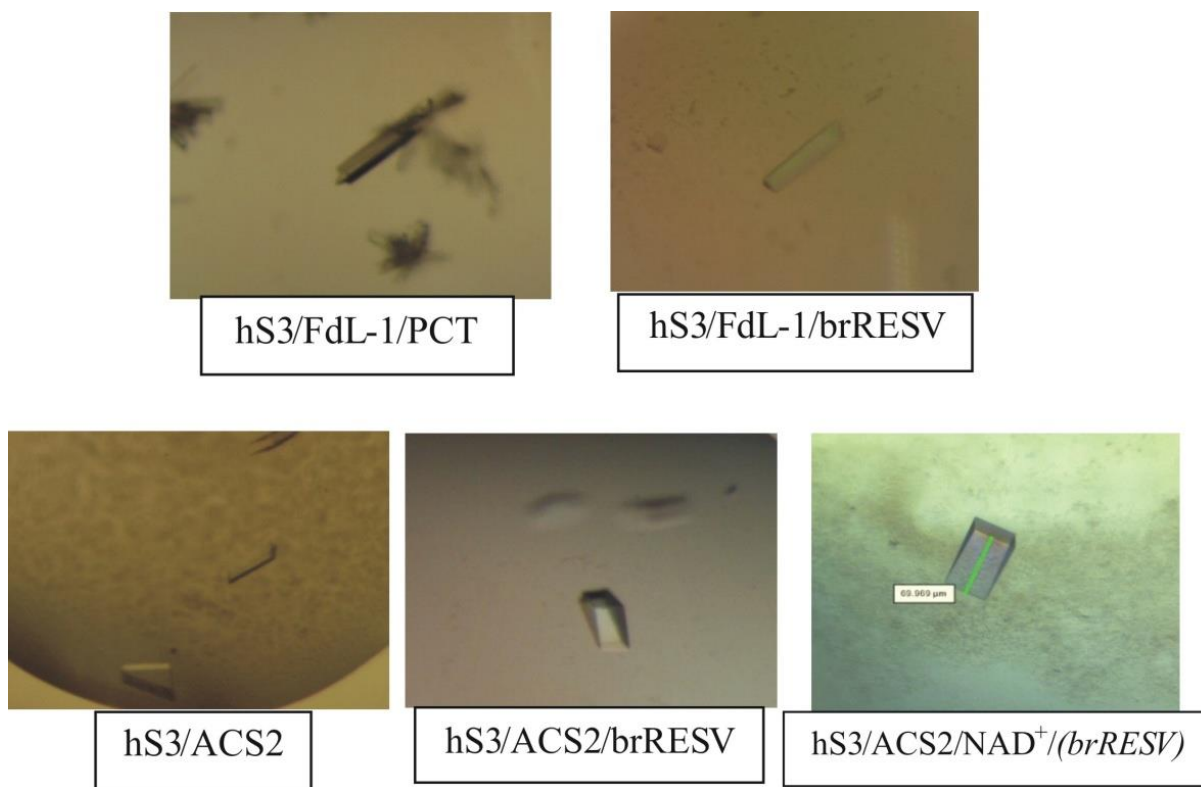


Figure 3.4. Crystals of different hSirt3 complexes with FdL-1 or ACS2 peptide and resveratrol related compounds in the presence or absence of NAD⁺. The compound labeled as italic was not found in the structures.



Figure 3.5. hSirt3 crystals in the presence of ACS2 peptide and brRESV were obtained in 30 different conditions with the same morphology. Three conditions were zoomed in as representative.

3.1.2.3. Crystal structures and inhibition mechanisms of hSirt3 in complex with resveratrol related compounds

3.1.2.3.1. hSirt3 in complex with FdL-1 peptide and piceatannol/polydatin

In the crystal structures of the complex hSirt3/FdL-1/PCT and hSirt3/FdL-1/PD, the compounds locate next to the coumarin ring of FdL-1 peptide (Figure 3.6A). The crystal contact was formed by the interaction between two fluorophores of FdL-1 peptide molecules that belong to two symmetry-related monomers (Figure 3.6B,C). PCT and PD bind to the protein at the same site and directly interact with FdL-1 peptide to induce non-productive substrate binding, thus inhibits hSirt3 activity (Gertz, et al., 2012).

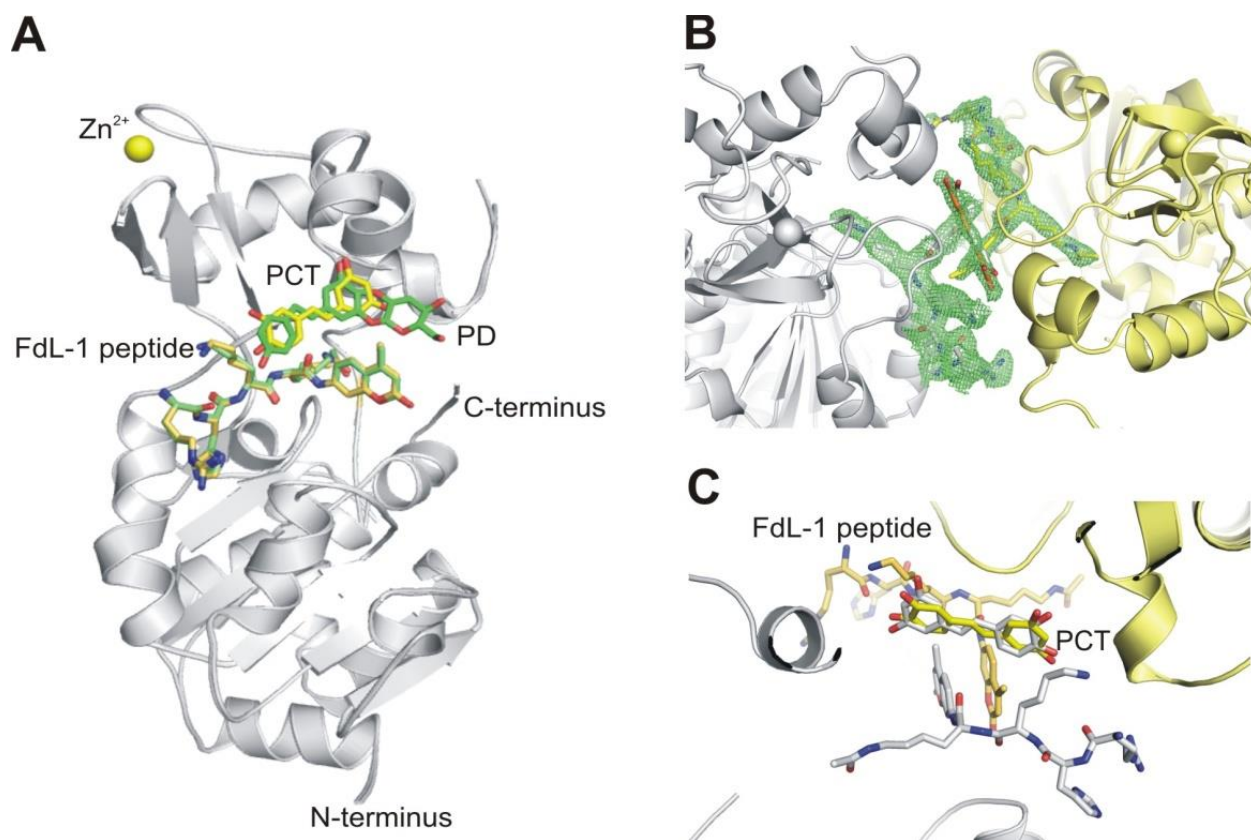


Figure 3.6. Crystal structure of hSirt3 in complex with PCT/PD and FdL-1 peptide. (A) Overall structures of the complex hSirt3/FdL-1/PCT and hSirt3/FdL-1/PD. PCT is shown in stick-yellow, PD in stick-green. FdL-1 peptides of two complexes are in stick and in the same color as the corresponding compound. (B, C) The interface with the neighboring symmetry-related monomer: Two FdL-1 peptides form π -stacking interactions and two PCT/PD molecules overlay each other. Omit $F_o - F_c$ difference density is contoured at 3.0σ . The symmetry-related monomer is in grey.

3.1.2.3.2. hSirt3 in complex with FdL-1 peptide and 4'-bromo-resveratrol

In the hSirt3/FdL-1/brRESV complex structure, the compound was found in the active site (Figure 3.7) and different from the PCT/PD binding site.

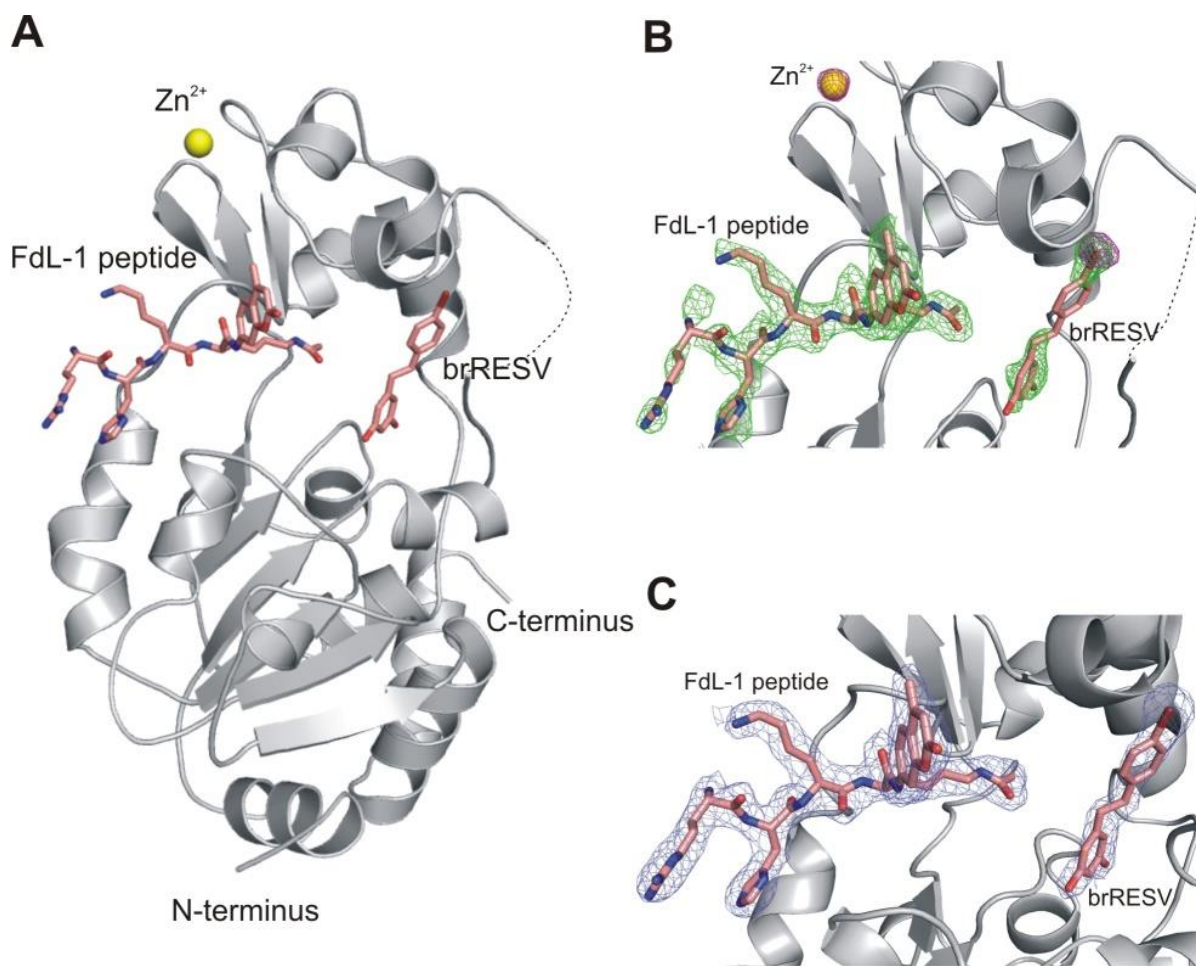


Figure 3.7. Crystal structure of hSirt3 in complex with brRESV and FdL-1 peptide. (A) Overall structure of hSirt3/FdL-1/brRESV complex. The dashed line indicates a loop not defined by electron density. (B) FdL-1 peptide and brRESV ligands of hSirt3, overlaid with omit F_0-F_c difference density (2.5σ ; green) and anomalous density (5σ ; magenta) showing the positions of Br and Zn^{2+} . (C) $2F_0-F_c$ electron density (1σ ; blue) of FdL-1 peptide and brRESV in hSirt3/FdL-1/brRESV complex.

A closer look at the compound binding site (Figure 3.8) shows that the A-ring hydroxyl groups of brRESV form hydrogen bonds with Asn229 and Asp231 of hSirt3. Furthermore, residues Ile230, Leu199, and Ile154 form a hydrophobic patch for A-ring binding, and Phe157, Leu195, and Phe180 a hydrophobic cleft for accommodating the B-ring. This cleft extends in a hydrophobic pocket (formed by Ile179, Leu173, and Tyr171) for binding the bromine atom, and Arg158 and Pro176 form a lid shielding this pocket from solvent.

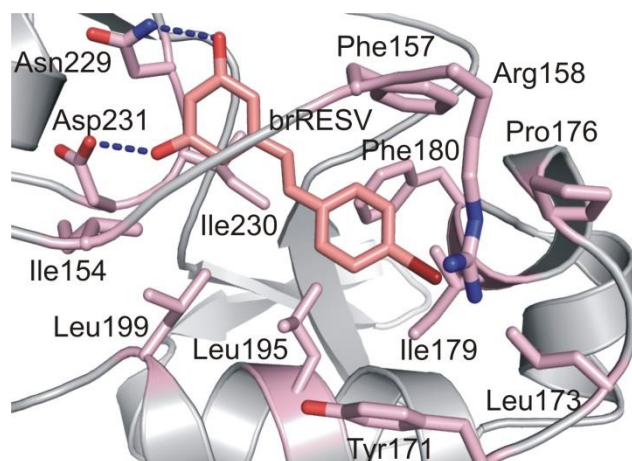


Figure 3.8. Closer view on the brRESV binding site showing interacting residues. Hydrogen bonds are indicated by dashed lines.

Superposition of the crystal structure of the complex hSirt3/FdL-1/brRESV and Sir2Tm in complex with p53 peptide and NAD⁺ (Hoff, et al., 2006) reveals that brRESV occupies part of the NAD⁺ binding pocket (Figure 3.9), thus prevents the C-pocket insertion of the NAD⁺ nicotinamide moiety necessary for catalysis.

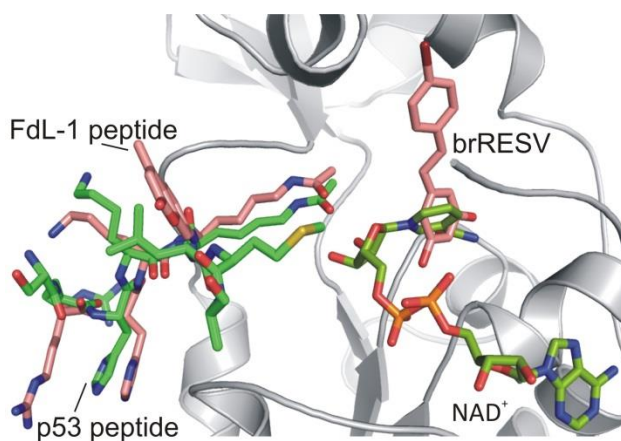


Figure 3.9. Superposition of the hSirt3/FdL-1/brRESV structure with a Sir2Tm/p53/NAD⁺ complex (PDB ID 2H4F) (Hoff, et al., 2006). FdL-1 peptide and brRESV are in pink, p53 peptide and NAD⁺ are in green. The protein part of the Sir2Tm/p53/NAD⁺ complex is omitted for clarity.

The overall hSirt3 and FdL1-peptide conformations in the superposition of the brRESV complex with hSirt3 bound to FdL-1 and other resveratrol-related compounds, PCT/PD, are identical (Figure 3.10). However, FdL-1 peptide conformations are different, in particular the fluorophore orientation. PCT/PD interact extensively with the FdL-1 fluorophore to induce non-productive peptide binding (Gertz, et al., 2012) whereas brRESV does not directly contact this substrate peptide but blocks productive NAD^+ binding.

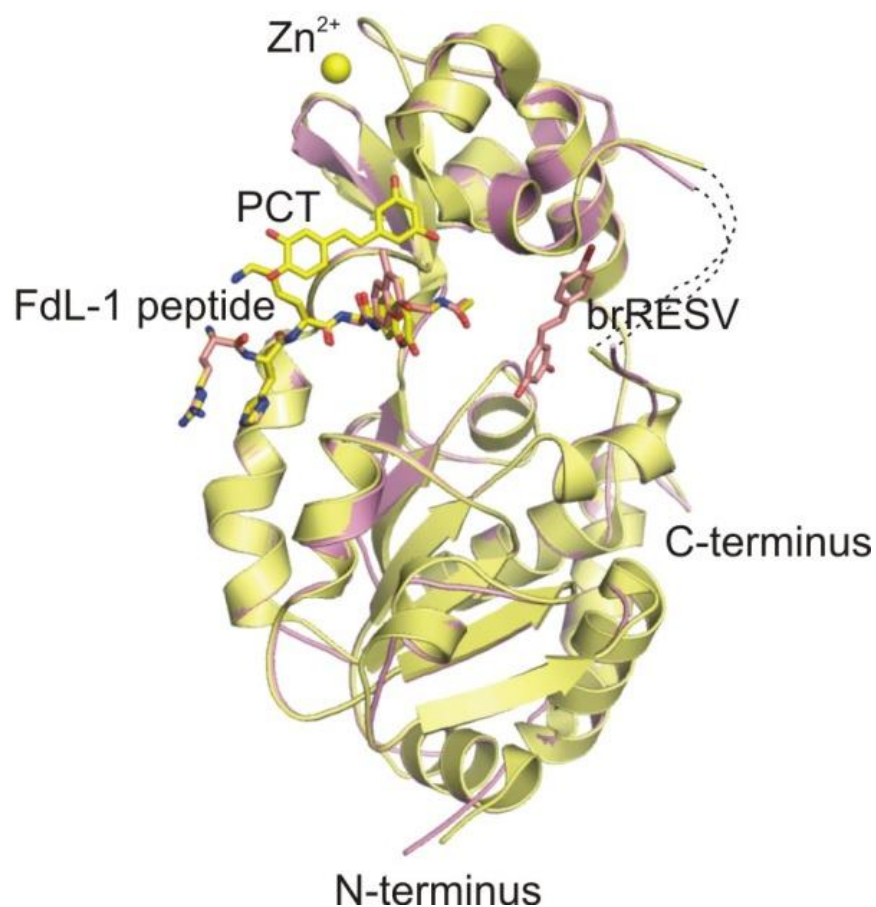


Figure 3.10. Superposition of the hSirt3/FdL-1/brRESV with the hSirt3/FdL-1/PCT complex. PCT is shown in stick-yellow, brRESV in stick-pink. FdL-1 peptides of two complexes are in stick and in the same color as the corresponding compound.

To test for competition between brRESV and FdL-1 peptide, IC_{50} values for brRESV inhibition of hSirt3 were determined at three different concentrations of FdL-1 peptide (50, 100,

and 200 μM). The IC_{50} value obtained were ~ 100 μM for all three peptide concentrations (Figure 3.11), indicating that the inhibitor brRESV does not compete against FdL-1.

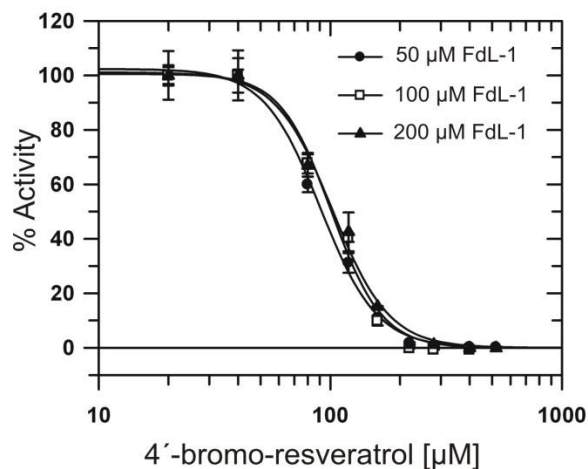


Figure 3.11. IC_{50} determination for brRESV inhibition of hSirt3 at 50, 100, and 200 μM FdL-1 substrate peptide.

We also investigated the competition between brRESV and NAD^+ for hSirt3 binding. The binding affinity of brRESV to the apo protein was 7.6 ± 0.9 μM , and the K_d increased to higher than 50 μM in the presence of 2 mM NAD^+ (Figure 3.12). The results reveal that brRESV competes with NAD^+ for binding to hSirt3, supporting the conclusion that the internal brRESV binding site is the one relevant for inhibition of hSirt3 activity.

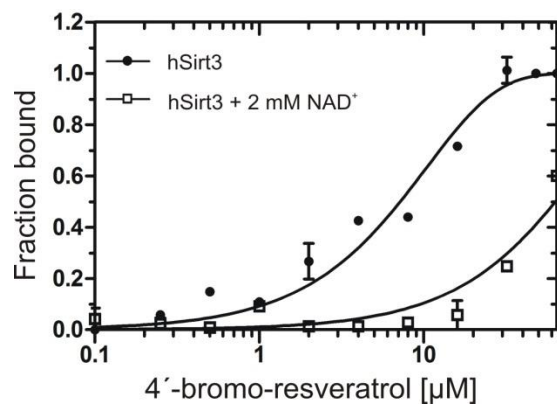


Figure 3.12. Binding affinity of brRESV to hSirt3 in the presence or absence of 2 mM NAD^+ .

3.1.2.3.3. hSirt3 in complex with ACS2 peptide and 4'-bromo-resveratrol

In the complex structure hSirt3/ACS2/brRESV, the compound molecule was found at the bottom of the Rossmann-fold domain, interacting with Arg139, Met331, and Arg335 (Figure 3.13). In this exposed position, the compound interacts only through its A-ring with this shallow hSirt3 pocket, and the bromo-containing aromatic ring points towards the symmetry-related monomer in the crystal lattice.

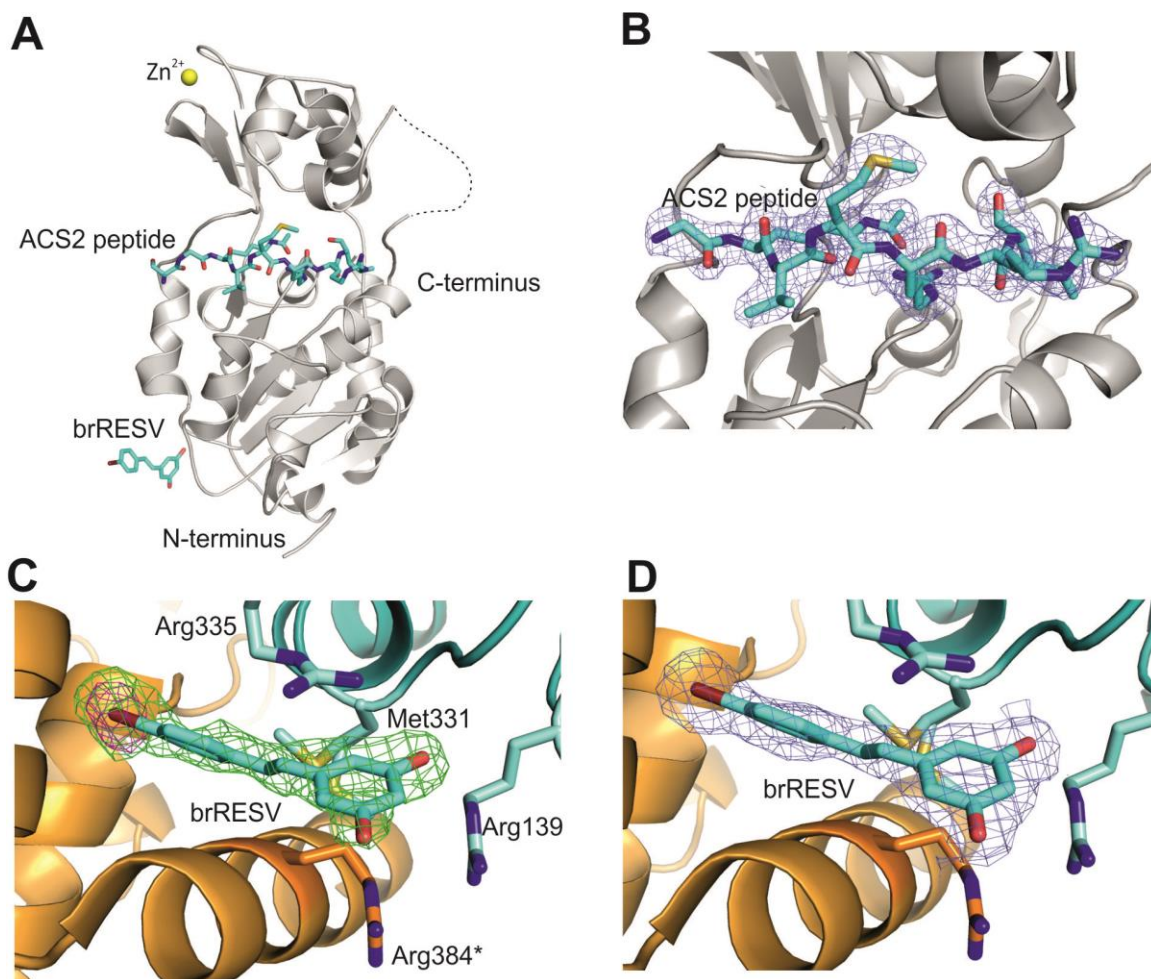


Figure 3.13. Crystal structure of hSirt3 in complex with brRESV and ACS2 substrate peptide. (A) Overall structure of hSirt3/ACS2/brRESV complex. A missing loop is indicated by a dashed line. (B) 2F_o-F_c electron density (1 σ; blue) of ACS2 peptide in hSirt3/ACS2/brRESV complex. (C) brRESV ligand of hSirt3, overlaid with omit F_o-F_c difference density (2.5 σ; green) and anomalous density (5 σ; magenta) showing the position of Br and surrounding residues important for compound binding. Residues from the symmetry-related monomer are labeled with a star. (D) 2F_o-F_c electron density (1 σ; blue) of brRESV in hSirt3/ACS2/brRESV complex.

The superposition of the hSirt3/brRESV complexes with FdL-1 and ACS2 peptide, respectively, reveals that the inhibitor cannot bind at the catalytic pocket when the ACS2 peptide is bound, since it would clash with the C-terminal part of this substrate peptide (Figure 3.14).

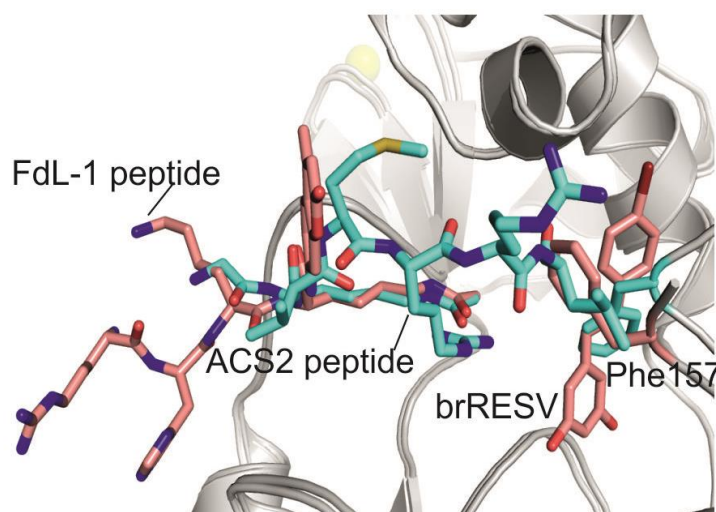


Figure 3.14. Superposition of the hSirt3/ACS2/brRESV structure with the hSirt3/FdL-1/brRESV complex. FdL-1 peptide and brRESV are in pink, ACS2 peptide is in cyan. Phe157 of the hSirt3/ACS2/brRESV and hSirt3/FdL-1/brRESV complex are shown in cyan and pink, respectively.

brRESV in the complex structure with hSirt3/ACS2-peptide does not show many interactions with hSirt3, rendering it a less likely inhibition site. Figure 3.15 illustrates the hydrogen bonds between brRESV with Arg139, Met331 (backbone), and Arg335 and additionally with Arg384 of the symmetry-related monomer.

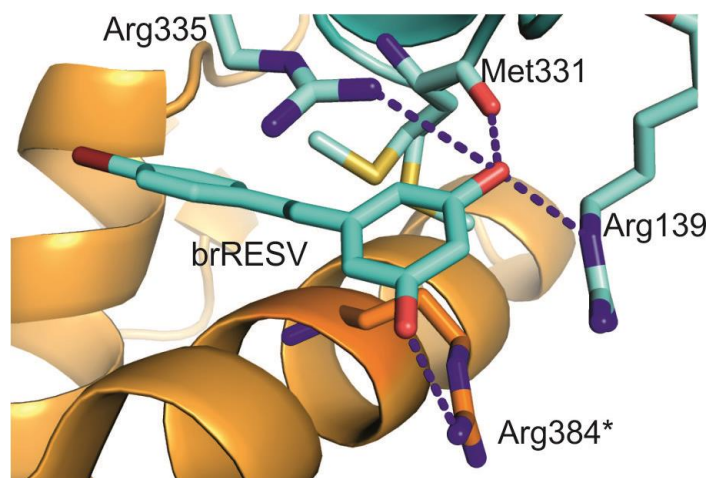


Figure 3. 15. Closer view on the brRESV binding site in the hSirt3/ACS2/brRESV complex showing interacting residues. Hydrogen bonds are indicated by dashed lines and residues of the next symmetry-related monomer are labeled with a star.

To test whether the surface site occupied by brRESV in its hSirt3/ACS2 complex is relevant for inhibition, the role of the interacting residues R139, M331, R335, and R384 were tested by site-directed mutagenesis to alanine. Microscale thermophoresis (MST) results indicate that the hSirt3-R335A variant has a slightly reduced binding affinity for the compound compared to wildtype hSirt3 (Figure 3.16A), but the change was not statistically significant. The hSirt3 variants R384A, R139A, and M331A showed no change in the affinity for the compound. Moreover, we performed activity assays with 500 μM ACS2 as peptide substrate and in presence of brRESV (at its IC_{50} concentration, 140 μM) to examine the effects on the activity of the mutant proteins. The screening indicated that the activity of hSirt3 R335A is slightly higher than for the other mutants and the wildtype protein (data not shown). The IC_{50} value of brRESV on the R335A variant activity was then determined. Figure 3.16B shows only a small shift for the brRESV inhibition curves between wildtype protein and the R335A variant, resulting in IC_{50} values of 143.0 ± 3.6 and 179.2 ± 12.3 μM , respectively. Therefore, the position of brRESV in the complex structure hSirt3/ACS2/brRESV seems not to be primarily responsible for the inhibitory effect of the compound on hSirt3.

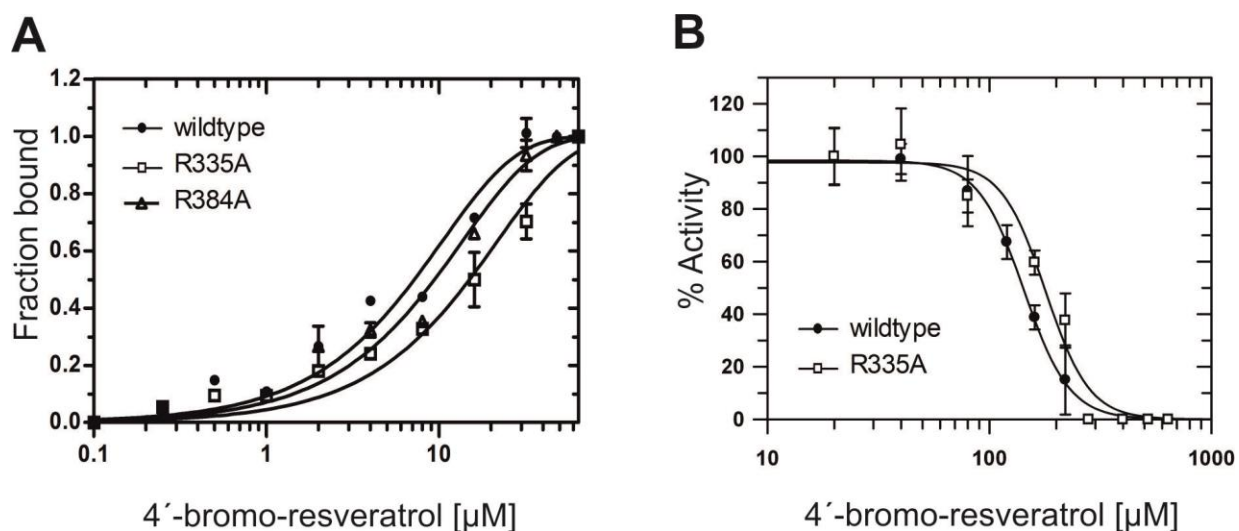


Figure 3.16. (A) Affinity measurements for binding of brRESV to hSirt3 wildtype as well as R335A and R384A variants. Error bars represent standard errors of two independent measurements. (B) IC_{50} determination of brRESV on wildtype hSirt3 or the R335A variant against 500 μM ACS2 peptide using MS. Error bars represent standard errors of linear fits to time series experiments.

To test for brRESV competition with ACS2 peptide, MS assays were performed to determine K_m and V_{\max} values for the peptide at different compound concentrations. The result shows that the higher the brRESV concentration, the more the K_m for substrate peptide increases, or affinity for substrate decreases, while the V_{\max} is not altered, indicating competitive inhibition (Figure 3.17).

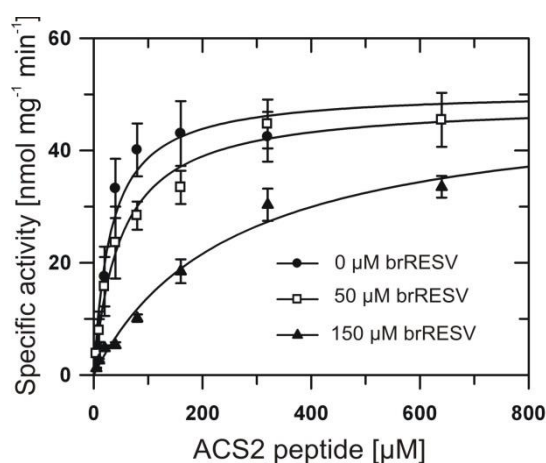


Figure 3.17. brRESV inhibition of hSirt3 with ACS2 peptide as a substrate. brRESV concentrations of 0, 50, and 150 μM resulted in K_m values for substrate peptide of 31.3 ± 9.0 , 48.6 ± 7.5 , and 253.3 ± 52.9 μM , respectively, while the V_{max} is roughly constant at ~ 50 $\text{nmol mg}^{-1} \text{min}^{-1}$. Error bars represent standard errors of linear fits to time series experiments.

This competition was confirmed through binding data from MST measurements. ACS2 peptide bound to apo hSirt3 with a K_d value of 64.4 ± 9.1 μM . In presence of 50 μM brRESV, the K_d value increased to more than 200 μM (Figure 3.18A). Consistently, binding affinity of brRESV to the apo protein was 7.6 ± 0.9 μM , and the K_d increased to higher than 37 μM in the presence of 500 μM ACS2 peptide (Figure 3.18B). Thus, brRESV inhibits hSirt3 through binding competition with ACS2 peptide substrate.

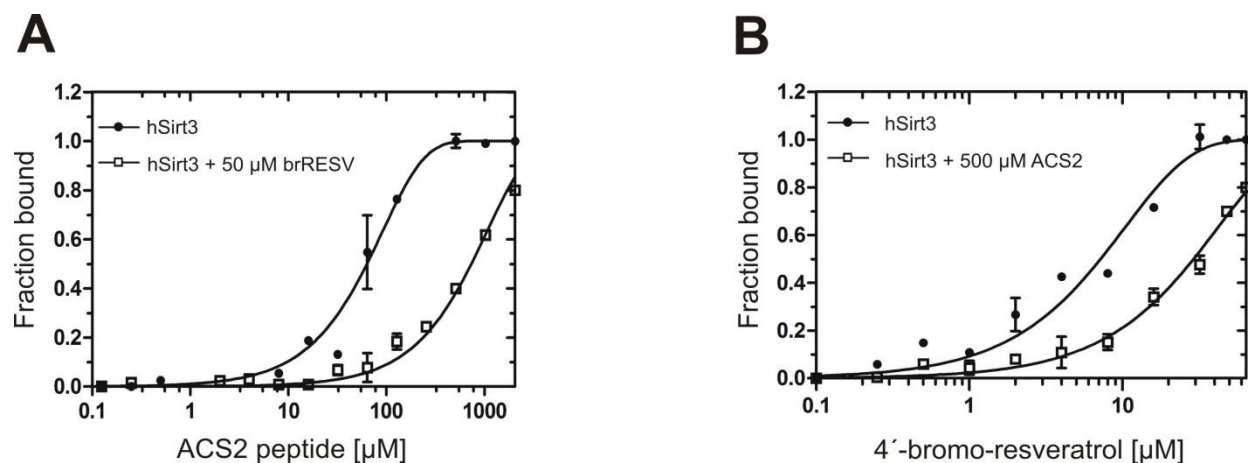


Figure 3.18. (A) Binding affinity of ACS2 peptide to hSirt3 in the presence or absence of 50 μM brRESV. **(B)** Binding affinity of brRESV to hSirt3 in the presence or absence of 500 μM ACS2 peptide. Error bars represent standard errors of two independent measurements.

3.1.3. Resveratrol unrelated compounds

3.1.3.1. SRT1720

The effect of SRT1720 on hSirt3 was investigated using FdL-1 and ACS2 peptide. The FdL assay indicates that 20 μM SRT1720 inhibits 92% hSirt3 activity but activates hSirt1 activity to 1.6 fold and has no effect on human Sirt2 (hSirt2) (Figure 3.19).

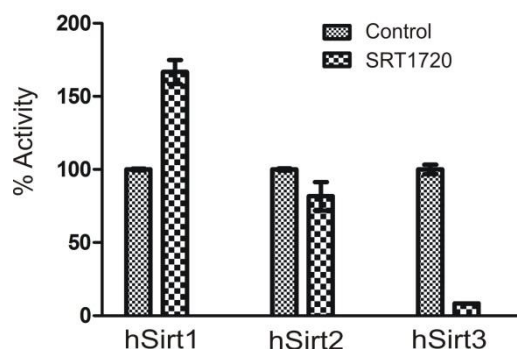


Figure 3.19. Effects of 20 μM SRT1720 on hSirt1, hSirt2 and hSirt3 in the FdL assay. Activities were normalized to the control in the absence of compounds. Error bars represent standard errors of two independent measurements.

MS was used to examine the effect of the compound on ACS2, the fluorophore-free peptide. The IC_{50} value of SRT1720 on hSirt3 is 11 ± 1 μM for ACS2 peptide (Figure 3.20).

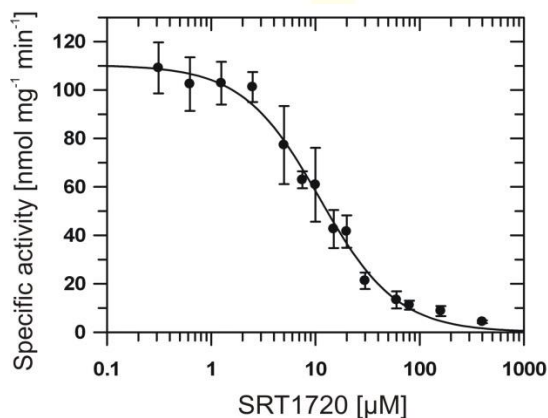


Figure 3.20. IC_{50} determination of SRT1720 on hSirt3 against 500 μM ACS2 peptide using MS. Error bars represent standard errors of linear fits to time series experiments.

Since SRT1720 was reported as a noncompetitive inhibitor of hSirt3 against NAD⁺ (Jin, et al., 2009), hSirt3 in complex with the compound was crystallized in the presence or absence of NAD⁺. Crystals were observed in many conditions with different morphologies (Figure 3.21). Crystals of the complex hSirt3/NAD⁺ were further soaked with SRT1720 at different time points.

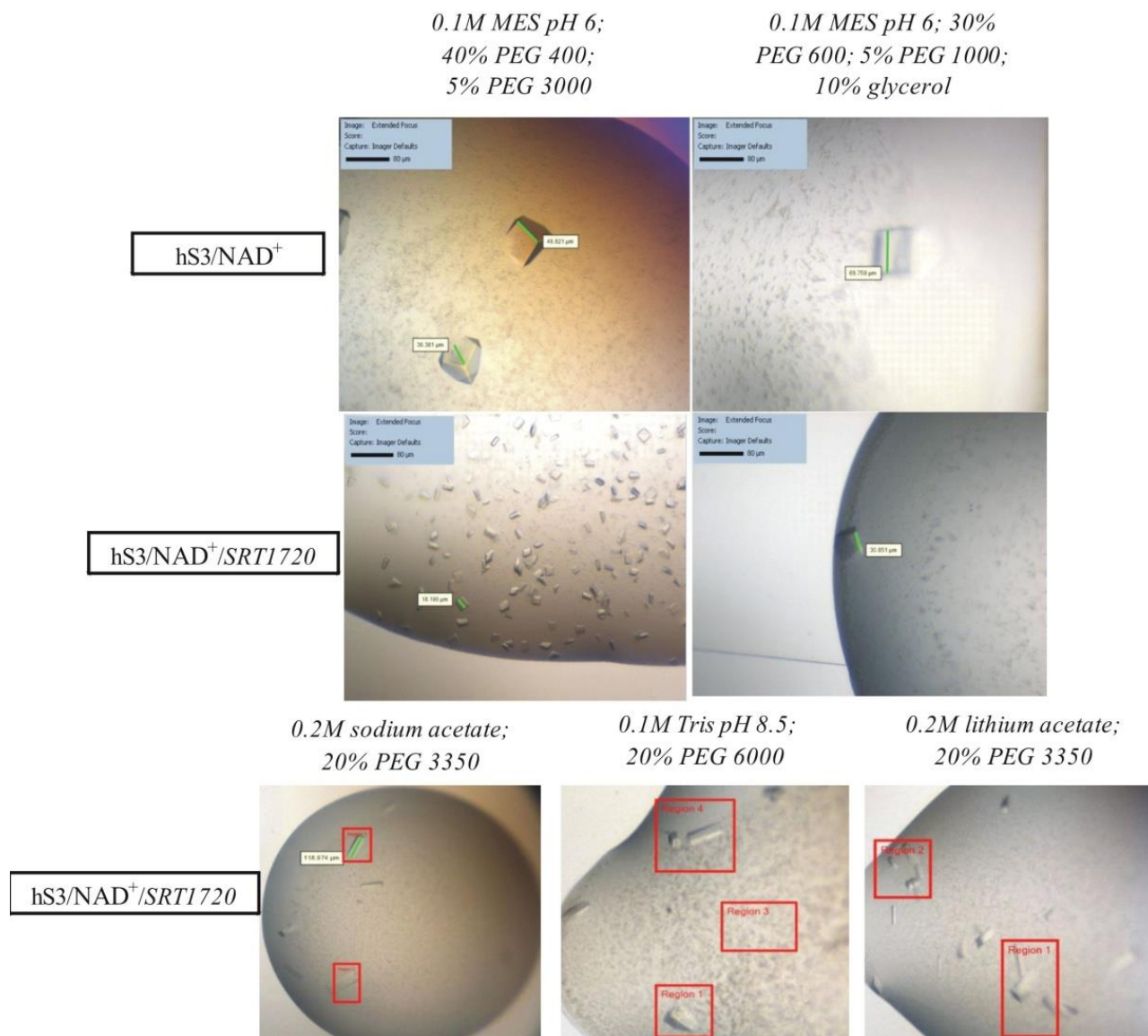


Figure 3.21. Crystals of hSirt3 in complex with NAD⁺ in the presence or absence of SRT1720. Since the compound was not found in the structures, it was labeled as italic.

In both cases, hSirt3/NAD⁺ soaking or co-crystallizing with SRT1720, the structures only showed the ADPR moiety of NAD⁺ and no density for the compound (Figure 3.22). This might indicate that NAD⁺ was hydrolyzed during crystallization that was mentioned in the Introduction section.

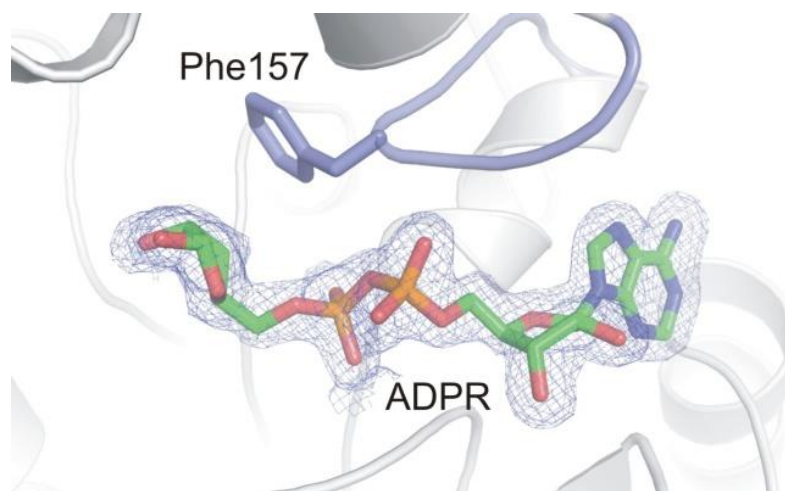


Figure 3.22. Active site of the hSirt3/ADPR complex. $2F_o-F_c$ electron density of ADPR is contoured at 1.0σ . The cosubstrate binding loop is shown in purple.

To prevent the hydrolysis of NAD⁺ during crystallization, we used inert carba-NAD⁺ (Szczepankiewicz, et al., 2012). This NAD⁺ analog is stable in crystallization conditions due to its ability to prevent the NAM displacement reactions. The replacement indeed resulted the crystal structure of a Sirt3/carba-NAD⁺/SRT1720 complex. The quinoxaline ring of SRT1720 interacts with NAM moiety of carba-NAD⁺ and Phe157 of the cosubstrate binding loop through π -stacking interaction (Figure 3.23). This observation explains the absence of the compound in Sirt3/NAD⁺ complex structure when using unstable NAD⁺ and indicates the role of NAD⁺, in particular NAM moiety, for the compound binding. Superposition of the complex hSirt3/carba-NAD⁺/SRT1720 with hSirt3/ACS2/carba-NAD⁺ (PDB ID 4FVT) (Szczepankiewicz, et al., 2012) reveals that the piperazine group and part of the connected imidazothiazole system of SRT1720 occupy the binding region of acetyl lysine (Figure 3.24); thus confirm the inhibition mechanism competitive with substrate peptide (Jin, et al., 2009). Due to the compound binding, the

cosubstrate binding loop was shifted and Phe157 was re-orientated whereas the carba-NAD⁺ conformation was almost unchanged (Figure 3.24).

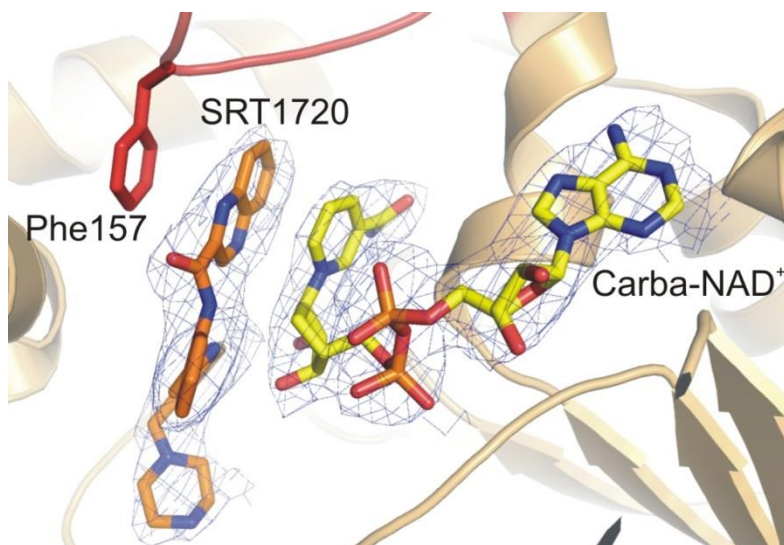


Figure 3.23. Active site of the hSirt3/carba-NAD⁺/SRT1720 complex. $2F_o-F_c$ electron density of carba-NAD⁺ and SRT1720 is contoured at 1.0σ . The cosubstrate binding loop is shown in red, SRT1720 in orange and carba-NAD⁺ in yellow.

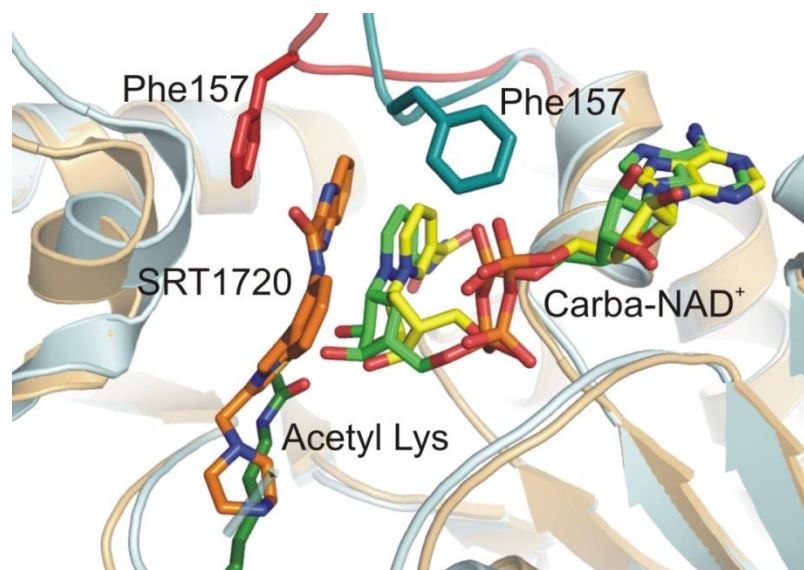


Figure 3.24. Superposition of the complex hSirt3/carba-NAD⁺/SRT1720 with hSirt3/ACS2/carba-NAD⁺ (green, PDB ID 4FVT) (Szczepankiewicz, et al., 2012).

To confirm the critical role of the NAM moiety of NAD^+ for the compound binding, the stability of hSirt3 towards thermal denaturation was measured using thermal shift assay (TSA) (Figure 3.25). In the presence of 50 μM SRT1720, the half-point of the hSirt3 melting transition (T_m) value increased from less than 324 K of the DMSO control to more than 326 K. The T_m value increased to more than 327 K when adding 500 μM NAD^+ in the presence of 50 μM SRT1720. The measurements imply that SRT1720 supports the hSirt3 stabilization and NAD^+ supports the compound binding.

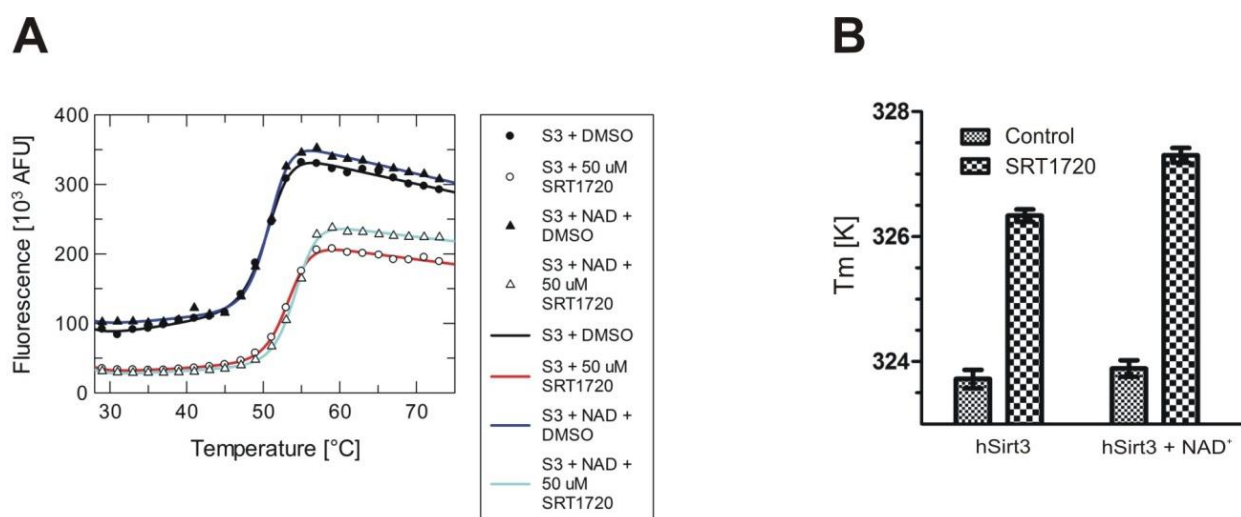


Figure 3.25. hSirt3 stability TSA test in presence or absence of 50 μM SRT1720 and/or 500 μM NAD^+ . (A) Transition curves. The lines shown are nonlinear fits for a two state transition. (B) Melting temperatures. Error bars represent standard errors of nonlinear fits.

The stability measurements of SRT1720 to hSirt3 are consistent with the binding data using microscale thermophoresis (MST) (Figure 3.26). The K_d value for the affinity of SRT1720 to hSirt3 is $7.5 \pm 1.3 \mu\text{M}$. In the presence of 500 μM NAD^+ , the K_d value decreased to $2.6 \pm 0.3 \mu\text{M}$. When adding 500 μM ADPR instead, the K_d value is $7.8 \pm 1.3 \mu\text{M}$ indicating that ADPR does not support the compound binding but NAD^+ with additional NAM moiety in comparison to ADPR provides a positive effect. The results of binding and stability measurements strengthen the conclusion of the contribution of NAD^+ , in particular its NAM moiety, in compound binding.

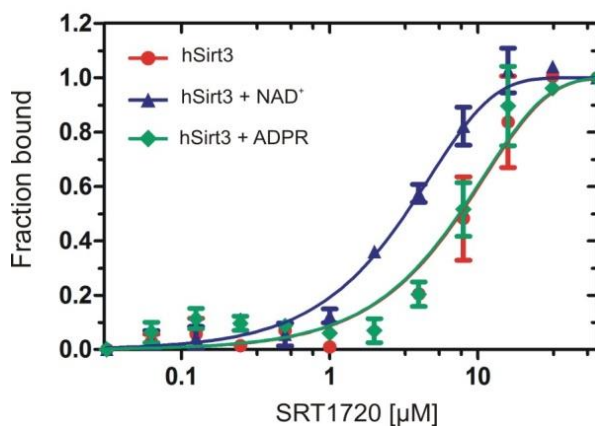


Figure 3.26. Binding affinity of SRT1720 to hSirt3 in the presence or absence of 500 μM NAD^+ or ADPR. Error bars represent standard errors of two independent measurements.

3.1.3.2. Ex-527

Ex527 was reported as a potent inhibitor of hSirt1 with the IC_{50} value of approximately 0.1 μM (Solomon, et al., 2006). It has much lower potency against hSirt3 with IC_{50} about 50 μM . In this study, hSirt3 was used as a model to understand the inhibition of this compound on sirtuins. In the crystal structure of the complex hSirt3/ NAD^+ /Ex-527, Ex-527 binds to hSirt3 at C pocket (Figure 3.27). When using ADPR instead, the compound can also bind to hSirt3 at the same site (Gertz, et al., 2013) indicating that the compound binds to the protein when the cosubstrate binding pocket is occupied either by NAD^+ or the product 2'-O-acetyl-ADP-ribose.

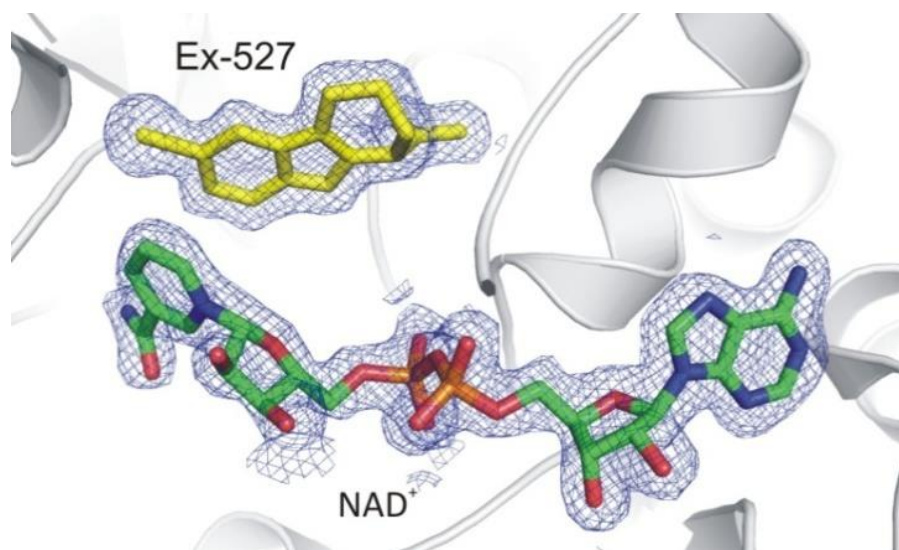


Figure 3.27. Active site of the hSirt3/ NAD⁺/Ex-527 complex. $2F_o - F_c$ electron density of NAD⁺ and Ex-527 is contoured at 1.0σ .

To examine whether Ex-527 can bind to hSirt3 during the step of forming O-alkylamidate intermediate, the crystal of hSirt3/ACS2 was soaked with NAD⁺ and Ex-527 in 80 minutes. The obtained structure showed very clear native O-alkylamidate intermediate state of the reaction but density for Ex-527 was not found (Figure 3.28). In comparison to the S-alkylamidate intermediate, the ribose moiety of the native O-alkylamidate intermediate has a different conformation (Figure 3.29). In combination with inhibition kinetics and binding analysis, the inhibition mechanism of Ex-527 on sirtuins was revealed to be that the compound stabilizes the closed enzyme conformation of the complex with 2'-O-acetyl-ADP-ribose, thus prevents product release (Gertz, et al., 2013).

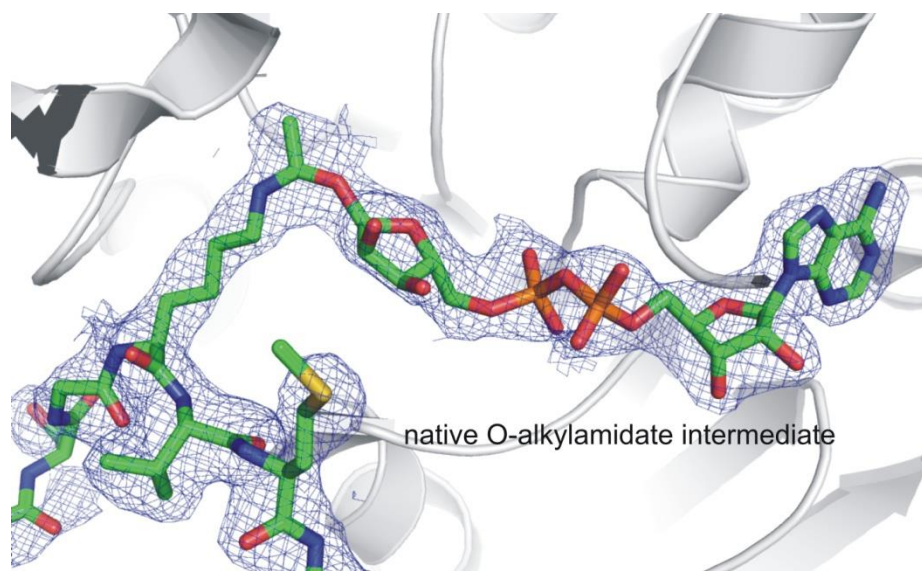


Figure 3.28. Active site of the hSirt3/ O-alkylamidate intermediate complex. $2F_o-F_c$ electron density of the intermediate is contoured at 1.0σ .

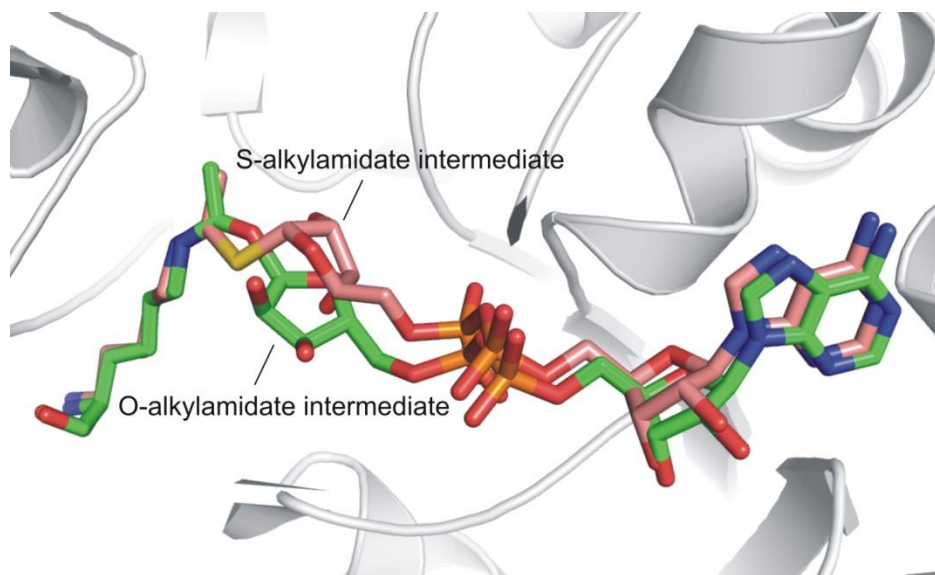


Figure 3.29. Superposition of the hSirt3/ O-alkylamidate intermediate complex with hSirt3/S-alkylamidate intermediate complex (pink, PDB ID 3GLT) (Jin, et al., 2009).

3.2. Sirt5 studies

3.2.1. Sirt5 purification

In a previous study, human Sirt5 (hSirt5) purification yielded high amount of the purified protein (Gertz, et al., 2012). However, crystallization trials resulted in twinned crystals and low occupancy of ligands. Therefore, zSirt5, an orthologue of hSirt5 was used in this study to overcome the issue. The zSirt5 purification protocol in this study was illustrated by a diagram in figure 3.30A. After the AC step, the highly expressed protein with the size of ~32 kDa was collected. The zSirt5 construct (30-298) is ~31 kDa and the His-tag is ~1 kDa. After TEV protease incubation and cation exchange, the His-tag was removed and zSirt5 was eluted in the fractions of the first peak with a small remaining contamination. After SEC, the last step of purification, the purified zSirt5 was obtained in the fractions B5 – B12 with the purity $\geq 95\%$ (Figure 3.30B). The yield of purification was 6 mg of the purified protein per 12 liters of the expressed media.

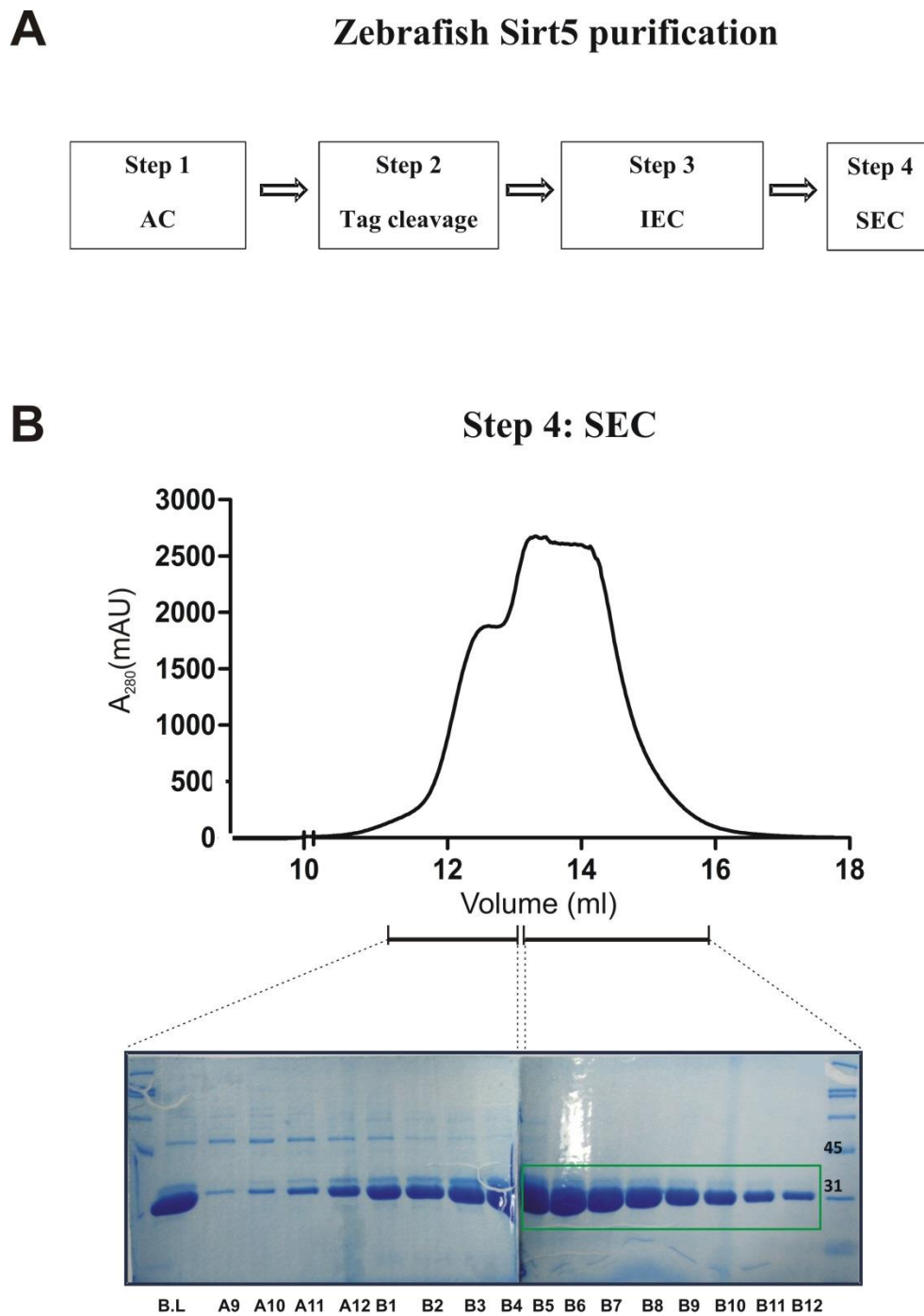


Figure 3.30. Zebrafish Sirt5 purification. (A) Four steps of zSirt5 purification. (B) Step 4: SEC, contamination was separated, purified zSirt5 including fractions B5-B12 (green box) was pooled for further studies. B.L, before loading.

3.2.2. Resveratrol and its related compounds are zSirt5 activators on FdL-1 peptide

Similar to Sirt3 study, the FdL assay was performed to investigate the effects of RESV and its related compounds including PCT, PD and brRESV on zSirt5. Among these compounds, 1 mM RESV can activate zSirt5 up to 12-fold, thus becoming the most potent activator of the enzyme (Figure 3.31). PCT, PD and brRESV slightly activate zSirt5 with nearly 3-fold in the presence of 0.2 mM and 6-fold in the presence of 1 mM compound concentration, except brRESV.

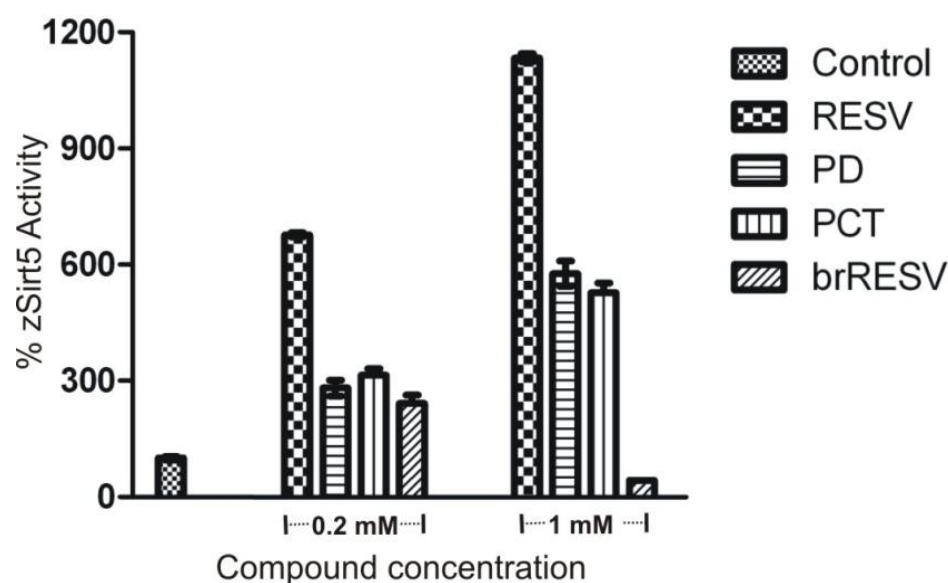


Figure 3.31. Activation of zSirt5 activity on FdL-1 peptide by resveratrol-related compounds at 0.2 mM and 1 mM compound concentration. Activities were normalized to the control in the absence of compound. Error bars represent standard errors of two independent measurements.

To prevent the artificial effect of FdL-1 peptide as mentioned in the Sirt3 study section, several fluorophore-free acetylated peptides were screened to find potent peptide substrates for zSirt5 using continuous assay. Among chosen peptides, p53 peptide is the most potent substrate of zSirt5 but not CPS1, the acetylated peptide derived from the physiological mammalian Sirt5 substrate (Figure 3.32). Lamin_B2 peptide is also a potent zSirt5 peptide substrate but has low solubility due to its rich hydrophobic residues. ME peptide has the similar linear of NADPH

consumption as CPS1 peptide indicating that it is also a zSirt5 substrate (Figure 3.32). ME and p53 peptide were chosen for further study. The regulations of resveratrol related compounds on these peptides were examined using MS. However, these compounds did not show significant effects (weak or unclear activation or inhibition) on the peptides (Figure 3.33).

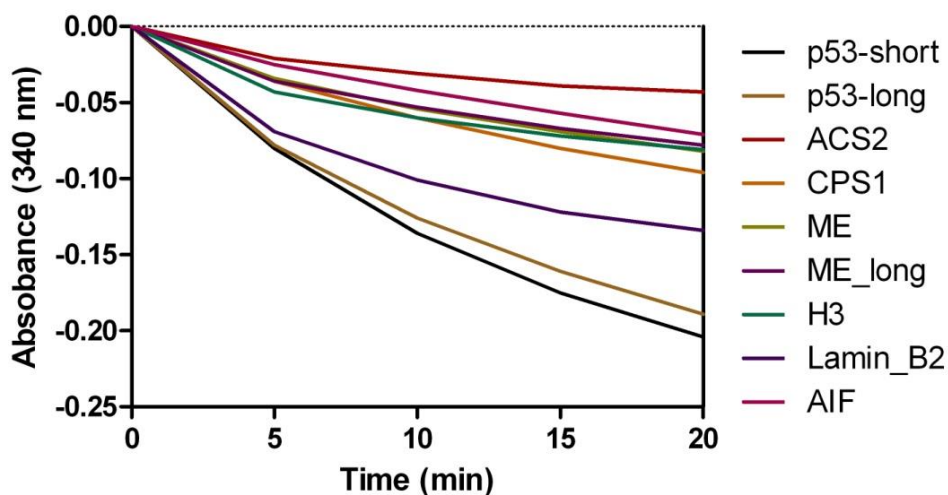


Figure 3.32. zSirt5 substrates were identified using continuous assays

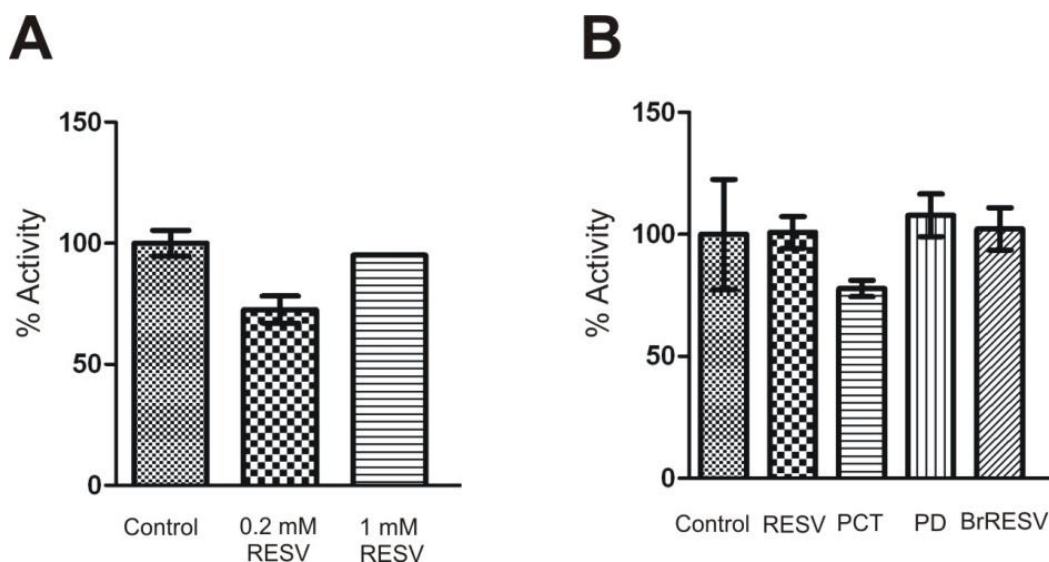


Figure 3.33. Insignificant effects of resveratrol related compounds on zSirt5 using MS. (A) p53 peptide. (B) ME peptide with 0.2 mM of each compound. Error bars represent standard errors of linear fits to time series experiments.

3.2.3. Crystallization trials and crystal structures of zSirt5 in complex with peptide substrates in the presence of resveratrol

Since RESV is the most potent activator of zSirt5 in comparison to its related compounds, it was used for crystallization study to determine the activation mechanism on the enzyme. Different crystallization trials including zSirt5 in the presence or absence of peptide substrate and RESV were setup. The diamond crystals were obtained from the condition containing the mixture of zSirt5 and RESV in comparison with no crystal when using DMSO as a control (Figure 3.34). The compound thus seems to be important for crystal growing. The crystals of the complex zSirt5/FdL-1 in the presence of RESV are in rod shape with a nice packing (Figure 3.34). However, the diffractions of these crystals are quite weak and the best data set is only 3.2 Å. The complex zSirt5/ME in the presence of RESV has very big rod crystals (Figure 3.34) and their diffractions are up to 2 Å. The complex zSirt5/p53 in the presence of RESV formed long stick crystals (Figure 3.34).

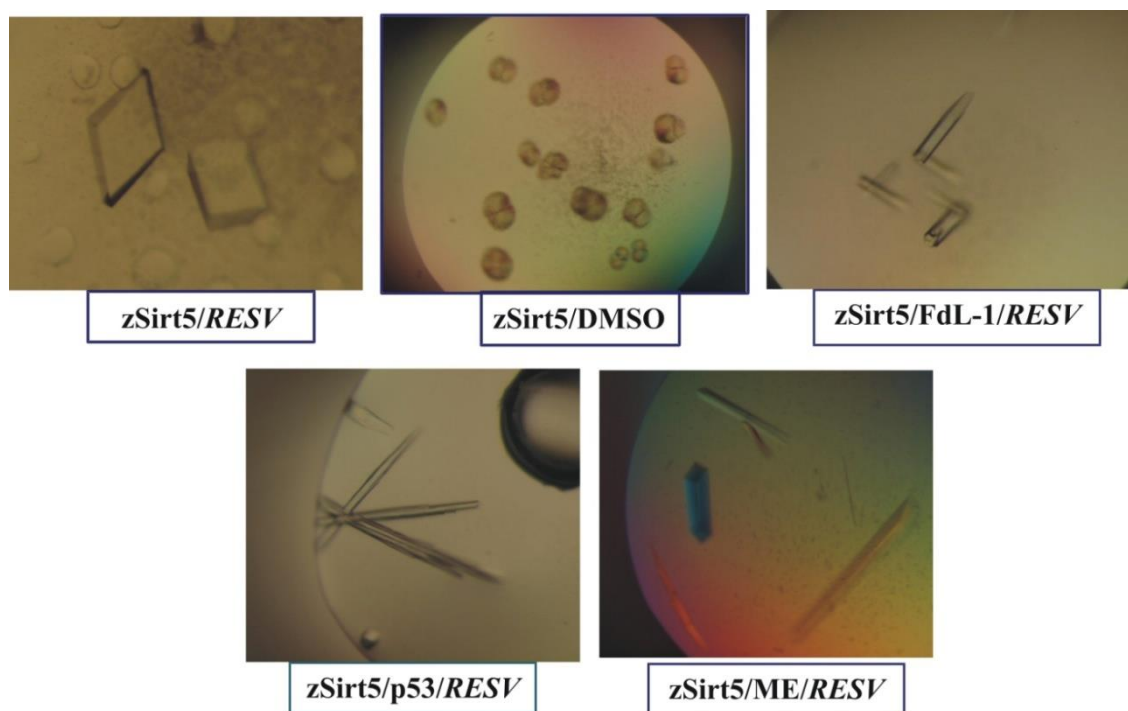


Figure 3.34. Crystals of different zSirt5 complexes with FdL-1 or p53 or ME peptide in the presence of RESV. Since the compound was not found in the structures, it was labeled as italic.

Similar to other sirtuin/peptide complexes, ME or p53 peptide binds to the cleft between the Rossmann-fold and zinc-binding domain of zSirt5 and the acetyl lysine binds into a hydrophobic tunnel pointing toward the catalytic residue His158 (Figure 3.35). No density fits to RESV implying the compound could not bind or bound with very low occupancy that could not be observed, consistent with the lack of an effect in activity assays with these peptides. Superposition of the complex zSirt5/ME/RESV and zSirt5/p53/RESV indicates that the protein has the same conformation in both structures (data not shown).

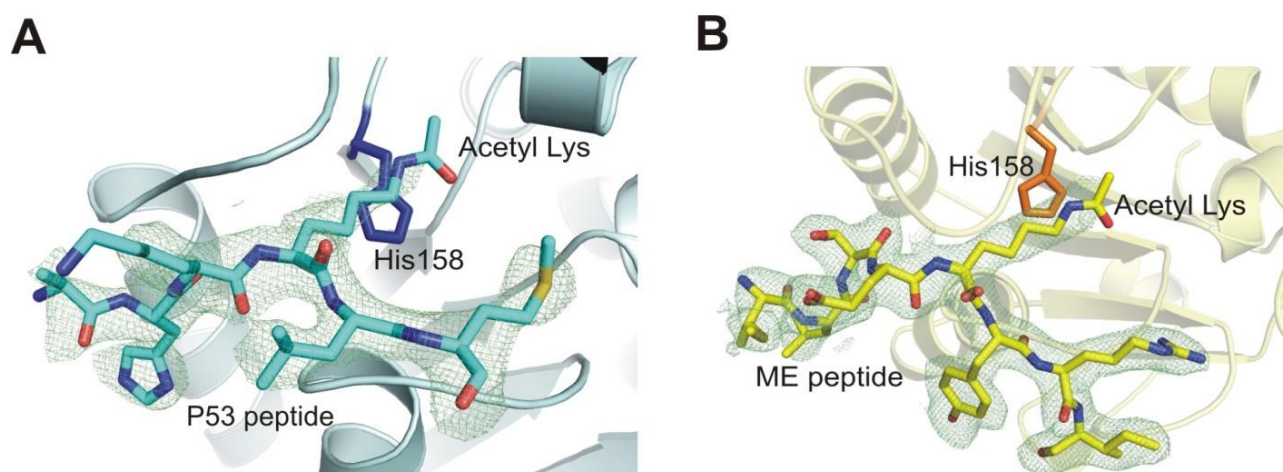


Figure 3.35. Active site of complex structures. (A) zSirt5/p53/RESV complex and (B) zSirt5/ME/RESV complex. Omit $F_o - F_c$ difference density is contoured at 3.0σ .

zSirt5 was crystallized in the presence of RESV but the obtained structure only showed the apo enzyme. The asymmetric unit of the apo-zSirt5 has four monomers whereas the complex zSirt5/FdL-1/RESV contains five zSirt5 monomers and the electron density of FdL-1 was found in only one monomer (Figure 3.36). RESV was included in the solution but not present in the structures. The protein packing may be caused by the unspecific binding between monomers including disulfide bonds formed by the residues Cys278.

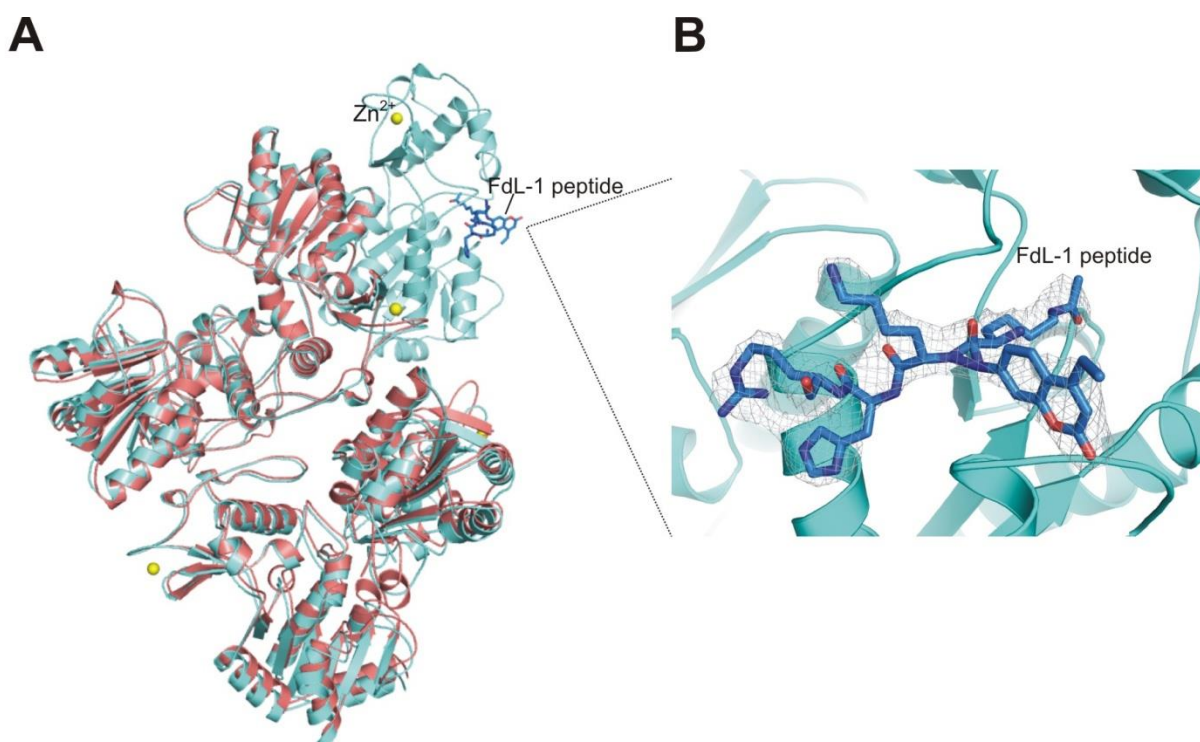


Figure 3.36. (A) Superposition of apo-zSirt5 (salmon pink) and the zSirt5/FdL-1/RESV complex (cyan), the density of the compound was not found. The asymmetric unit of apo structure is tetramer and of the zSirt5/FdL-1/RESV is pentamer but only one monomer contains FdL-1 peptide. zSirt5 is shown in cartoon, Zn²⁺ as a sphere and the peptide is in stick representation. (B) Active site of the monomer containing FdL-1 peptide. 2F_o-F_c electron density of FdL-1 peptide is contoured at 1.0σ.

Superposition of the FdL-1-containing monomer and apo monomer reveals two positions of conformation change: the loop 250 – 260 and the loop 277 – 284 (Figure 3.37). The loop 250 – 260 is peptide-binding loop, thus it moves closer to the peptide when the peptides bind to the protein. The loop 277 – 284 is on the surface of monomer contacts. Figure 3.38 shows the crystal contact of FdL-1 containing monomer of the zSirt5/FdL-1/RESV complex. The peptide is close to the loop 277 – 284 of the next symmetry-related monomer indicating that the loop conformation is also influenced by the presence of the peptide. The overall conformations of the complex zSirt5/FdL-1/RESV and zSirt5/ME/RESV are almost identical except a slight difference in the loop 277-284 (Figure 3.39). This may cause by different sequences and lengths of the peptides. Therefore, the loop 277-284 conformation is very flexible and depends on the presence, sequence and length of peptides.

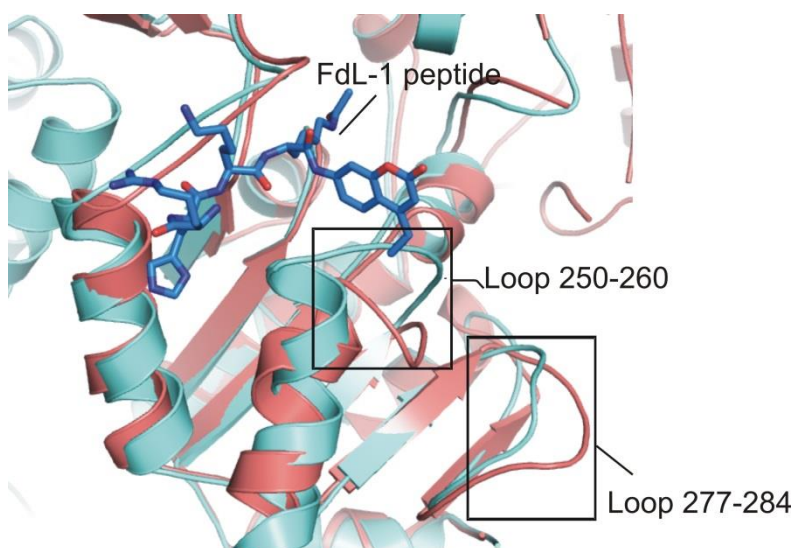


Figure 3.37. Superposition of apo-zSirt5 (salmon pink) and the FdL-1 containing zSirt5 monomer (cyan) with the positions of conformation changes showed in black boxes: loop 250-260 and loop 277-284.

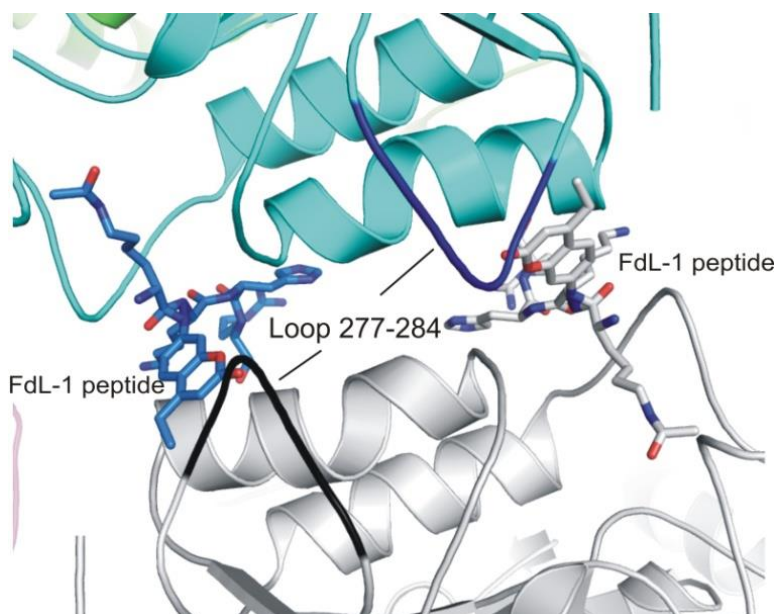


Figure 3.38. Crystal contact of the zSirt5/FdL-1/RESV complex. The symmetry-related monomer is shown in grey. The FdL-1 peptide and the loop 277-284 of the complex is in dark blue and of the symmetry-related monomer is in grey-black.

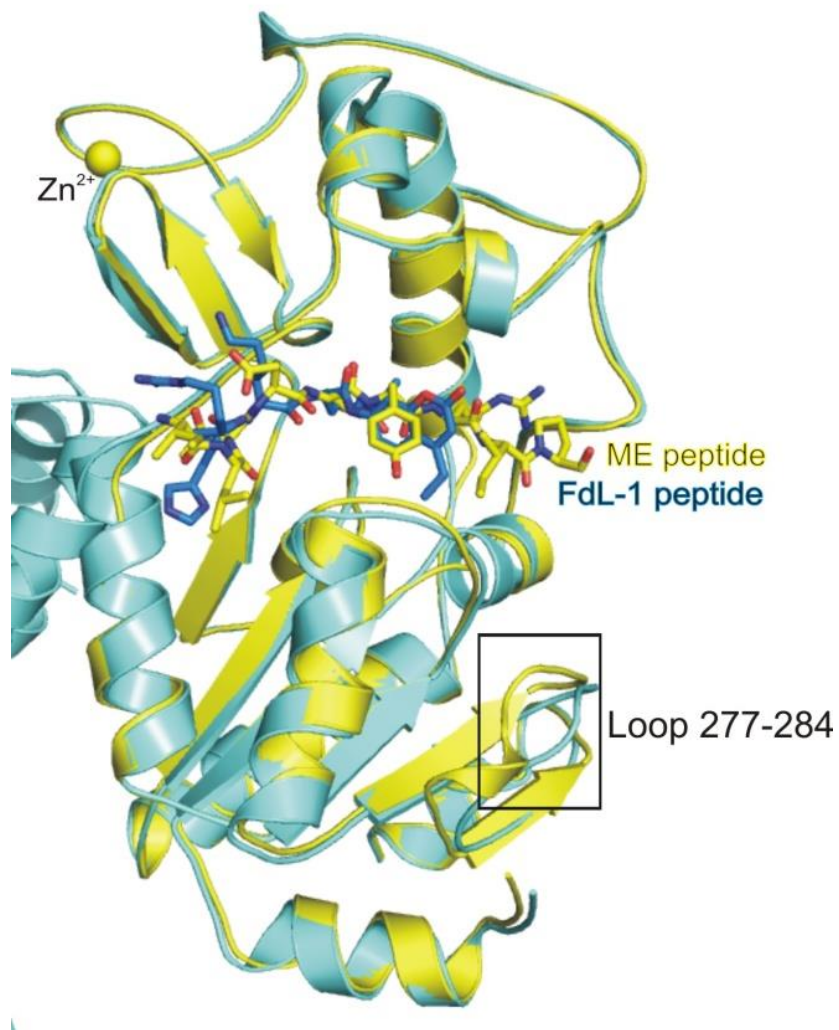


Figure 3.39. Superposition of the complex *zSirt5/FdL-1/RESV* (cyan) and *zSirt5/ME/RESV* (yellow). *zSirt5* is shown in cartoon, Zn^{2+} as a sphere and the peptide is in stick representation.

4. Discussion

4.1. Sirt3 studies

4.1.1. Resveratrol and its related compounds

Resveratrol and its related compounds are hSirt3 inhibitors with brRESV as the most potent candidate. Unlike PCT or PD which directly interact with the FdL-1 fluorophore for the inhibition effect, brRESV in the FdL-1 complex occupies a part of the C pocket where the NAM moiety of NAD⁺ binds to initialize the reaction and where NAM can bind to an alkylimidate complex (Sauve, et al., 2006) for the reverse reaction. In comparison to the Sir2Tm/NAM complex structure (Avalos, et al., 2005), the 1-OH group of the brRESV A-ring plays a role like the NAM carboxamide group, which also interacts with the conserved Asp101 in Sir2Tm (Asp231 in hSirt3) (Figure 4.1). A novel binding site for the 4'-bromo-reveratrol B-ring in hSirt3/FdL-1 complex provides a base to develop a new class of sirtuin inhibitors.

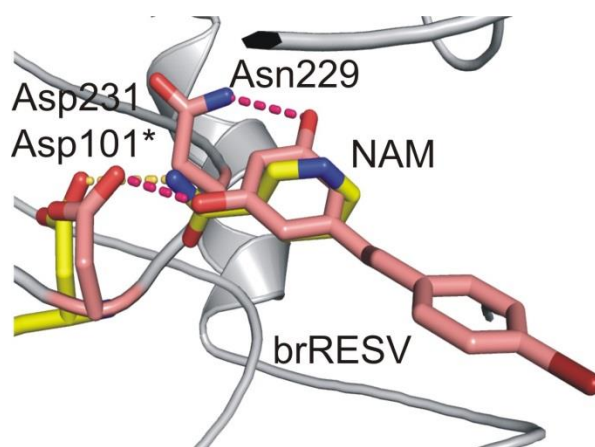


Figure 4.1. Superposition of the complex hSirt3/FdL-1/brRESV with Sir2Tm/p53/NAM (PDB ID 1YC5) (Avalos, et al., 2005). Dashed lines indicate hydrogen bonds of the brRESV A-ring hydroxyl groups and of the NAM carboxamide group to protein residues. brRESV is shown in pink and NAM in yellow. The protein part of the Sir2Tm/p53/NAM complex is omitted for clarity. Sir2Tm residues are labeled with a star.

Superposition of the complex hSirt3/ACS2/brRESV and hSirt3/FdL-1/brRESV reveals that a loop of a symmetry related monomer in the FdL-1 complex prevents the compound to bind to this allosteric site (Figure 4.2). RESV was reported as the most potent natural small molecule activator on Sirt1 and its orthologs (Howitz, et al., 2003). An activation mechanism of this compound on Sirt1 has not been successfully investigated due to the lacking of a Sirt1/RESV complex structure. Superposition of the hSirt3/ACS2/brRESV complex with a hSirt1 model indicates that the N-terminal extension could contribute to the external brRESV binding site. The residue Glu230 that is essential for Sirt1 activation (Hubbard, et al., 2013) is located next to this binding site, thus it might be the allosteric activation site in hSirt1 (Figure 4.3).

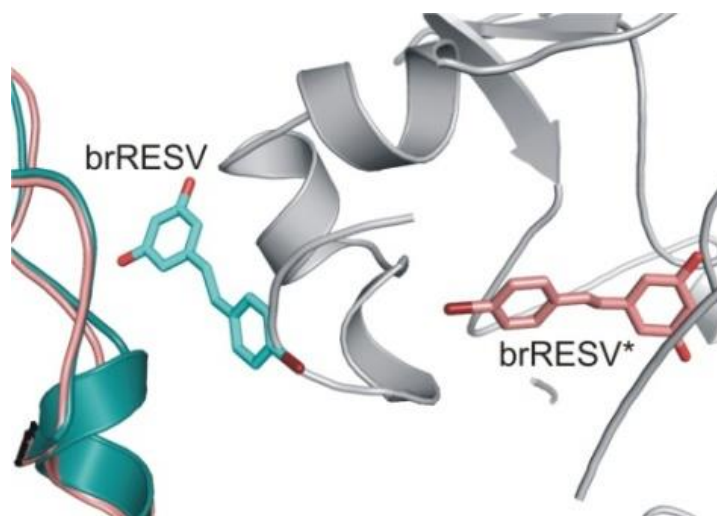


Figure 4.2. Analysis of crystal contacts. Superposition of the complex hSirt3/ACS2/brRESV (blue) and hSirt3/FdL-1/brRESV (pink and grey). brRESV of the ACS2 complex (cyan) clashes with the substrate binding loop of the symmetry related monomer (grey) of the FdL-1 complex. brRESV of the symmetry related FdL-1 complex is shown in pink and labeled with a star.

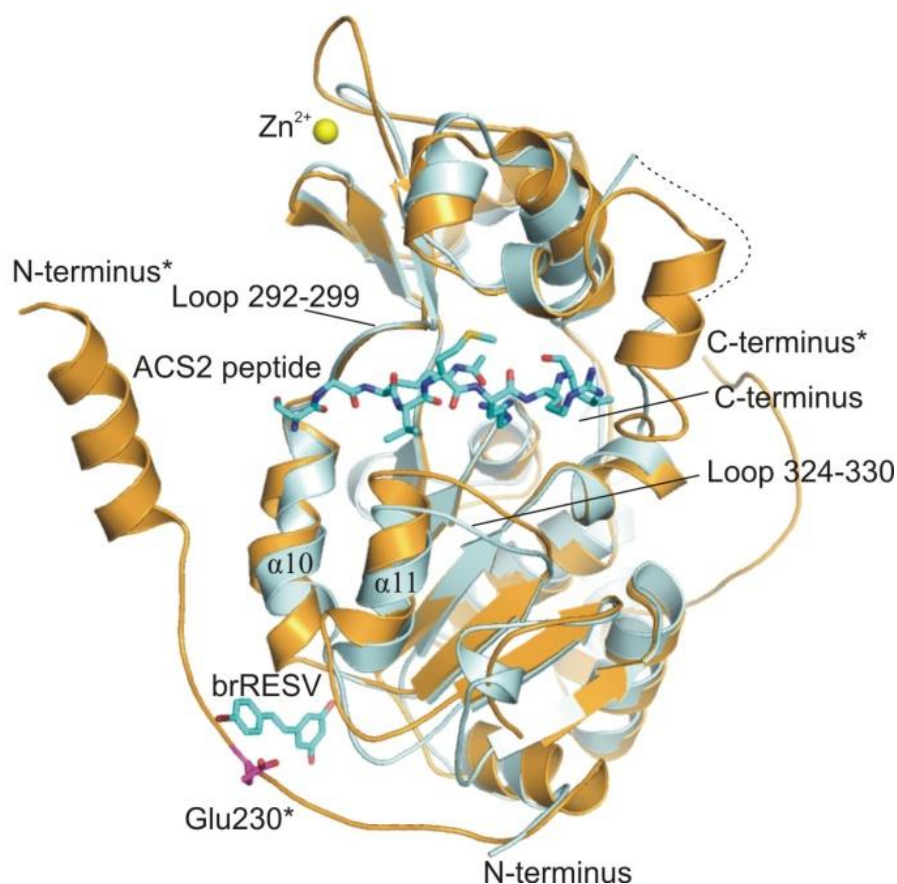


Figure 4.3. Superposition of the complex hSirt3/ACS2/brRESV with a homology model of hSirt1. brRESV (cyan) of hSirt3 (blue) is close to the putative position of Glu230 of hSirt1 (magenta and orange, respectively) suggesting the involvement of the compound binding site to an allosteric hSirt1 activation mechanism. hSirt1 N- and C-terminus and Glu230 are labeled with a star. A missing hSirt3 loop is indicated by a dashed line.

4.1.2. Resveratrol unrelated compounds

SRT1720 was known as a potent synthetic activator on Sirt1 with a much higher effect than RESV (Milne, et al., 2007). SRT1720 inhibits hSirt3 with high potency and isoform selectivity. Although it showed competitive inhibition with substrate peptide and uncompetitive with NAD⁺ using kinetic analysis (Jin, et al., 2009), the lacking of a complex structure with details about the binding site prevents full understanding of the inhibition mechanism. The hSirt3/carba-NAD⁺/SRT1720 complex structure in this study reveals the molecular inhibition

mechanism of the compound. Consistent with the kinetic study (Jin, et al., 2009), the compound interacts with NAM moiety of NAD^+ and Phe157 of the cosubstrate binding loop to form π -stacking sandwich and interferes substrate peptide by occupying a part of acetyl lysine. Further improvements to obtain more effective inhibitor can be developed from the novel binding site of SRT1720. It can be strengthening either the π -stacking interaction or substrate peptide competition. Based on the inhibition mechanism of Ex-527 (Gertz, et al., 2013) and the binding site of SRT1720 in hSirt3 complex structure, an activation mechanism of SRT1720 on Sirt1 can be speculated. SRT1720 would clash with the acetyl ribose moiety of the product (Figure 4.4) indicating that the compound might bind to Sirt1 after product formation and support product release.

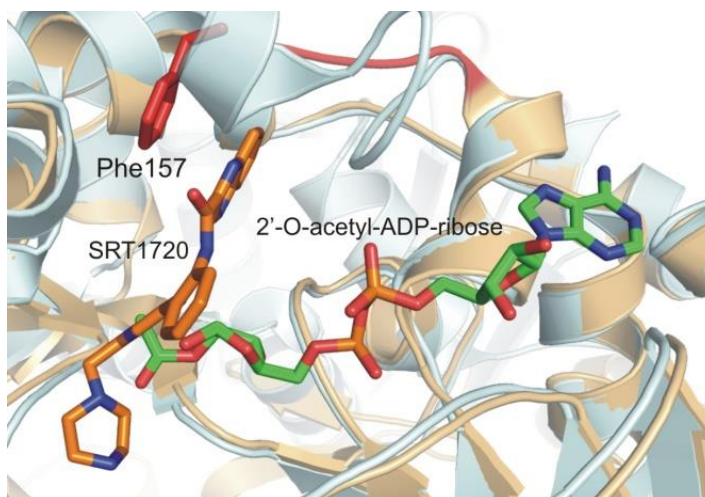


Figure 4.4. Superposition of the complex hSirt3/carba- NAD^+ /SRT1720 with hSirt3/OAcADPR/Ex-527 (PDB ID 4BVH) (Gertz, et al., 2013). SRT1720 (orange) would clash with the product 2'-O-acetyl-ADP-ribose (green). Carba- NAD^+ and Ex-527 were omitted for clarity.

The inhibitor Ex-527 has high selectivity for Sirt1 and lower potency on other isoforms (Solomon, et al., 2006). Ex-527 binds to sirtuins at the C pocket but extends in a different direction in comparison to the internal binding site of brRESV in the FdL-1 complex (Figure 4.5). The Ex-527 molecule extends perpendicular to its carbamide in a hydrophobic pocket close

to the acetyl-Lys binding site whereas brRESV extends toward a pocket close to the enzyme's surface. The crystal structure of the complex hSirt3/NAD⁺/Ex-527 and hSirt1/NAD⁺/Ex-527 (Zhao, et al., 2013) indicate that the compound can interact with the ribose and NAM moiety of NAD⁺, force NAD⁺ to bind in non-productive conformation and thus affects the peptide binding. However, a previous study indicated that the compound is an uncompetitive inhibitor of Sirt1 against both peptide substrate and NAD⁺ (Napper, et al., 2005). Based on competition experiments on the base exchange activity observed after intermediate formation, it was suggested to bind after binding of both substrates, and possibly to act by preventing the release of one or both of the products, 2'-O-acetyl-ADP-ribose and the acetylated peptide (Napper, et al., 2005). Moreover, the uncompetitive inhibition behavior in kinetic experiments was confirmed in our lab; thus the hSirt3/NAD⁺/Ex-527 complex structure appears not to be relevant for the inhibition mechanism. Our study reveals that Ex-527 inhibits sirtuins by binding to the product 2'-O-acetyl-ADP-ribose complex to prevent product release. The complex hSirt3/OAADPr/Ex-527 explains the kinetics mentioned above. In addition, we confirmed that the compound binds to the enzyme after intermediate formation and one product molecule per enzyme molecule is formed before inhibition.

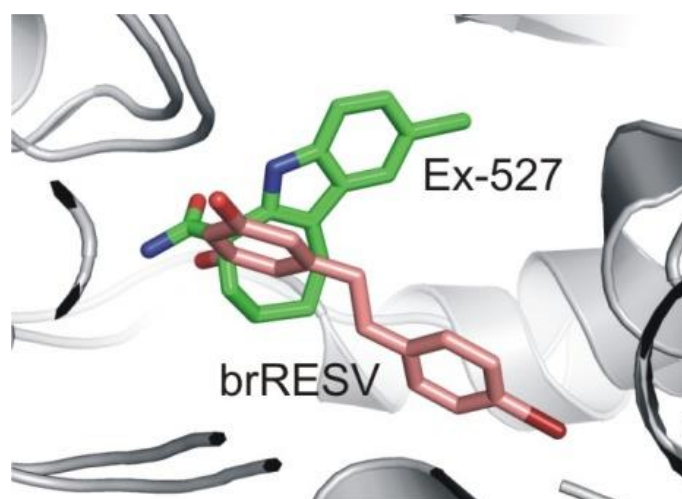


Figure 4.5. Superposition of the complex hSirt3/FdL-1/brRESV with hSirt3/OAcADPR/Ex-527 (PDB ID 4BVH) (Gertz, et al., 2013). Both brRESV (pink) and Ex-527 (green) occupy the C-site but extend in different directions.

4.2. Sirt5 studies

An effort to investigate the activation mechanism of RESV on zSirt5 has not been successful. The compound was not found in crystal structures of zSirt5 complex that might due to its low solubility. However, the study obtained different zSirt5 structures including the apo structure and the protein in complex with different peptide substrates. Therefore, it provides structural models for further study on screening and investigating the regulation of other small molecule compounds with higher solubility, potency and selectivity on zSirt5.

References

- Ahn, B.H., Kim, H.S., Song, S., Lee, I.H., Liu, J., Vassilopoulos, A., Deng, C.X., and Finkel, T. (2008). A role for the mitochondrial deacetylase Sirt3 in regulating energy homeostasis. *Proc Natl Acad Sci USA* 105, 14447-14452.
- Ahuja, N., Schwer, B., Carobbio, S., Waltregny, D., North, B.J., Castronovo, V., Maechler, P., and Verdin, E. (2007). Regulation of Insulin Secretion by SIRT4, a Mitochondrial ADP-ribosyltransferase. *J Biol Chem* 282, 33583-33592.
- Alcaín, F.J., and Villalba, J.M. (2009). Sirtuin activators. *Expert Opin Ther Pat* 19, 403-414.
- Arima, K., Uéda, K., Sunohara, N., Hirai, S., Izumiyama, Y., Tonozuka-Uehara, H., and Kawai, M. (1998). Immunoelectron-microscopic demonstration of NACP/ α -synuclein-epitopes on the filamentous component of Lewy bodies in Parkinson's disease and in dementia with Lewy bodies. *Brain Res* 808, 93-100.
- Avalos, J.L., Bever, K.M., and Wolberger, C. (2005). Mechanism of sirtuin inhibition by nicotinamide: altering the NAD(+) cosubstrate specificity of a Sir2 enzyme. *Mol Cell* 17, 855-868.
- Barber, M.F., Michishita-Kioi, E., Xi, Y., Tasselli, L., Kioi, M., Moqtaderi, Z., Tennen, R.I., Paredes, S., Young, N.L., Chen, K., et al. (2012). SIRT7 links H3K18 deacetylation to maintenance of oncogenic transformation. *Nature* 487, 114-118.
- Bedalov, A., Gatabont, T., Irvine, W.P., Gottschling, D.E., and Simon, J.A. (2001). Identification of a small molecule inhibitor of Sir2p. *Proc Natl Acad Sci U S A* 98, 15113-15118.
- Beher, D., Wu, J., Cumine, S., Kim, K.W., Lu, S.-C., Atangan, L., and Wang, M. (2009). Resveratrol is Not a Direct Activator of SIRT1 Enzyme Activity. *Chem Biol Drug Des* 74, 619-624.
- Beirowski, B., Gustin, J., Armour, S.M., Yamamoto, H., Viader, A., North, B.J., Michán, S., Baloh, R.H., Golden, J.P., Schmidt, R.E., et al. (2011). Sir-two-homolog 2 (Sirt2) modulates peripheral myelination through polarity protein Par-3/atypical protein kinase C (aPKC) signaling. *Proc Natl Acad Sci USA* 108, E952-E961.
- Blum, C.A., Ellis, J.L., Loh, C., Ng, P.Y., Perni, R.B., and Stein, R.L. (2011). SIRT1 modulation as a novel approach to the treatment of diseases of aging. *J Med Chem* 54, 417-432.

- Borra, M.T., Langer, M.R., Slama, J.T., and Denu, J.M. (2004). Substrate specificity and kinetic mechanism of the Sir2 family of NAD⁺-dependent histone/protein deacetylases. *Biochemistry* 43, 9877-9887.
- Borra, M.T., Smith, B.C., and Denu, J.M. (2005). Mechanism of human SIRT1 activation by resveratrol. *J Biol Chem* 280, 17187-17195.
- Cantó, C., and Auwerx, J. (2009). Caloric restriction, SIRT1 and longevity. *Trends Endocrinol Metab* 20, 325-331.
- Cen, Y. (2010). Sirtuins inhibitors: The approach to affinity and selectivity. *Biochim Biophys Acta* 1804, 1635-1644.
- Chang, J.H., Kim, H.C., Hwang, K.Y., Lee, J.W., Jackson, S.P., Bell, S.D., and Cho, Y. (2002). Structural basis for the NAD-dependent deacetylase mechanism of Sir2. *J Biol Chem* 277, 34489-34498.
- Chen, L. (2011). Medicinal chemistry of sirtuin inhibitors. *Curr Med Chem* 18, 1936-1946.
- Chen, V.B., Arendall, W.B., 3rd, Headd, J.J., Keedy, D.A., Immormino, R.M., Kapral, G.J., Murray, L.W., Richardson, J.S., and Richardson, D.C. (2010). MolProbity: all-atom structure validation for macromolecular crystallography. *Acta Crystallogr D Biol Crystallogr* 66, 12-21.
- Cohen, E., Paulsson, J.F., Blinder, P., Burstyn-Cohen, T., Du, D., Estepa, G., Adame, A., Pham, H.M., Holzenberger, M., Kelly, J.W., et al. (2009). Reduced IGF-1 Signaling Delays Age-Associated Proteotoxicity in Mice. *Cell* 139, 1157-1169.
- Cosgrove, M.S., Bever, K., Avalos, J.L., Muhammad, S., Zhang, X., and Wolberger, C. (2006). The structural basis of sirtuin substrate affinity. *Biochemistry* 45, 7511-7521.
- Du, J., Zhou, Y., Su, X., Yu, J.J., Khan, S., Jiang, H., Kim, J., Woo, J., Kim, J.H., Choi, B.H., et al. (2011). Sirt5 is a NAD-dependent protein lysine demalonylase and desuccinylase. *Science* 334, 806-809.
- Emsley, P., and Cowtan, K. (2004). Coot: Model-Building Tools for Molecular Graphics. *Acta Cryst Section D* 60, 2126-2132.
- Feldman, J.L., Dittenhafer-Reed, K.E., and Denu, J.M. (2012). Sirtuin Catalysis and Regulation. *J Biol Chem* 287, 42419-42427.

-
- Fischer, F., Gertz, M., Suenkel, B., Lakshminarasimhan, M., Schutkowski, M., and Steegborn, C. (2012). Sirt5 deacylation activities show differential sensitivities to nicotinamide inhibition. *PLoS One* 7, e45098.
- Frye, R.A. (2000). Phylogenetic classification of prokaryotic and eukaryotic Sir2-like proteins. *Biochem Biophys Res Commun* 273, 793-798.
- Gertz, M., Fischer, F., Nguyen, G.T.T., Lakshminarasimhan, M., Schutkowski, M., Weyand, M., and Steegborn, C. (2013). Ex-527 inhibits Sirtuins by exploiting their unique NAD⁺-dependent deacetylation mechanism. *P Natl Acad Sci* 110, E2772-E2781.
- Gertz, M., Nguyen, G.T., Fischer, F., Suenkel, B., Schlicker, C., Franzel, B., Tomaschewski, J., Aladini, F., Becker, C., Wolters, D., et al. (2012). A molecular mechanism for direct sirtuin activation by resveratrol. *PLoS One* 7, e49761.
- Gertz, M., and Steegborn, C. (2010). Function and regulation of the mitochondrial Sirtuin isoform Sirt5 in Mammalia. *Biochim Biophys Acta* 1804, 1658-1665.
- Grozinger, C.M., Chao, E.D., Blackwell, H.E., Moazed, D., and Schreiber, S.L. (2001). Identification of a class of small molecule inhibitors of the sirtuin family of NAD-dependent deacetylases by phenotypic screening. *J Biol Chem* 276, 38837-38843.
- Haass, C., and Selkoe, D.J. (2007). Soluble protein oligomers in neurodegeneration: lessons from the Alzheimer's amyloid beta-peptide. *Nat Rev Mol Cell Bio* 8, 101-112.
- Haigis, M.C., Mostoslavsky, R., Haigis, K.M., Fahie, K., Christodoulou, D.C., Murphy, A.J., Valenzuela, D.M., Yancopoulos, G.D., Karow, M., Blander, G., et al. (2006). SIRT4 inhibits glutamate dehydrogenase and opposes the effects of calorie restriction in pancreatic beta cells. *Cell* 126, 941-954.
- Haigis, M.C., and Sinclair, D.A. (2010). Mammalian sirtuins: biological insights and disease relevance. *Annu Rev Pathol* 5, 253-295.
- Hallows, W.C., Lee, S., and Denu, J.M. (2006). Sirtuins deacetylate and activate mammalian acetyl-CoA synthetases. *Proc Natl Acad Sci U S A* 103, 10230-10235.
- Heltweg, B., Gathbonton, T., Schuler, A.D., Posakony, J., Li, H., Goehle, S., Kollipara, R., Depinho, R.A., Gu, Y., Simon, J.A., et al. (2006). Antitumor activity of a small-molecule inhibitor of human silent information regulator 2 enzymes. *Cancer Res* 66, 4368-4377.

- Hoff, K.G., Avalos, J.L., Sens, K., and Wolberger, C. (2006). Insights into the sirtuin mechanism from ternary complexes containing NAD⁺ and acetylated peptide. *Structure* 14, 1231-1240.
- Howitz, K.T., Bitterman, K.J., Cohen, H.Y., Lamming, D.W., Lavu, S., Wood, J.G., Zipkin, R.E., Chung, P., Kisielewski, A., Zhang, L.L., et al. (2003). Small molecule activators of sirtuins extend *Saccharomyces cerevisiae* lifespan. *Nature* 425, 191-196.
- Hubbard, B.P., Gomes, A.P., Dai, H., Li, J., Case, A.W., Considine, T., Riera, T.V., Lee, J.E., E, S.Y., Lamming, D.W., et al. (2013). Evidence for a Common Mechanism of SIRT1 Regulation by Allosteric Activators. *Science* 339, 1216-1219.
- Jackson, M.D., and Denu, J.M. (2002). Structural Identification of 2'- and 3'-O-Acetyl-ADP-ribose as Novel Metabolites Derived from the Sir2 Family of β -NAD⁺-dependent Histone/Protein Deacetylases. *J Biol Chem* 277, 18535-18544.
- Jiang, M., Wang, J., Fu, J., Du, L., Jeong, H., West, T., Xiang, L., Peng, Q., Hou, Z., Cai, H., et al. (2012). Neuroprotective role of Sirt1 in mammalian models of Huntington's disease through activation of multiple Sirt1 targets. *Nat Med* 18, 153-158.
- Jin, L., Galonek, H., Israelian, K., Choy, W., Morrison, M., Xia, Y., Wang, X., Xu, Y., Yang, Y., Smith, J.J., et al. (2009). Biochemical characterization, localization, and tissue distribution of the longer form of mouse SIRT3. *Protein Sci* 18, 514-525.
- Jin, L., Wei, W., Jiang, Y., Peng, H., Cai, J., Mao, C., Dai, H., Choy, W., Bemis, J.E., Jirousek, M.R., et al. (2009). Crystal structures of human SIRT3 displaying substrate-induced conformational changes. *J Biol Chem* 284, 24394-24405.
- Kabsch, W. (2010). Xds. *Acta Crystallogr D Biol Crystallogr* 66, 125-132.
- Kaeberlein, M., McDonagh, T., Heltweg, B., Hixon, J., Westman, E.A., Caldwell, S.D., Napper, A., Curtis, R., DiStefano, P.S., Fields, S., et al. (2005). Substrate-specific activation of sirtuins by resveratrol. *J Biol Chem* 280, 17038-17045.
- Kaeberlein, M., McVey, M., and Guarente, L. (1999). The SIR2/3/4 complex and SIR2 alone promote longevity in *Saccharomyces cerevisiae* by two different mechanisms. *Genes Dev* 13, 2570-2580.
- Kanfi, Y., Naiman, S., Amir, G., Peshti, V., Zinman, G., Nahum, L., Bar-Joseph, Z., and Cohen, H.Y. (2012). The sirtuin SIRT6 regulates lifespan in male mice. *Nature* 483, 218-221.

- Kawahara, T.L.A., Michishita, E., Adler, A.S., Damian, M., Berber, E., Lin, M., McCord, R.A., Ongaigui, K.C.L., Boxer, L.D., Chang, H.Y., et al. (2009). SIRT6 Links Histone H3 Lysine 9 Deacetylation to NF- κ B-Dependent Gene Expression and Organismal Life Span. *Cell* 136, 62-74.
- Lakshminarasimhan, M., Rauh, D., Schutkowski, M., and Steegborn, C. (2013). Sirt1 activation by resveratrol is substrate sequence-selective. *Aging*.
- Landry, J., Slama, J.T., and Sternglanz, R. (2000). Role of NAD⁺ in the Deacetylase Activity of the SIR2-like Proteins. *Biochem Biophys Res Commun* 278, 685-690.
- Li, W., Zhang, B., Tang, J., Cao, Q., Wu, Y., Wu, C., Guo, J., Ling, E.A., and Liang, F. (2007). Sirtuin 2, a Mammalian Homolog of Yeast Silent Information Regulator-2 Longevity Regulator, Is an Oligodendroglial Protein That Decelerates Cell Differentiation through Deacetylating α -Tubulin. *J Neurosci* 27, 2606-2616.
- Lin, S.-J., Kaeberlein, M., Andalis, A., Sturtz, L., Defossez, P.-A., Culotta, V., Fink, G., and Guarente, L. (2002). Calorie restriction extends *Saccharomyces cerevisiae* lifespan by increasing respiration. *Nature* 418, 344-348.
- Lin, S.J., Defossez, P.A., and Guarente, L. (2000). Requirement of NAD and SIR2 for life-span extension by calorie restriction in *Saccharomyces cerevisiae*. *Science* 289, 2126-2128.
- Lombard, D.B. (2009). Sirtuins at the Breaking Point: SIRT6 in DNA Repair. *Aging* 1, 12-16.
- Lombard, D.B., Alt, F.W., Cheng, H.L., Bunkenborg, J., Streeper, R.S., Mostoslavsky, R., Kim, J., Yancopoulos, G., Valenzuela, D., Murphy, A., et al. (2007). Mammalian Sir2 homolog SIRT3 regulates global mitochondrial lysine acetylation. *Mol Cell Biol* 27, 8807-8814.
- Lombard, D.B., and Miller, R.A. (2012). Ageing: sorting out the sirtuins. *Nature* 483, 166-167.
- Longo, V.D., and Fontana, L. (2010). Calorie restriction and cancer prevention: metabolic and molecular mechanisms. *Trends Pharmacol Sci* 31, 89-98.
- Mai, A., Massa, S., Lavu, S., Pezzi, R., Simeoni, S., Ragno, R., Mariotti, F.R., Chiani, F., Camilloni, G., and Sinclair, D.A. (2005). Design, synthesis, and biological evaluation of sirtinol analogues as class III histone/protein deacetylase (Sirtuin) inhibitors. *J Med Chem* 48, 7789-7795.
- Mao, Z., Hine, C., Tian, X., Van Meter, M., Au, M., Vaidya, A., Seluanov, A., and Gorbunova, V. (2011). SIRT6 Promotes DNA Repair Under Stress by Activating PARP1. *Science* 332, 1443-1446.

- Martinez-Pastor, B., and Mostoslavsky, R. (2012). Sirtuins, Metabolism, and Cancer. *Front Pharm* 3.
- Masoro, E.J. (2005). Overview of caloric restriction and ageing. *Mech Ageing Dev* 126, 913-922.
- Masoro, E.J. (1990). The Retardation of Aging and Disease by Dietary Restriction. *J Nutr* 120, 139-139.
- McCay, C.M., Crowell, M.F., and Maynard, L.A. (1989). The effect of retarded growth upon the length of life span and upon the ultimate body size. 1935. *Nutrition* 5, 155-171; discussion 172.
- Medda, F., Russell, R.J.M., Higgins, M., McCarthy, A.R., Campbell, J., Slawin, A.M.Z., Lane, D.P., Lain, S., and Westwood, N.J. (2009). Novel Cambinol Analogs as Sirtuin Inhibitors: Synthesis, Biological Evaluation, and Rationalization of Activity. *J Med Chem* 52, 2673-2682.
- Michan, S., and Sinclair, D. (2007). Sirtuins in mammals: insights into their biological function. *Biochem J* 404, 1-13.
- Michishita, E., McCord, R.A., Berber, E., Kioi, M., Padilla-Nash, H., Damian, M., Cheung, P., Kusumoto, R., Kawahara, T.L., Barrett, J.C., et al. (2008). SIRT6 is a histone H3 lysine 9 deacetylase that modulates telomeric chromatin. *Nature* 452, 492-496.
- Michishita, E., Park, J.Y., Burneskis, J.M., Barrett, J.C., and Horikawa, I. (2005). Evolutionarily conserved and nonconserved cellular localizations and functions of human SIRT proteins. *Mol Biol Cell* 16, 4623-4635.
- Milne, J.C., Lambert, P.D., Schenk, S., Carney, D.P., Smith, J.J., Gagne, D.J., Jin, L., Boss, O., Perni, R.B., Vu, C.B., et al. (2007). Small molecule activators of SIRT1 as therapeutics for the treatment of type 2 diabetes. *Nature* 450, 712-716.
- Min, J., Landry, J., Sternglanz, R., and Xu, R.-M. (2001). Crystal Structure of a SIR2 Homolog NAD Complex. *Cell* 105, 269-279.
- Motta, M.C., Divecha, N., Lemieux, M., Kamel, C., Chen, D., Gu, W., Bultsma, Y., McBurney, M., and Guarente, L. (2004). Mammalian SIRT1 Represses Forkhead Transcription Factors. *Cell* 116, 551-563.
- Mueller, U., Darowski, N., Fuchs, M.R., Forster, R., Hellmig, M., Paithankar, K.S., Puhlinger, S., Steffien, M., Zocher, G., and Weiss, M.S. (2012). Facilities for macromolecular crystallography at the Helmholtz-Zentrum Berlin. *J Synchrotron Radiat* 19, 442-449.

- Murshudov, G.N., Vagin, A.A., and Dodson, E.J. (1997). Refinement of macromolecular structures by the maximum-likelihood method. *Acta Crystallogr D Biol Crystallogr* 53, 240-255.
- Nakagawa, T., Lomb, D.J., Haigis, M.C., and Guarente, L. (2009). SIRT5 Deacetylates carbamoyl phosphate synthetase 1 and regulates the urea cycle. *Cell* 137, 560-570.
- Napper, A.D., Hixon, J., McDonagh, T., Keavey, K., Pons, J.F., Barker, J., Yau, W.T., Amouzegh, P., Flegg, A., Hamelin, E., et al. (2005). Discovery of indoles as potent and selective inhibitors of the deacetylase SIRT1. *J Med Chem* 48, 8045-8054.
- Nguyen, G.T.T., Schaefer, S., Gertz, M., Weyand, M., and Steegborn, C. (2013). Structures of human sirtuin 3 complexes with ADP-ribose and with carba-NAD⁺ and SRT1720: binding details and inhibition mechanism. *Acta Crystallogr D* 69, 1423-1432.
- North, B.J., Marshall, B.L., Borra, M.T., Denu, J.M., and Verdin, E. (2003). The human Sir2 ortholog, SIRT2, is an NAD⁺-dependent tubulin deacetylase. *Mol Cell* 11, 437-444.
- Pacholec, M., Bleasdale, J.E., Chrnyk, B., Cunningham, D., Flynn, D., Garofalo, R.S., Griffith, D., Griffior, M., Loulakis, P., Pabst, B., et al. (2010). SRT1720, SRT2183, SRT1460, and resveratrol are not direct activators of SIRT1. *J Biol Chem* 285, 8340-8351.
- Pagans, S., Pedal, A., North, B.J., Kaehlcke, K., Marshall, B.L., Dorr, A., Hetzer-Egger, C., Henklein, P., Frye, R., McBurney, M.W., et al. (2005). SIRT1 Regulates HIV Transcription via Tat Deacetylation. *PLoS Biol* 3, e41.
- Pan, P.W., Feldman, J.L., Devries, M.K., Dong, A., Edwards, A.M., and Denu, J.M. (2011). Structure and Biochemical Functions of SIRT6. *J Biol Chem* 286, 14575-14587.
- Park, S.-J., Ahmad, F., Philp, A., Baar, K., Williams, T., Luo, H., Ke, H., Rehmann, H., Taussig, R., Brown, Alexandra L., et al. (2012). Resveratrol Ameliorates Aging-Related Metabolic Phenotypes by Inhibiting cAMP Phosphodiesterases. *Cell* 148, 421-433.
- Peng, C., Lu, Z., Xie, Z., Cheng, Z., Chen, Y., Tan, M., Luo, H., Zhang, Y., He, W., Yang, K., et al. (2011). The First Identification of Lysine Malonylation Substrates and Its Regulatory Enzyme. *Mol Cell Proteomics* 10.
- Pillai, V.B., Sundaresan, N.R., Kim, G., Gupta, M., Rajamohan, S.B., Pillai, J.B., Samant, S., Ravindra, P.V., Isbatan, A., and Gupta, M.P. (2010). Exogenous NAD Blocks Cardiac Hypertrophic Response via Activation of the SIRT3-LKB1-AMP-activated Kinase Pathway. *J Biol Chem* 285, 3133-3144.

-
- Pirola, L., and Frojdo, S. (2008). Resveratrol: one molecule, many targets. *IUBMB Life* 60, 323-332.
- Rogina, B., and Helfand, S.L. (2004). Sir2 mediates longevity in the fly through a pathway related to calorie restriction. *Proc Natl Acad Sci USA* 101, 15998-16003.
- S. Mohar, D. (2012). The Sirtuin System: The Holy Grail of Resveratrol? *J Clin Exp Cardiol* 03.
- Sack, M.N. (2011). Emerging characterization of the role of SIRT3-mediated mitochondrial protein deacetylation in the heart. *Am J Physiol Heart Circ Physiol* 301, H2191-H2197.
- Sambrook, J., and Russell, D.W. (2001). *Molecular Cloning: A Laboratory Manual*. Cold Spring Harbor Laboratory; 3rd edition.
- Sanders, B.D., Jackson, B., and Marmorstein, R. (2010). Structural basis for sirtuin function: What we know and what we don't. *Biochim Biophys Acta* 1804, 1604-1616.
- Sanders, B.D., Zhao, K., Slama, J.T., and Marmorstein, R. (2007). Structural Basis for Nicotinamide Inhibition and Base Exchange in Sir2 Enzymes. *Mol Cell* 25, 463-472.
- Sauve, A.A. (2010). Sirtuin chemical mechanisms. *Biochim Biophys Acta* 1804, 1591-1603.
- Sauve, A.A., and Schramm, V.L. (2003). Sir2 regulation by nicotinamide results from switching between base exchange and deacetylation chemistry. *Biochemistry* 42, 9249-9256.
- Sauve, A.A., Wolberger, C., Schramm, V.L., and Boeke, J.D. (2006). The biochemistry of sirtuins. *Annu Rev Biochem* 75, 435-465.
- Sauve, A.A., and Youn, D.Y. (2012). Sirtuins: NAD⁺-dependent deacetylase mechanism and regulation. *Curr Opin Chem Biol* 16, 535-543.
- Schlicker, C., Gertz, M., Papatheodorou, P., Kachholz, B., Becker, C.F., and Steegborn, C. (2008). Substrates and regulation mechanisms for the human mitochondrial sirtuins Sirt3 and Sirt5. *J Mol Biol* 382, 790-801.
- Schuetz, A., Min, J., Antoshenko, T., Wang, C.L., Allali-Hassani, A., Dong, A., Loppnau, P., Vedadi, M., Bochkarev, A., Sternglanz, R., et al. (2007). Structural basis of inhibition of the human NAD⁺-dependent deacetylase SIRT5 by suramin. *Structure* 15, 377-389.
- Schuttelkopf, A.W., and van Aalten, D.M. (2004). PRODRG: a tool for high-throughput crystallography of protein-ligand complexes. *Acta Crystallogr D Biol Crystallogr* 60, 1355-1363.

-
- Sebastian, C., Satterstrom, F.K., Haigis, M.C., and Mostoslavsky, R. (2012). From Sirtuin Biology to Human Diseases: An Update. *J Biol Chem* 287, 42444-42452.
- Smith, B.C., and Denu, J.M. (2007). Mechanism-Based Inhibition of Sir2 Deacetylases by Thioacetyl-Lysine Peptide†. *Biochemistry* 46, 14478-14486.
- Smith, B.C., and Denu, J.M. (2007). Sir2 Deacetylases Exhibit Nucleophilic Participation of Acetyl-Lysine in NAD⁺ Cleavage. *J Am Chem Soc* 129, 5802-5803.
- Smith, B.C., Hallows, W.C., and Denu, J.M. (2009). A continuous microplate assay for sirtuins and nicotinamide-producing enzymes. *Anal Biochem* 394, 101-109.
- Solomon, J.M., Pasupuleti, R., Xu, L., McDonagh, T., Curtis, R., DiStefano, P.S., and Huber, L.J. (2006). Inhibition of SIRT1 catalytic activity increases p53 acetylation but does not alter cell survival following DNA damage. *Mol Cell Biol* 26, 28-38.
- Someya, S., Yu, W., Hallows, W.C., Xu, J., Vann, J.M., Leeuwenburgh, C., Tanokura, M., Denu, J.M., and Prolla, T.A. (2010). Sirt3 Mediates Reduction of Oxidative Damage and Prevention of Age-Related Hearing Loss under Caloric Restriction. *Cell* 143, 802-812.
- Sundaresan, N.R., Vasudevan, P., Zhong, L., Kim, G., Samant, S., Ravindra, P.V., Pillai, V.B., Gupta, M., Cunningham, J.M., Deng, C.-X., et al. (2012). The sirtuin SIRT6 blocks IGF-Akt signaling and development of cardiac hypertrophy by targeting c-Jun. *Nat Med* 8, 1643-1650.
- Szczepankiewicz, B.G., Dai, H., Koppetsch, K.J., Qian, D., Jiang, F., Mao, C., and Perni, R.B. (2012). Synthesis of Carba-NAD and the Structures of Its Ternary Complexes with SIRT3 and SIRT5. *J Org Chem* 77, 7319-7329.
- Tanner, K.G., Landry, J., Sternglanz, R., and Denu, J.M. (2000). Silent information regulator 2 family of NAD- dependent histone/protein deacetylases generates a unique product, 1-O-acetyl-ADP-ribose. *P Natl Acad Sci* 97, 14178-14182.
- Tanny, J.C., Dowd, G.J., Huang, J., Hilz, H., and Moazed, D. (1999). An Enzymatic Activity in the Yeast Sir2 Protein that Is Essential for Gene Silencing. *Cell* 99, 735-745.
- Trapp, J., Meier, R., Hongwiset, D., Kassack, M.U., Sippl, W., and Jung, M. (2007). Structure-activity studies on suramin analogues as inhibitors of NAD⁺-dependent histone deacetylases (sirtuins). *ChemMedChem* 2, 1419-1431.

- Um, J.-H., Park, S.-J., Kang, H., Yang, S., Foretz, M., McBurney, M.W., Kim, M.K., Viollet, B., and Chung, J.H. (2010). AMP-Activated Protein Kinase–Deficient Mice Are Resistant to the Metabolic Effects of Resveratrol. *Diabetes* 59, 554-563.
- Vagin, A.A., and Isupov, M.N. (2001). Spherically averaged phased translation function and its application to the search for molecules and fragments in electron-density maps. *Acta Crystallogr D Biol Crystallogr* 57, 1451-1456.
- Valenzano, D.R., Terzibasi, E., Genade, T., Cattaneo, A., Domenici, L., and Cellerino, A. (2006). Resveratrol Prolongs Lifespan and Retards the Onset of Age-Related Markers in a Short-Lived Vertebrate. *Curr Biol* 16, 296-300.
- Van Gool, F., Gallí, M., Gueydan, C., Kruys, V., Prevot, P.-P., Bedalov, A., Mostoslavsky, R., Alt, F.W., De Smedt, T., and Leo, O. (2009). Intracellular NAD levels regulate tumor necrosis factor protein synthesis in a sirtuin-dependent manner. *Nat Med* 15, 206-210.
- Vaziri, H., Dessain, S.K., Eaton, E.N., Imai, S.-I., Frye, R.A., Pandita, T.K., Guarente, L., and Weinberg, R.A. (2001). hSIR2/SIRT1 Functions as an NAD-Dependent p53 Deacetylase. *Cell* 107, 149-159.
- Verdin, E., Hirschey, M.D., Finley, L.W.S., and Haigis, M.C. (2010). Sirtuin regulation of mitochondria: energy production, apoptosis, and signaling. *Trends Biochem Sci* 35, 669-675.
- Villalba, J.M., and Alcáin, F.J. (2012). Sirtuin activators and inhibitors. *BioFactors* 38, 349-359.
- Wang, Y., and Tissenbaum, H.A. (2006). Overlapping and distinct functions for a *Caenorhabditis elegans* SIR2 and DAF-16/FOXO. *Mech Ageing Dev* 127, 48-56.
- Wienken, C.J., Baaske, P., Rothbauer, U., Braun, D., and Duhr, S. (2010). Protein-binding assays in biological liquids using microscale thermophoresis. *Nat Commun* 1, 100.
- Wood, J.G., Rogina, B., Lavu, S., Howitz, K., Helfand, S.L., Tatar, M., and Sinclair, D. (2004). Sirtuin activators mimic caloric restriction and delay ageing in metazoans. *Nature* 430, 686-689.
- Yu, S.S., Cai, Y., Ye, J.T., Pi, R.B., Chen, S.R., Liu, P.Q., Shen, X.Y., and Ji, Y. (2012). Sirtuin 6 protects cardiomyocytes from hypertrophy in vitro via inhibition of NF- κ B-dependent transcriptional activity. *Br J Pharmacol*, 10.1111/j.1476-5381.2012.01903.x.
- Yuan, J., Minter-Dykhouse, K., and Lou, Z. (2009). A c-Myc-SIRT1 feedback loop regulates cell growth and transformation. *J Cell Biol* 185, 203-211.

-
- Zhao, K., Chai, X., Clements, A., and Marmorstein, R. (2003). Structure and autoregulation of the yeast Hst2 homolog of Sir2. *Nat struct biol* 10, 864-871.
- Zhao, K., Harshaw, R., Chai, X., and Marmorstein, R. (2004). Structural basis for nicotinamide cleavage and ADP-ribose transfer by NAD(+)-dependent Sir2 histone/protein deacetylases. *Proc Natl Acad Sci U S A* 101, 8563-8568.
- Zhao, X., Allison, D., Condon, B., Zhang, F., Gheyi, T., Zhang, A., Ashok, S., Russell, M., Macewan, I., Qian, Y., et al. (2013). The 2.5 Å crystal structure of the SIRT1 catalytic domain bound to nicotinamide adenine dinucleotide (NAD⁺) and an indole (EX527 analog) reveals a novel mechanism of histone deacetylase inhibition. *J Med Chem*.
- Zhou, Y., Zhang, H., He, B., Du, J., Lin, H., Cerione, R.A., and Hao, Q. (2012). The bicyclic intermediate structure provides insights into the desuccinylation mechanism of human sirtuin 5 (SIRT5). *J Biol Chem* 287, 28307-28314.

Appendix

Appendix A: A list of crystallization conditions of diffraction quality crystals. The ligand labeled as *italic* was not found in structures.

Complex	Condition of Diffraction-quality Xtals			Initial screening
	Salt	Buffer	Precipitant	
hSirt3/ACS2	1 M Ammonium sulfate	0.1 M BisTris pH 5.5	1% (w/v) PEG 3350	JCSG+ 2.38
	0.2 M Ammonium sulfate	0.1 M BisTris pH 5.5	25% (w/v) PEG 3350	JCSG+ 2.43
hSirt3/FdL-1/PCT	0.2 M Sodium chloride	0.1 M HEPES pH 7.0	10% (v/v) Isopropanol	JCSG+ 2.3
hSirt3/FdL-1/brRESV	0.2 M Sodium chloride	0.1 M HEPES pH 7.0	10% (v/v) Isopropanol	JCSG+ 2.3
hSirt3/ACS2/brRESV	0.25 M Ammonium sulfate	0.1 M BisTris pH 6.0 – 6.6	21% (w/v) PEG 3350	JCSG+ 2.43 And many other conditions
hSirt3/ACS2/NAD⁺/brRESV		0.1 M MES pH 6.0	40% (v/v)PEG 400; 5% (w/v)PEG 3000	JCSGIII 61
hSirt3/ NAD⁺		0.1 M MES pH 6.0	40% (v/v)PEG 400; 5% (w/v)PEG 3000	JCSGIII 61
		0.1M MES pH 6.0	30% (v/v) PEG 600; 5% (w/v) PEG 1000;	JCSGIV 71

			10% (v/v) glycerol	
hSirt3/ NAD⁺/SRT1720		0.1M MES pH 6.0	40% (v/v)PEG 400; 5% (w/v)PEG 3000	JCSGIII 61
		0.1M MES pH 6.0	30% (v/v) PEG 600; 5% (w/v) PEG 1000; 10% (v/v) glycerol	JCSGIV 71
hSirt3/ carba-NAD⁺/SRT1720	0.2 M Sodium fluoride		20% (w/v) PEG 3350	JCSGII 29
hSirt3/ NAD⁺/Ex-527	0.2 M Ammonium nitrate		20% (w/v) PEG 3350	JCSG+ 1.27
zSirt5/p53/RESV		0.2M tri-Lithium citrate	14% (w/v) PEG 3350	JCSGI 9
zSirt5/ME/RESV		0.2M tri-Lithium citrate	20% (w/v) PEG 3350	JCSGI 9
zSirt5/FdL-1/RESV	0.15 M Sodium citrate	0.1 M BisTrisPropane pH 6.5	20% (w/v) PEG 3350	PACT 71
zSirt5/RESV		0.1 M Sodium cacodylate pH 6.5	1 M tri-Sodium citrate	JCSG+ 2.1

Appendix B: Tables Table I. Data collection and refinement statistics

	hSirt3/FdL-1/ 4'-bromo-resveratrol	hSirt3/ACS2/ 4'-bromo-resveratrol
Space group	R32	P2 ₁ 2 ₁ 2
Unit cell constants	a = b = 114.8 Å, c = 123.7 Å	a = 52.6 Å, b = 159.7 Å, c = 34.7 Å
Resolution (Å)	46.1 – 2.2	37.4 – 2.0
Unique reflections	30849	37699
<I / σ> (outermost shell)	16.1 (2.9)	11.5 (2.0)
Completeness (outermost shell) (%)	99.9 (100)	98.6 (99.0)
R _{meas} ^(a) (outermost shell) (%)	7.8 (58.6)	6.5 (57)
Total number of reflections used	15293	19508
Number of atoms in asymmetric unit		
Protein	2068	2070
Ligands	95	79
Water	136	127
R.m.s. deviations:		
Bond length (Å)	0.02	0.02
Bond angles (°)	2.1	1.8
Average B factor (Å ²)		
Protein	38.0	41.4
Peptide	44.5	46.5
4'-bromo-resveratrol	65.9	33.9
Zinc ions	24.4	42.5
Final R _{cryst} /R _{free} ^{(b)(c)} (%)	17.6/23.2	20.8/26.4

	hSirt3/ACS2	hSirt3/FdL-1/Piceatannol	hSirt3/FdL-1/Polydatin
Space group	C222 ₁	R32	R32
Unit cell constants	a = 77.4 Å, b = 128.9 Å c = 76.9 Å	a = b = 114.6 Å, c = 123.7 Å	a = b = 114.6 Å, c = 123.9 Å
Resolution (Å)	33.8 - 2.35	38.7– 2.3	35.9 - 2.3
Unique reflections	16333	14069	12434
$\langle I / \sigma \rangle$	15.38 (3.14)	19.95 (4.26)	16.84 (3.88)
Completeness	99.6 (99.6)	99.9 (99.9)	99.9 (99.7)
(outermost shell) (%)			
R _{meas} ^(a) (outermost shell)	9.2 (58.5)	9.1 (52.7)	10.1 (56.7)
(%)			
Total reflections Used	15516	13365	13318
Final R _{cryst} /R _{free} ^{(b)(c)} (%)	16.4/21.7	17.4/24.1	17.4/22.2
R.m.s. deviations:			
bond length (Å)	0.017	0.015	0.015
bond angles (°)	1.92	1.87	1.88

	hSirt3/ADPR	hSirt3/carba-NAD⁺/SRT1720
Space group	P2 ₁ 2 ₁ 2	C2
Unit cell constants	a = 63.9 Å, b = 66.7 Å, c = 66.9 Å β = 90°	a = 227.8 Å, b = 246.1 Å, c = 127.3 Å, β = 123.9°
Resolution (Å)	47.2 – 1.3	45.8 – 3.25
Unique reflections	69702	91148
<I/ σ> (outermost shell)	15.1 (1.2)	9.3 (1.1)
Completeness (outermost shell) (%)	98.4 (96.8)	99.4 (99.6)
R _{meas} ^(a) (outermost shell) (%)	8.8 (136.2)	14.4 (144.0)
Protein chains in asymmetric unit	1	12
No. of amino acids	272	3275
No. of protein atoms	2489	25548
No. of ligand atoms	41	936
No. of waters	266	0
No. of solvent atoms (except water)	20	24
No. of metals	2	12
R.m.s. deviations:		
Bond length (Å)	0.02	0.02
Bond angles (°)	2.3	2.4
Average B factor (Å ²)		
Protein	20.4	20.0
Ligands	15.0	86.2
Water	37.9	---
Final R _{cryst} /R _{free} ^{(b)(c)} (%)	13.8/17.9	22.7/24.7

	hSirt3/NAD⁺/Ex-527	hSirt3/native intermediate
Space group	P2 ₁ 2 ₁ 2	C222 ₁
Unit cell constants	a = 60.9 Å, b = 63.4 Å, c = 66.4 Å	a = 78.0 Å, b = 131.3 Å, c = 76.5 Å
Resolution (Å)	45.8 – 2.0	38.2 – 2.5
Unique reflections	17814	12915
<I / σ> (outermost shell)	15.6 (2.9)	20.8 (3.8)
Completeness (outermost shell) (%)	99.3 (95.4)	92.4 (93.9)
R _{meas} ^(a) (outermost shell) (%)	11.0 (64.7)	7.2 (52.3)
No. of amino acids	270	273
No. of protein atoms	2183	2144
No. of intermediate atoms	0	101
No. of ligand atoms	97	0
No. of waters	123	57
No. of solvent atoms (except water)	18	63
No. of metals	1	1
R.m.s. deviations:		
Bond length (Å)	0.02	0.02
Bond angles (°)	2.0	1.9
Average B factor (Å ²)		
Protein	20.0	41.2
Intermediate		53.5
Ligands include Zn	16.7	28.3
Water	25.0	39.6
Final R _{cryst} /R _{free} ^{(b)(c)} (%)	16.3/20.9	18.2/24.8

	<i>zSirt5/ME/Resveratrol</i>	<i>zSirt5/p53/Resveratrol</i>
Space group	I222	C222
Unit cell constants	a = 56.9 Å, b = 77.6 Å c = 139.4 Å	a = 84.5 Å, b = 105.4 Å, c = 65.9 Å
Resolution (Å)	19.93 – 2.0	46.6 – 2.45
Unique reflections	21218	11155
$\langle I / \sigma \rangle$	20.70 (4.20)	15.75 (3.6)
Completeness (outermost shell) (%)	99.7 (100)	99.9 (99.9)
$R_{\text{meas}}^{(a)}$ (outermost shell) (%)	4.8 (33.9)	9.7 (53.2)
Total reflections Used	20157	41463
Current $R_{\text{cryst}}/R_{\text{free}}^{(b)(c)}$ (%)	20.6/27.5	20.2/27.7
R.m.s. deviations:		
bond length (Å)	0.018	0.013
bond angles (°)	1.93	1.60

	<i>zSirt5/FdL-1/Resveratrol</i>	<i>zSirt5/Resveratrol</i>
Space group	I222	R32
Unit cell constants	a = 146.6 Å, b = 148.1 Å c = 248.8 Å	a = b = 230.8 Å, c = 167.0 Å
Resolution (Å)	19.9 – 3.2	46.2 - 2.6
Unique reflections	44932	52309
$\langle I / \sigma \rangle$	13.35 (3.38)	22.62 (4.18)
Completeness (outermost shell) (%)	99.8 (99.8)	100 (100)
$R_{\text{meas}}^{(a)}$ (outermost shell) (%)	12.0 (52.8)	7.5 (51.1)
Total reflections Used	42685	49693
Current $R_{\text{cryst}}/R_{\text{free}}^{(b)(c)}$ (%)	18.3/24.2	18.5/24.6
R.m.s. deviations:		
bond length (Å)	0.016	0.016
bond angles (°)	2.13	1.90

$$(a) R_{\text{meas}} = \frac{\sum_h \sqrt{\frac{n_h}{n_h - 1}} \sum_i^{n_h} |\hat{I}_h - I_{h,i}|}{\sum_h \sum_i^{n_h} I_{h,i}} \quad \text{with} \quad \hat{I}_h = \frac{1}{n_h} \sum_i^{n_h} I_{h,i}$$

$$(b) R_{\text{cryst}} = \frac{\sum \left| |F_{\text{obs}}| - |F_{\text{calc}}| \right|}{\sum |F_{\text{obs}}|}; \quad |F_{\text{obs}}| \text{ is the observed and } |F_{\text{calc}}| \text{ the calculated structure factor}$$

amplitude.

(c) R_{free} was calculated from 5% of measured reflections omitted from refinement.

(Eidesstattliche) Versicherungen und Erklärungen

(§ 5 Nr. 4 PromO)

Hiermit erkläre ich, dass keine Tatsachen vorliegen, die mich nach den gesetzlichen Bestimmungen über die Führung akademischer Grade zur Führung eines Doktorgrades unwürdig erscheinen lassen.

(§ 8 S. 2 Nr. 5 PromO)

Hiermit erkläre ich mich damit einverstanden, dass die elektronische Fassung meiner Dissertation unter Wahrung meiner Urheberrechte und des Datenschutzes einer gesonderten Überprüfung hinsichtlich der eigenständigen Anfertigung der Dissertation unterzogen werden kann.

(§ 8 S. 2 Nr. 7 PromO)

Hiermit erkläre ich eidesstattlich, dass ich die Dissertation selbständig verfasst und keine anderen als die von mir angegebenen Quellen und Hilfsmittel benutzt habe.

Ich habe die Dissertation nicht bereits zur Erlangung eines akademischen Grades anderweitig eingereicht und habe auch nicht bereits diese oder eine gleichartige Doktorprüfung endgültig nicht bestanden.

(§ 8 S. 2 Nr. 9 PromO)

Hiermit erkläre ich, dass ich keine Hilfe von gewerbliche Promotionsberatern bzw. -vermittlern in Anspruch genommen habe und auch künftig nicht nehmen werde.

.....
Ort, Datum, Unterschrift